ERDC/GSL TR-19-20

Geotechnical and Structures Laboratory

US Army Corps
of Engineers®
Engineer Research and
Development Center

ERDC
ENGINEER RESEARCH & DEVELOPMENT CENTER

Investigation of the Mechanisms for the Delamination Resistance Found In Bio-Engineered Composites Found in Nature: Bi-Layered Exoskeleton Fish Scales

Wayne D. Hodo

April 2019

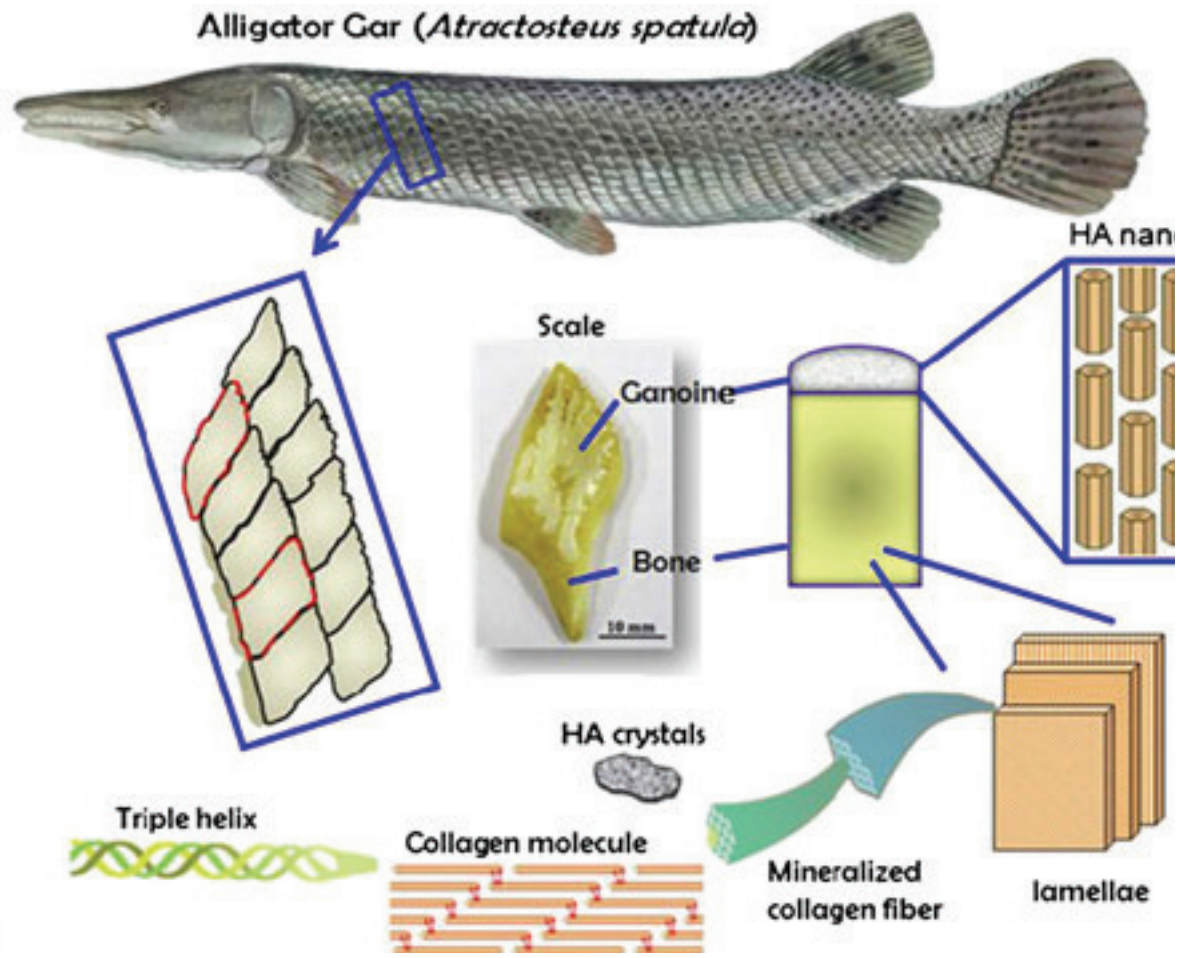

The U.S. Army Engineer Research and Development Center (ERDC) solves the nation's toughest engineering and environmental challenges. ERDC develops innovative solutions in civil and military engineering, geospatial sciences, water resources, and environmental sciences for the Army, the Department of Defense, civilian agencies, and our nation's public good. Find out more at www.erdc.usace.army.mil.

To search for other technical reports published by ERDC, visit the ERDC online library at http://acwc.sdp.sirsi.net/client/default.

ERDC/GSL TR-19-20
April 2019

Investigation of the Mechanisms for the Delamination Resistance Found In Bio-Engineered Composites Found in Nature: Bi-Layered Exoskeleton Fish Scales

Wayne D. Hodo

Geotechnical and Structures Laboratory
U.S. Army Engineer Research and Development Center
3909 Halls Ferry Road
Vicksburg, MS 39180-6199

Final report

Prepared for U.S. Army Corps of Engineers
Washington, DC 20314-1000

Under Military Engineering AT22 under Work Package # 256 Material Modeling For Force Protection (PE 61101, Task 02) Project Number MR018, "Investigation of Delamination Resistant Bio-Laminates (6.1/ILIR 002)."

Abstract

The focus of this study was to learn how nature integrates hard and soft materials at each length scale to form a layered composite that better resists delamination. This research provided a detailed description, using novel experiments, to explain how hard and soft materials have been mixed/integrated at each length scale, optimized by volume fractions, which affect the fish scales' mechanical response due to external loading. The results from the study showed the following:

1. The combination of the hard (inorganic minerals) and soft (organic collagen fibers) are integrated instead of being glued at the nano scale. At the micron scale for the two-layered composite, the outer dental enamel (hard) layered interface uses a sawtooth-shaped joint to connect to the inner bone (hard open-like foam) layer. At the millimeter scale, the material and mechanical properties are gradually graded through the thickness away from the interface.
2. The outer hard layer has 90 percent hard (inorganic minerals) and 10 percent (collagen fibers) by volume. Whereas, the inner bone layer has 60 percent hard (inorganic minerals) and 40 percent (organic collagen fibers) by volume. The property variation seems to delocalize stresses, which increase delamination resistance at the interface.

Contents

Figures and Tables

Figures

Tables

Preface

This study was conducted for the U.S. Army Engineer Research and Development Center for the Military Engineering AT22 Program under Work Package 256 Material Modeling for Force Protection (PE 61101, Task 02) Project Number MR018, "Investigation of Delamination Resistant Bio-Laminates (6.1/ILIR 002)."

The work was performed by the Airfields and Pavements Branch (GMA) of the Engineering Systems and Materials Division (GM), U.S. Army Engineer Research and Development Center, Geotechnical and Structures Laboratory (ERDC-GSL). At the time of publication, Dr. Timothy W. Rushing was Chief, CEERD-GMA; Dr. Gordon W. McMahon was Chief, CEERD-GM; and Ms. Pamela G. Kinnebrew, CEERD-GZT, was the Technical Director for Military Engineering. The Deputy Director of ERDC-GSL was Mr. Charles W. Ertle II, and the Director was Mr. Bartley P. Durst.

COL Ivan P. Beckman was the Commander of ERDC, and Dr. David W. Pittman was the Director.

List of Abbreviations and Terms

α-Al_2O_3	Aluminum Oxide
2σ	Two Standard Deviations
AASHTO	American Association of State Highway and Transportation Officials
$AgC_{22}H_{43}O_2$	Silver Behenate
AFM	Atomic Force Microscopy
Al	Aluminum
ATR	Attenuated Total Reflectance
ATR-FTIR	Attenuated Total Reflectance- Fourier Transform Infrared Spectroscopy
B-Ap	Bio-Apatite
C/B-Ap	Collagen + Bio-Apatite
C	Carbon
Ca	Calcium
$CaCO_3$	Calcium Carbonate
CO_3	Carbonate
CBR	California Bearing Ratio
CH_x	Hydrocarbons
Cl	Chlorine
COOH	Carboxyl
CP	Cross-Polarization
CP-CH	Cross-Polarization Carbon-Hybridized
CP-CSA	Cross-Polarization Chemical Shift Anisotropy
CP-DD	Cross-Polarization Dipolar De-phasing
CP-DDD	Cross-Polarization Dipolar De-phasing Difference
CP-TOSS	Cross-Polarization Total Carbon Speciation
Cryst.	Crystals

DEM	Discrete Element Method
DMA	Dynamic Mechanical Analysis
DOE	Design of Experiments
Deter.	Determination
D_S	Contact Damping
D_m	Machine Damping
DTI	Drop Tower Impact
E'	Storage Modulus
E"	Loss Modulus
EELS	Electron Energy Loss Spectroscopy
EPMA	Electron Microprobe Analyzer
ERDC	Engineer and Research Development Center
F	Fluorine
F_o	Harmonic Force Amplitude
FEA	Finite Element Analysis
FEM	Finite Element Method
Fe	Iron
FIB	Focused Ion Beam
FTIR	Fourier Transform Infrared Spectroscopy
G	Gravitational Constant
Ge	Germanium
H	Hydrogen
h_o	Harmonic Displacement
H	Hypothesis
HAADF	High Angle Annular Dark Field
HAp	Hydroxyapatite
HR-SEM	High Resolution Scanning Electron Microscopy

INI	Instrumented Nanoindentation
IRE	Internal Reflection Element
ITZ	Interfacial Transition Zone
K	Potassium
k_f	Finite Stiffness
k_s	Spring Stiffness
m	Mass
Mg	Magnesium
Mn	Manganese
μm-UC	Micropillar Uniaxial Compression
μm-XANES	Microcomputed Synchrotron X-Ray Absorption Near Edge Structure
μm-XCT	Micro X-Ray Computed Tomography
μm-XEDS	Microcomputed X-Ray Energy-Dispersive Spectroscopy
μm-XRD	Microcomputed Synchrotron X-Ray Diffraction
μm-XRF	Microcomputed Synchrotron X-Ray Fluorescence
Mg	Magnesium
Mn	Manganese
N	Nitrogen
Na	Sodium
NIH	National Institutes of Health
O	Oxygen
OH^-	Hydroxide
P	Phosphorus
PO_4	Phosphate
PBS	Phosphate-Buffered Saline
ppm	Parts-Per-Million

Prot.	Protein
ROI	Return on Investment
S	Contact Stiffness
S	Sulfur
Si	Silica
Sr	Strontium
Speciat.	Speciation
SS-NMR	Solid-State Nuclear Magnetic Resonance
STEM	Scanning Transmission Electron Microscopy
STEM-HAADF	Scanning Transmission Electron Microscopy-High Angle Annular Dark Field
STEM-EELS	Scanning Transmission Electron Microscopy-Electron Energy Loss Spectroscopy
tan Φ	Phase Lag or Phase Angle
TEM	Transmission Electron Microscopy
Ti	Titanium
TGA	Thermal Gravimetric Analysis
UC	Uniaxial Compression
UT	Uniaxial Tension
Var.	variables
Zn	Zinc

Unit Conversion Factors

Multiply	By	To Obtain
angstroms	0.1	nanometers
degrees Fahrenheit	(F-32)/1.8	degrees Celsius
microns	1.0 E-06	meters
pounds (mass)	0.45359237	kilograms

1 Introduction

1.1 Motivation

As a result of recent budget restraints, the U.S. Army has looked to reduce production cost for some of its military assets. For example, the Army has determined a huge cost savings can be accomplished by reducing the gross vehicle weight for the Mine-Resistant Ambush Protected (MRAP) personnel carrier by 33 percent (Joint Light Tactical Vehicle 2015). The MRAP weighs 7 to 15 tons and cost $300k to $550k (base models)/vehicle to build (Mine-Resistant Ambush Protected 2015); whereas, the next generation Joint Light Tactical Vehicle (JLTV) is expected to weigh 4.5 to 10 tons and cost $230k to $270k (base models)/vehicle to build (Joint Light Tactical Vehicle 2015). To be able to cut cost up to 51 percent while maintaining military personnel safety, engineered composite materials will need to be used. Engineered composite (inhomogeneous) materials are well-known for their superior structural properties. Composites are attractive because they can have the superior structural properties of being impact/penetration resistant, lightweight, high-strength, high-stiffness and can provide good fatigue and corrosion resistance (Figure 1.1) (Structural Composites and Sandwich Panels 2015). Additionally, engineered composites are multilayered systems that have interfaces that are glued. In the general sense, composite materials are defined as two or more physically and chemically distinct materials which, when combined, have improved properties over the individual materials (Strong 2008). When comparing engineering composites to other structural materials such as steel, concrete, and foams, we find: (a) steel has high-strength, high-fracture toughness but is extremely heavy, (b) concrete has high-strength but is very brittle, has little fracture toughness, and is very heavy, (c) foam is impact resistant, lightweight, but has low fracture-toughness and low-strength.

Although composites are promising and offer mutually exclusive material properties (high-strength, high-fracture toughness, and lightweight) that are not found in other structural materials, they are prone to delamination at the glued layered interface. Usually manmade engineered composites tend to delaminate when impacted because the glued layers de-bond. Delamination at layer interfaces is the primary mechanism that leads to the failure of composite materials, Figure 1.2 (Makhecha 2005, Columbia

Accident Investigation Board 2003). As an example, if engineered composites are used as sandwich panels on space shuttles, they can become damaged by impact. As an outcome of the impact damage, the glued sandwich panels may delaminate and fail almost instantaneously if exposed to the extreme thermal temperatures and weight of gravity, causing the shuttle to explode (Makhecha 2005, Columbia Accident Investigation Board 2003).

Figure 1.1. Schematic of multilayered composite material system (Structural Composites and Sandwich Panels 2015).

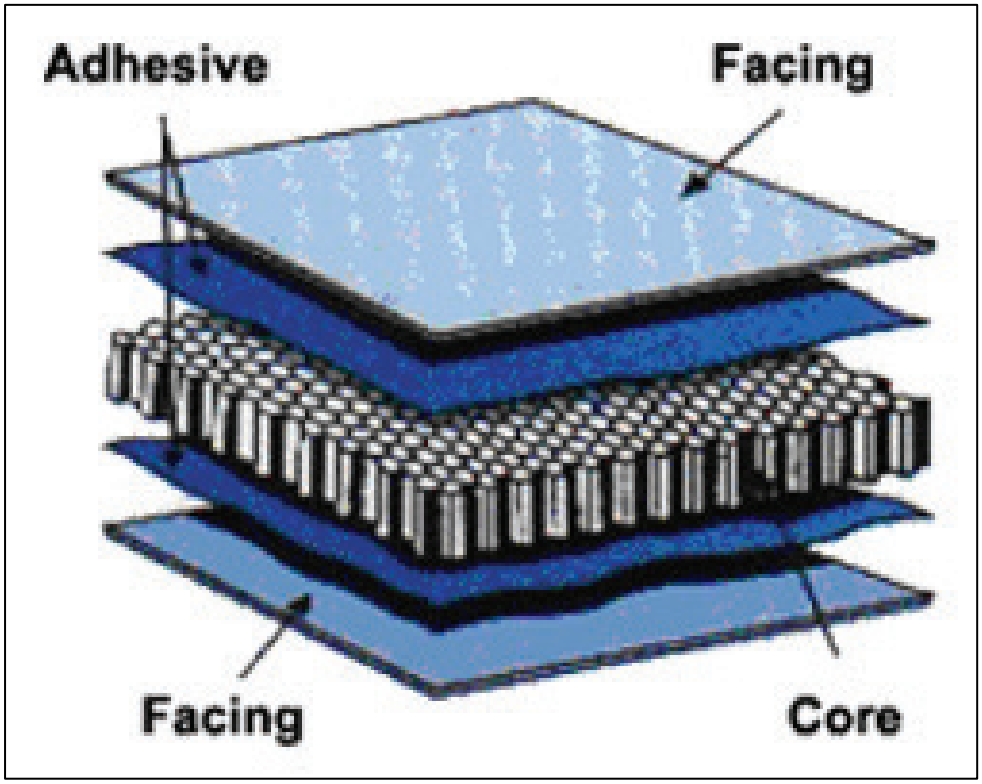

In contrast to manmade composites, most superior performing materials (high-strength, high-toughness, and lightweight) found in nature are layered composite systems that use a two-component mixture of materials that are integrated at each length scale from the nano- to millimeters to form what is called a “hierarchal structure.” From the nano- to micron-length scale the hard materials (similar to metals) are mixed with soft materials (similar to polymers) then varied by volume fractions, spatial proximity, and directional placement in the layers to produce a delamination resistant composite system. These delaminate-resistant biocomposite structures (e.g., alligator gar [*Atractosteus spatula]* exoskeleton fish scale) have mechanical properties that vastly exceed the

properties of their relatively weak constituents, as seen in Figure 1.3 (Wegst et al. 2010). Shown in Ashby's chart "a," Figure 1.3, are the specific values (that is, normalized by density) at the millimeter scale after integrating the hard and soft material, the natural composites can have values of strength and toughness that are very comparable to those of most metals and alloys.

Figure 1.2. Composites fail by delamination when impacted, foam-tile delamination led to Columbia space shuttle disaster (Columbia Accident Investigation Board 2003).

Figure 1.3. Ashby design chart of mechanical properties showing fracture toughness plotted against Young's modulus for natural and engineered composite materials (Wegst et al. 2010; Hodo 2015).

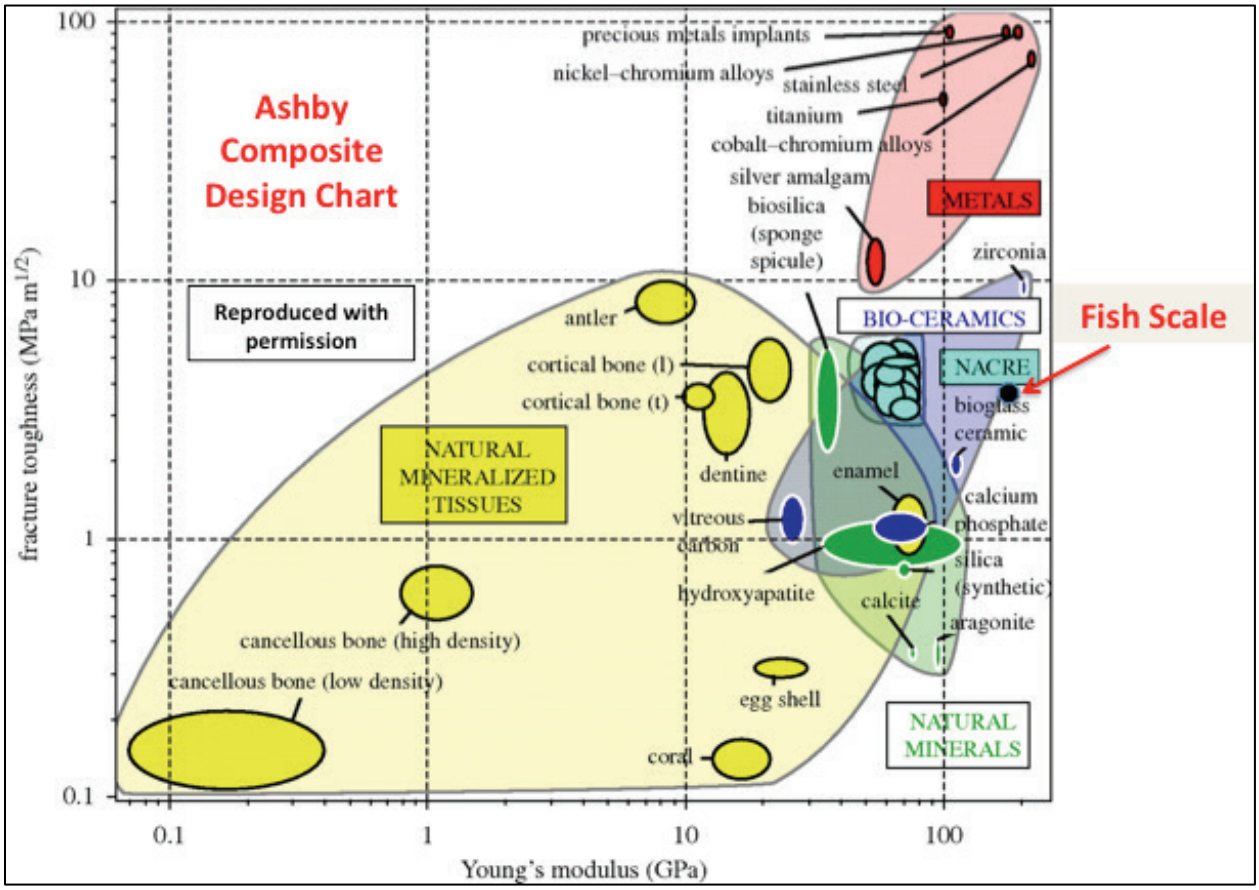

Specifically, shown in Figure 1.3, the engineering properties of the fish scales' two individual layer components are similar to the outer dental enamel (hard) and inner cancellous bone (soft, sponge-like foam). The hard enamel is lightweight, has high-strength but is brittle, and has a low fracture toughness; whereas the sponge-like cancellous bone is lightweight, but it is soft, low-strength and has low fracture toughness. However, when the (hard) enamel is mixed with the (soft) sponge-like cancellous bone, they combine to make a lightweight, fish-scale layered composite that has high strength with good fracture toughness whose engineering properties are comparable to metal alloys.

1.2 Problem

Most superior performing materials found in nature possess a hierarchal composite structure. The formation of the weak individual constituents found in fish scale composite is a function of its environmental conditions (i.e., water temperature and soluble minerals). Within each layer, at the

micron scale, there are subtle variations in the spatial proximity and directional placement of the hard and soft materials. The fish scale is made up of 90 percent hard (inorganic minerals) and 10 percent soft (polymer-like organic collagen fibers) by volume. However, knowledge is lacking on how nature integrates hard and soft materials at each length scale to form a layered composite that is lightweight, has high strength with good fracture toughness, but does not delaminate.

1.3 Scientific objective

The objective of this research effort is to:

1. Investigate how nature might produce a composite made from a hard (inorganic mineral) and soft (polymer-like organic fibers) to form a layered structure that exhibits superior performing delamination resistance when externally loaded.
2. Explain how the hard and soft materials are integrated in the fish scale to form a layered structure that is lightweight and has high strength with good fracture toughness so they may not delaminate.
3. Suggest what fish-scale design principles can be applied to the design of manmade engineered composite systems.

1.4 Hypothesis (*H*)

The hypothesis (*H*) is that the fish scales resist cracks and delamination because of the mixing and integration of materials occurring at millimeter, micron, and nano scales. Evidently, the fish scale's hard (inorganic minerals) and soft (polymer like organic fibers) material volume fractions and variations within the layers reduces the local stresses that lead to delamination and crack formation caused by impact/penetration.

1.5 Approach

To meet the objectives of this research effort and to test the hypothesis, I further experimentally investigated from the nano- to millimeter-length scale the delamination resistant mechanisms in fish scale. At each length scale a detailed description was provided of how the hard and soft materials were mixed, what the material variations were within the layers, and what effect did the materials and variations have on mechanical properties in the composite system.

1.6 Research innovation

Previous research conducted by others has suggested that from the nano- to millimeter-length scale, the individual components of the fish scale are glued rather than integrated to form layers in the composite. However, sufficient evidence has yet to be provided that neither proves nor disproves the suggested assumption. The innovation of this research is that for the first time a detailed description was provided as to how hard and soft materials are mixed and integrated at each length to form a layered structure. In addition, my research provided details on how the hard and soft materials vary by volume fractions, spatial proximity, and directional placement within the layers. Furthermore, the material variations were compared to mechanical properties of modulus and hardness and, for the first time, energy dissipation was used to explain why the natural composite has high strength, good toughness, and may not delaminate.

As an additional outcome of my research, to be able to meet my research objective and sufficiently test the hypothesis, a fundamental material science approach was used to develop an experimental protocol. Currently, there are no satisfactory standard combined protocols for investigating the material integration, local mechanical properties, material variation and integration at each length scale (millimeter, micron, and nano). Therefore, the development of the experimental protocol was needed so that the material variation and integration from the nano- to millimeter-length scale could be adequately explained. The experimental protocol used in this research is based on fundamental principles as opposed to the applied research methods of trial and error. The approach used here makes use of design concepts rather than iterative techniques that are employed across the engineering and scientific communities.

1.7 Organization of report

Chapter 2 of this document provides a detailed overview of the current state of knowledge for exoskeleton fish scales and the experimental methods used in the characterization of bio-composites. Chapter 3 describes the experimental plan, materials, and methods used in this study. Chapter 4 provides the experimental data, analysis, and results for type, integration, and variation of materials, and mechanical properties for the layers at each length scale. Chapter 5 discusses the specific questions raised by the hypothesis, insight provided for the biological design

principles, and suggested methodologies for developing bioinspired engineered composite designs that exhibit advanced high performance. Chapter 6 provides the summary, contributions/conclusions from this research, and offers recommendations for future work.

2 State of Knowledge

2.1 Advanced engineered composites overview

Advanced engineered composites have been widely used by public and private sectors for marine, automotive, transportation, and aerospace industries (Gururaja 2012). In general, composites are used because no single structural material can be found that has all of the desired characteristics to meet the demands for specific applications. Engineered composites are robust and are often preferred by designers because individual materials are used in concert for the enhancement of performance characteristics. For instance, heterogeneous (dissimilar) carbon fiber-reinforced polymers (CFRPs) materials are used wherever high strength-to-weight ratio and rigidity are key to performance such as in airplane wings (Jones 1999). The wings must be light for air flight and durable enough to resist torsion, compressive, tensile, shearing, and flexural failure.

In recent years, the composites that are in use are comprised of advanced materials and typically function under extreme operating conditions. For example, high earthquake areas, subzero temperature environments, nuclear blasts, or instances of penetration effects caused by mid-to-high rate situations are the extreme conditions in which the composites should be able to perform well. Therefore, the myriad attributes advanced composites offer that may be used to meet designers' tailored requirements are: (a) tailorable physical and mechanical properties (e.g., anisotropic strengthening, toughness, durable, lightweight, high stiffness/crush resistance, strength-to-weight ratios and complex geometries, (b) conductive properties (e.g., optical or electrical ranging from none, to low, to high), (c) corrosion resistance, (d) thermal/flammable resistance, and (e) renewability/recyclability (Gibson 1994).

2.2 Current limitations of advanced engineered composites

One of the most critical aspects when designing composites is to prevent de-bonding/delamination of layers and at interfacial transition zones (ITZs) of dissimilar materials. For example, engineered sandwich panel composites have the superior properties of being lightweight and temperature resistant and have been consistently used on space shuttle surfaces, thereby making space travel possible. However, an accident

occurred 1 February 2003 during the Columbia space mission, when the surface layer of the composites panel space shuttle received impact damage from a foreign object. As an outcome of the impact damage, the composite panel became unglued and delaminated. The space shuttle could no longer perform as designed. Failure occurred almost instantaneously because the damaged, de-bonded surface areas were exposed to the extreme thermal temperatures (3000°F) and gravity of at least 5G (where G is the gravitational constant is approximately equal to 6.674×10^{-11} N m^2/kg^2), causing the shuttle to explode. (Makhecha 2005, Columbia Accident Investigation Board 2003).

The capability to prevent composites from delaminating has eluded designers. Engineered composites are vulnerable to delamination when impacted or penetrated (Qiao et al. 2008; Geubelle and Baylor 2008). Delamination at the interface is the primary mechanism that leads to the failure of composite materials (Tippetts 2005). The interface is an important factor controlling the stiffness, strength, and fracture properties for composite materials at the macro scale (Needleman 1989). Because of expanding needs for new high-performance materials that are cheaper and environmentally acceptable, researchers have turned to nature for answers by investigating superior performing biological materials.

2.3 Biological materials overview

Over the last two decades, both design engineers and researchers have turned to nature with the hopes of understanding how biological materials are efficiently created to have superior properties such as high-strength, high toughness, and lightweight (Wegst and Ashby 2004). Researchers have learned nature does not design structures. Rather, it designs for functionality using whatever materials are indigenous to the geographical location. Functionality is what dictates the formation of the structure (Srinivasan et al. 1991; Weiner et al. 2000). From an evolutionary standpoint, the biological materials adapted to their environment by enhancing their functionality in response to external stimuli. The adaptation by biological organisms has traceable developmental processes documenting how the systems adjust to their ever-changing surroundings. The motifs that are common in the development of biological materials are shown in Figure 2.1. I summarized the previous research efforts as to how the three integrated stages occur (Goodsell 2004, Oyen 2011, Ehrilich 2010, Luz and Mano 2009, Sarikaya et al. 1999).

Figure 2.1. Three integrated stages of developmental processes for adaptive biological materials.

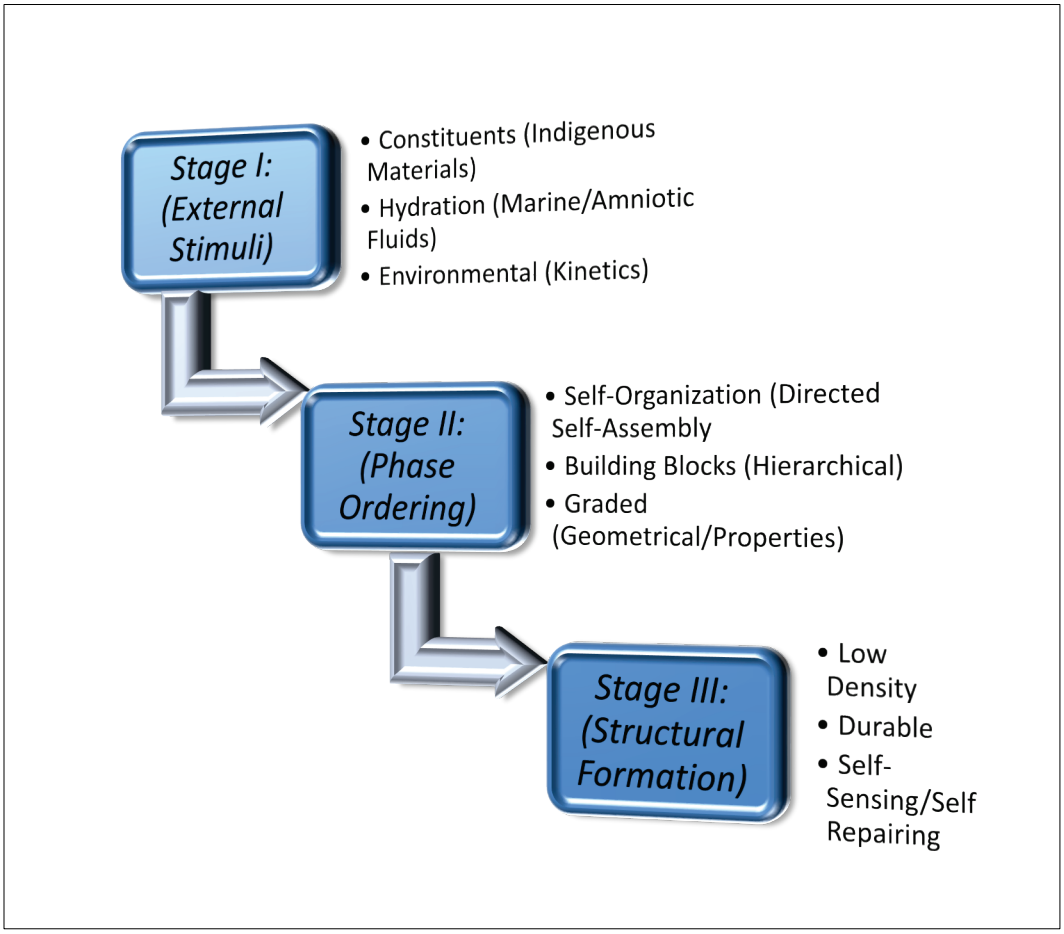

The three sequential occurring stages are *External Stimuli*, *Phase Ordering*, and *Structural Formation*. *Stage I* is where nature acquires indigenous materials to be used for its constructs. Biological materials routinely make use of the commonly available periodic elements: carbon(C), nitrogen (N), calcium (Ca), hydrogen (H), oxygen (O), silica (Si), phosphorus (P), iron (Fe), and magnesium (Mg), which then form into proteins and minerals (Meyers et al. 2008). Nature uses the same periodic elements to serve different purposes in the structural development process. For instance, the periodic elements of Ca, C, and O can form calcium carbonate ($CaCO_3$).

In the Nacre *(Mother of Pearl)* layer for the mollusks seashells, $CaCo_3$ is the main molecule that drives the structural formation of high-strength mineralized aragonite layers within the seashell (Figure 2.2). Yet, in bone and tooth, $CaCO_3$ assumes the role of solubilizing agent used for promoting ion transport within the hydroxyapatite molecule. The

hydroxyapatite molecule is the primary constituent responsible for developing the high-strength mineralized structural layers found in bone and tooth (Goodsell 2004, Ehrilich 2010, Meyers et al. 2008).

Figure 2.2 Schematic and scanning electron microscope images of the structural arrangement for aragonite crystal layers found in nacre (Meyers et al. 2008).

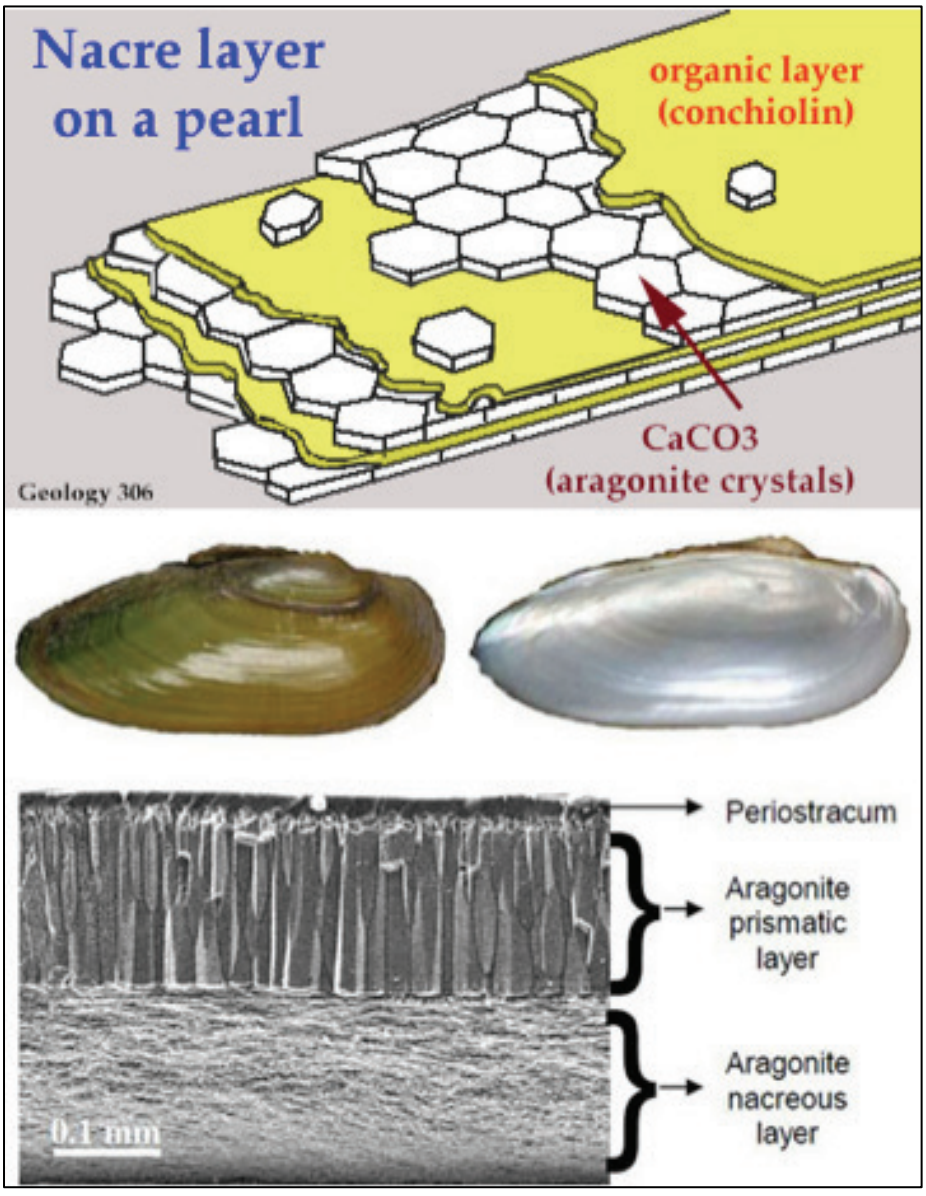

Another important aspect of all biological material formation is the hydration state. Nature uses hydration to facilitate the organism's development starting from the incubation period through the end of cessation. The environmental conditions provide the efficient energy source to drive the reaction kinetics, usually occurring at ambient temperature with

standard pressure and hydration states as determined by the required functionality (e.g., structural formation/geometry and mechanical property development). More importantly, nature responds to the environmental conditions to maintain a delicate balance between the role the periodic elements play in the construction and functionality of the organisms.

Next, *Stage II* begins with self-organizing the media and metrics defined in *Stage I*. The entity then uses the directed self-assembly process to attach the building blocks at each length scale with the variation in how the materials are integrated. In *Stage II*, the way materials are mixed, distributed, and integrated plays a key role in the amplification of properties that governs the formation of the multifunctionality for the system. The amplification of properties is very complex and unique for each length scale starting from the atomic level through the macro level (one angstrom to one millimeter) depending on the characteristic length for the system.

After nature has systematically gathered, organized, and measured the ingredients within the confines of the environmental constraints, as denoted in *Stages I-II*, finally *Stage III* can begin. The construction of biological material structure encompasses several aspects of formation. Biological materials, specific to structures that have undergone the bio-mineralization process, develop characteristics during formation of being low density, durable, self-sensing, and able to repair themselves when damaged (Mann 2001).

2.4 Mineralized biological composites

A mineralized biological composite constitutes two phases: hard (inorganic minerals) matrix phase integrated with a soft (polymer-like organic fiber reinforcement phase) (Dunlop and Fratzl 2010, Baohua and Huajian 2010, Wegst et al. 2015, Dubey and Tomar 2010, Yang et al. 2012). Scientists discovered the biomineralized composites are advanced because of their length scale dependent material ordering, grading of mechanical properties, and functional role, and they have exhibited superior performance under extreme conditions (Meyers et al. 2011, Fratzl 2007). Subsequent to the scientist's discovery, design engineers have become fascinated with the novel characteristics and the possibilities of learning from nature how to synthesize bioinspired materials and structures for use in engineering applications (Barthelat 2007, Bhushan

2009). Examples of superior performing advanced mineralized biological composites are bone, teeth, and exoskeleton fish scales (Chen et al. 2012).

2.4.1 Exoskeleton fish scale

Material designers are in need of multifunctional composite materials that can readily meet a variety of in-service requirements (e.g., mechanical, sensing, or repairing) (Hanus and Harris 2013). Exploring simpler structured biomaterials other than bone and tooth is advantageous and can have a huge payoff for the composites community (Hanus and Harris 2013). Exoskeleton fish scales are another one of Mother Nature's biomineralized analogues that exhibit superior performance characteristics. Scientists are extremely challenged with the characterization, interpretation of processes, and functionality of the complex biomineralized systems such as nacre, bone, and tooth. By investigating less complex biological constructs, there is a greater chance for designers to use "biomimicry" or "bioinspiration" for synthesizing, designing, and manufacturing superior performing advanced composites.

Designers are frequently challenged when vetting new composite materials systems, especially those biological material composites deemed superior performing in nature. The new composites will need to: (a) meet engineering requirements, (b) have performance characteristics that are scalable from the nano to macro level, (c) be affordable to produce, and (d) be environmentally safe. By studying the less complicated structure of exoskeleton fish scale, designers are more likely to develop future advanced composites materials that can better meet the challenging need to maintain the nation's infrastructure, aircraft, and automobiles. Also, the fish scale can be used as a stepping stone for understanding more complicated material systems.

Designers have recently shown great interest in studying exoskeleton fish scales for potential use in a wide variety of engineering applications. Researchers have observed that the protective biomineralized hard outer layer seems to function as body armor for the fish (Bruet et al. 2008, Song et al. 2010). The fish scales are especially attractive for study because they are relatively simple and involve fewer discrete layers, yet the fish scale exhibits superior mechanical response and has comparable nanoindentation moduli with bone and tooth (Oyen 2011, Chen et al. 2011). From a design engineer's vantage point, when fewer components are incorporated there is higher probability the composite's design will:

(a) meet specifications, (b) require less optimization, and (c) can ultimately be manufactured. Therefore, the designer is more likely to develop a superior performing advanced composite structure with the in-service lifecycle maintenance requirements that are manageable and affordable (Hoa 2009, Ashby et al. 2007, Salonitis et al. 2010). The remaining portion of this section will discuss the current state of knowledge for the exoskeleton fish scale.

Nature has synthesized the scales of fish to serve many purposes attracting several researchers in their studies of evolution, functions, structures, and properties (Chen et al. 2012; Sire 1989a, 1989b, 1995; Sudo et al. 2002; Richter and Smith 1995; Wiley 1976; Williamson 1849; Alfaro et al. 2008; Bartol et al. 2003; Raschi and Tabit 1992). Although several classes of fish have been investigated, scientists/observationists have been able to find only one fish scale group that forms extremely hard, high-strength exterior biomineralized lightweight layers, Figure 2.3 (Yang et al. 2013a, Goodrich 1907).

The bony fish scale group is called ganoid. Ganoid scales are found in the Actinopterygii: gar and birchir fish class. The inception of both fish happened during the "Cretaceous" time period, occurring 66-144 million years ago (Gottfried and Krause 1998, Daget et al. 2001). The fish developed before the continental plates broke apart to form the African, South American, and Asian continents. As a result, the birchir and gar had widespread distribution in locations as diverse as Spain, India, Cuba, and North and Central America (Gayet and Meunier 1991; Domingo et al. 2009; Kumar et al. 2005; Smith et al. 2006; Gayet et al. 2002). Table 2.1 presents the speciation and general structural features for the gar and birchir fish that have been studied (Allison et al. 2013; Yang et al. 2013a; Géraudie 1988).

The ganoid scales are multilayered with mechanically graded modulus and hardness properties. The outermost layer is the strongest with strength decreasing and toughness increasing for innermost layers (Allison et al. 2013). The scales are diamond-shaped, with the outer edges of the scale being thinner to allow overlapping (Figure 2.4) (Shark 2015). Peg-and-socket joints along with sharpey fibers connect the adjacent overlapping scales (Figure 2.5) (Bruet et al. 2008). The overlapped connectors create a layer of uniform thickness that matches the scales' interior orthogonal thickness (Figure 2.6).

Figure 2.3 Images of different fish scale types and their overlaps; (a)-(b) Placoid, (c)-(d) Ganoid, (e)-(f) Cycloid, (g)-(h) Ctenoid. (Cosmoid scales not shown) (Yang et al. 2013a).

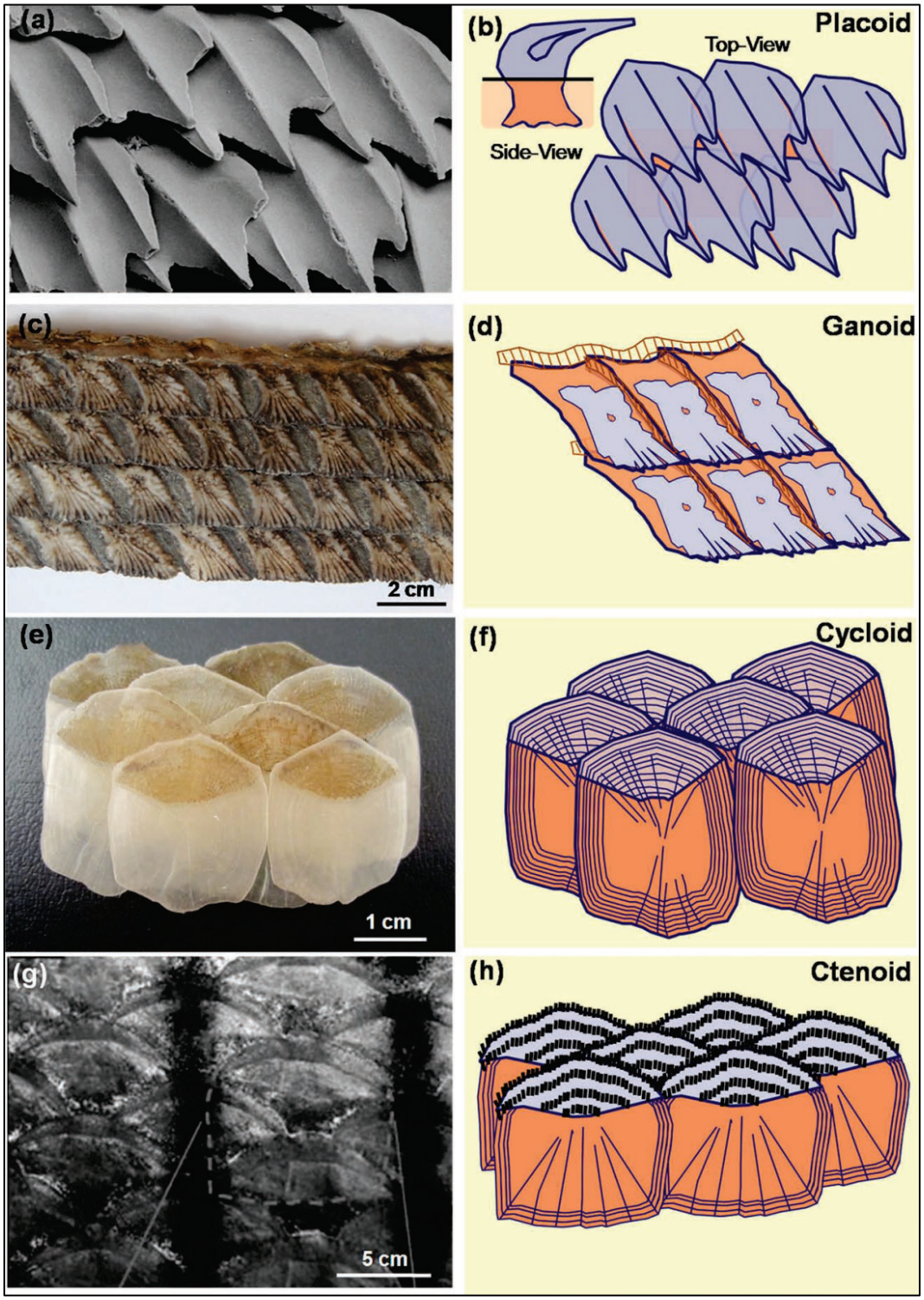

Although the ganoid scales of the gar and birchir fish have very similar speciation and general structural features, the two fish have differing structural layer arrangements. Examples of differing structural layer arrangements for the Senegal birchir (*Polypterus senegalus*) and Mississippi alligator gar fish (*Atractosteus spatula*) are illustrated in Figures 2.7 and 2.8, respectively (Bruet et al. 2008). The most commonly reported layer labels are provided for each fish type. Earlier layer designations provided by observationists have varied. For instance, the work discussed in Smith et al. (2006) pointed out there has been a long-standing debate since the 1850s whether or not the *polypterus* is a three- or four-layered system.

Table 2.1. Speciation and general structural features for gar and birchir fish (Allison et al. 2013, Yang et al. 2013a, Géraudie 1988).

	Fish Species	
Speciation Profile	**Gar**	**Birchir**
Temporal Range	Late Cretaceous–Recent	Cretaceous–Recent
Kingdom	Animalia	Animalia
Phylum	Chordata	Chordata
Class	Actinopterygii (Ray-Finned Fishes)	Actinopterygii (Ray-Finned Fishes)
Sub-Class	Neopterygii	Cladistia
Order	Lepisosteiformes	Polypteriformes
Family	Lepisosteidae	Polypteridae
Genera	[1]*Atractosteus*; *Lepisosteus*	[1]*Polypterus*; *Erpetoichthys*
Structural Member	Bone/Tooth/Scale	Bone/Tooth/Scale
Constituent Materials	Hydroxyapatite Mineral; Collagen Fibers	Hydroxyapatite Mineral; Collagen Fibers
Structural Features	• Biomineralized; • Multilayered; • Hierarchical • Functionally Graded • Composite	• Biomineralized; • Multilayered; • Hierarchical • Functionally Graded • Composite

[1] Most frequently studied.

In recent years, because of advanced microscope technology, the number of layers found in each fish type has been determined with more certainty (Bruet et al. 2008, Allison et al. 2013, Yang et al. 2013a). The Mississippi alligator gar fish scale has been shown to have two layers (outer ganoine + inner lamellar bone) and the Senegal birchir fish scale has four layers (outermost ganoine + 1st inner dentine + 2nd inner isopedine + inner most bone) (Bruet et al. 2008, Allison et al. 2013, Yang et al. 2013a).

Figure 2.4. Images of different fish scale types and their shapes (Shark 2015).

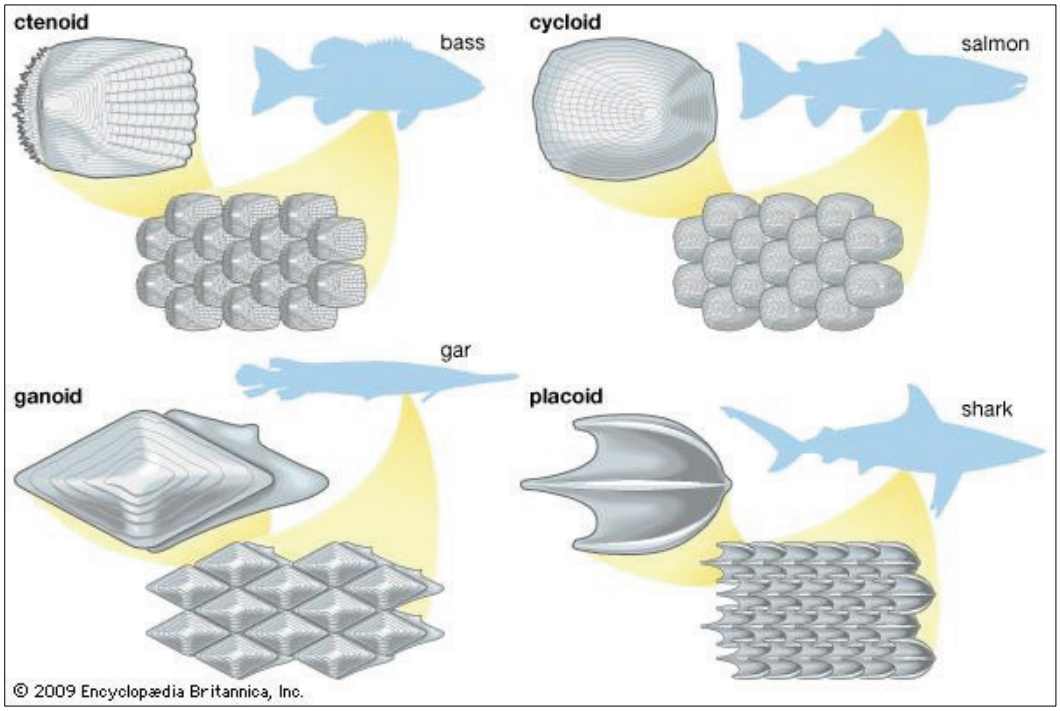

However, the comparisons made to other better understood biological materials are still open for questions. Observers have long debated the dissimilarities and resemblances of the structure and formation/growth mechanisms for each individual fish and also when comparing the birchir to the gar fish, along with other biomineralized composite materials such as bone and tooth (Williamson 1849; Goodrich 1907; Wiley 1976; Géraudie 1988; Sire 1989a, 1989b; Gayet and Meunier 1991; Sire 1995; Gottfried and Krause 1998; Daget et al. 2001; Gayet et al. 2002). Subsequently, the debate has led researchers to postulate the inherent mechanical response is directly related to the fish scale's intrinsic structure arrangement and chemical composition. The general postulate has been proven many times over; however, the structural specific layer make-up, formation, and growth mechanisms for the two fish scales are still not clear (Smith et al. 2006, Géraudie 1988).

Figure 2.5. Birchir fish with peg and socket connecting scales (Bruet et al. 2008).

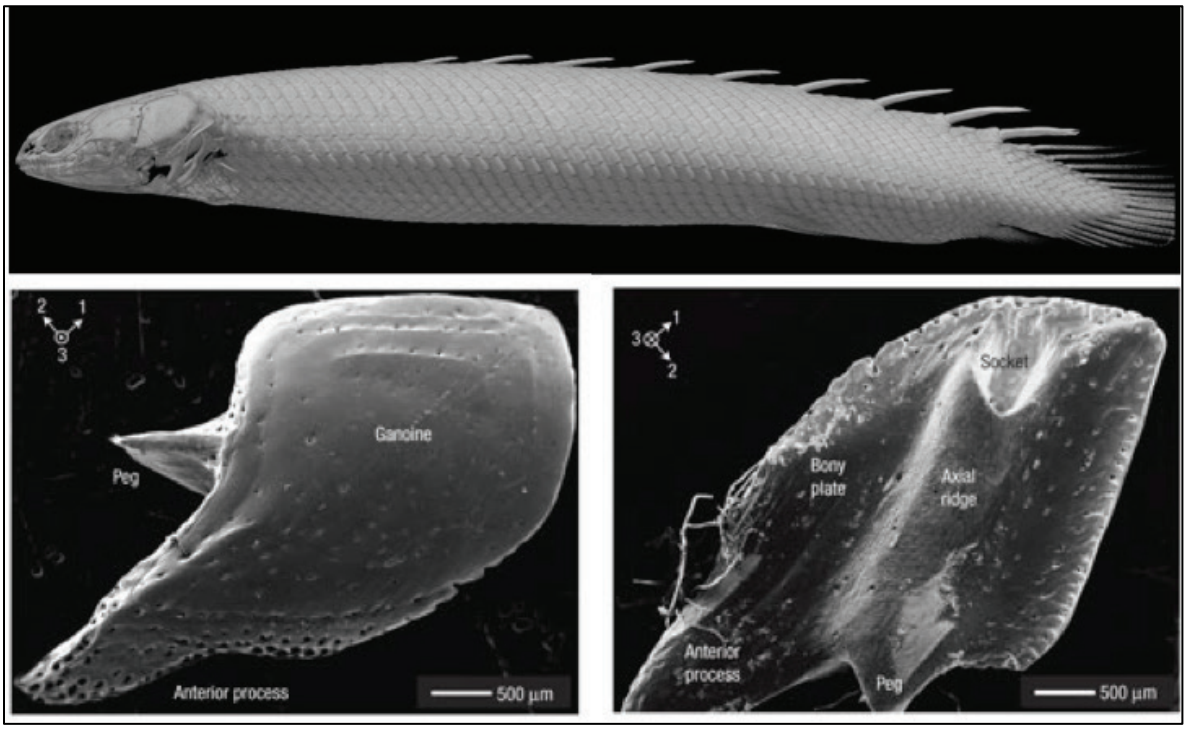

Figure 2.6. 3-D printed prototype demonstrating peg-and-socket joint connecting the adjacent overlapping birchir ganoid scales (Images courtesy of the U.S. Army's Institute for Soldier Nanotechnology located at Massachusetts Institute of Technology).

Figure 2.7. Structural layer arrangements for the Senegal birchir (*Polypterus senegalus*) (Bruet et al. 2008).

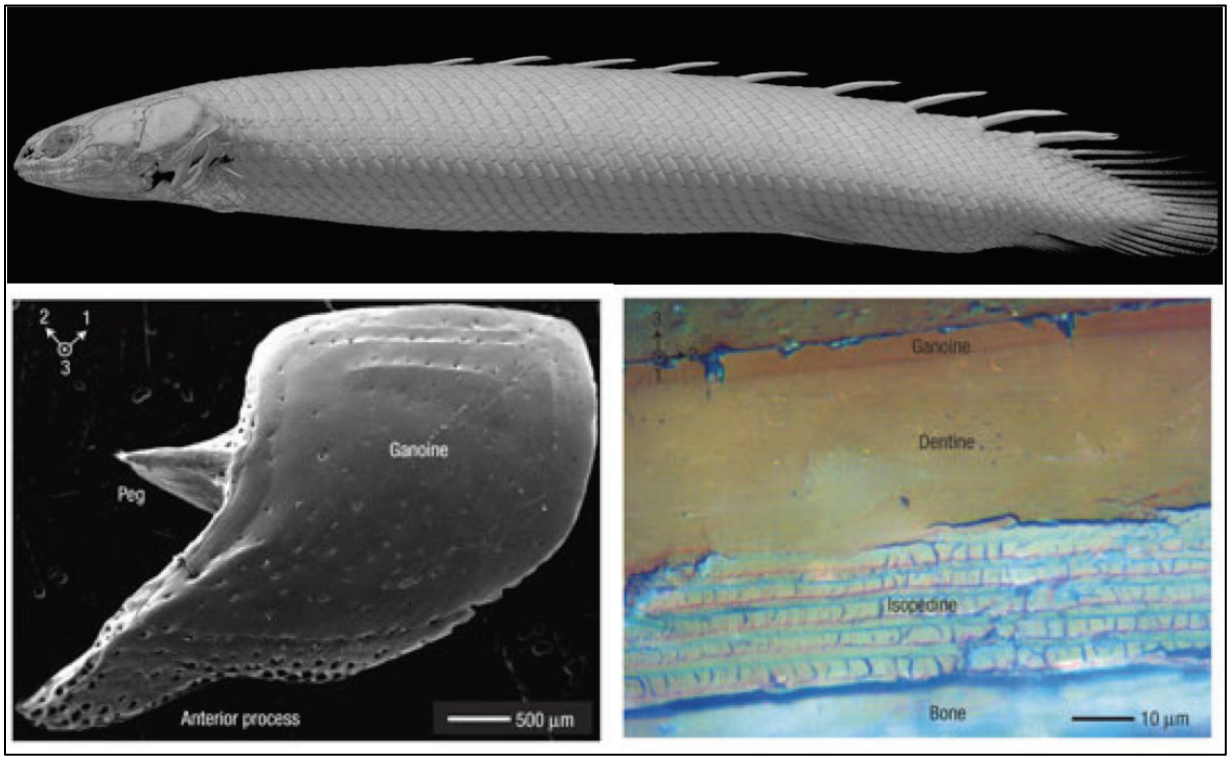

Figure 2.8. Structural layer arrangements for the Mississippi alligator gar fish (*Atractosteus spatula*) (Images courtesy of the U.S. Army's Engineer Research and Development Center [ERDC]-Geotechnical and Structures Laboratory [GSL] located in Vicksburg, MS).

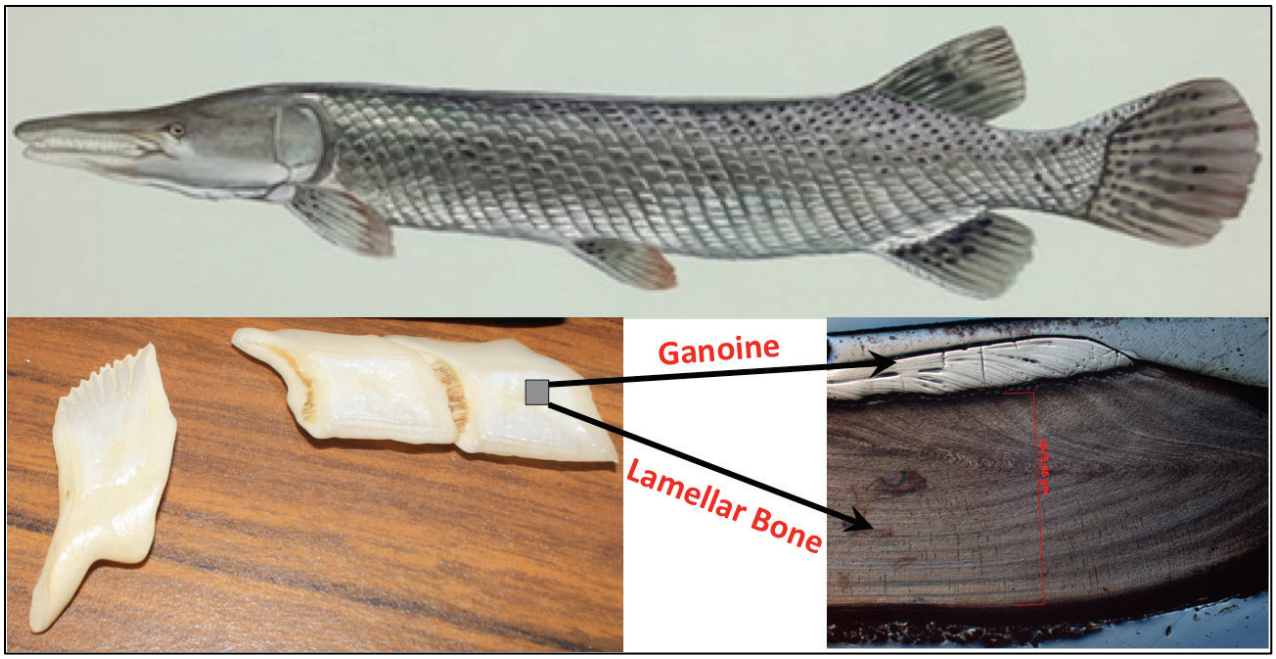

From a detailed review of literature, the material compositional differences in the two fish are subtle. Also, there are few differences in the local mechanical properties (elastic modulus and hardness) determined from nanoindentation experimentation. Elastic modulus and hardness appears to be similar within the ganoine layers and when taking measurements across the interface into the dentin layers and lamellar bone for the birchir and gar fish, see Figures 2.9 and 2.10, respectively (Bruet et al. 2008; Allison et al. 2013; Yang et al. 2013a, 2013b); although, from microindentation experiments and simulations, the measured global response indicates the birchir is better at resisting uniaxial loading when compared to the gar, see (corresponding) Figures 2.11 and 2.12, (Bruet et al. 2008; Song et al. 2011; Chandler et al. 2014).

Figure 2.9. Illustration of nanoindentation measured elastic modulus and hardness for Birchir fish scale (Bruet et al. 2008).

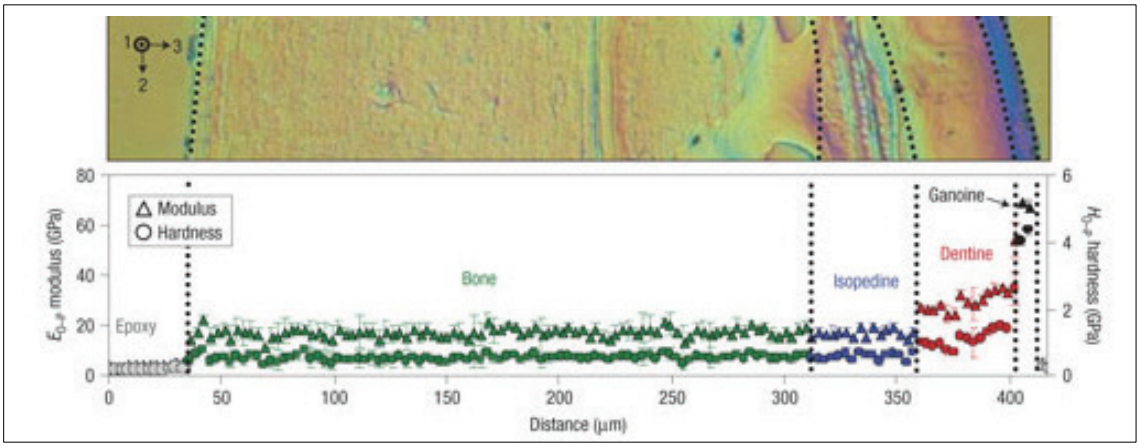

Evidently, increased resistance is attributed to the number of layers found in the birchir. Such use of layered structures is well-known to design engineering. For example, pavement design makes use of the principle of starting with the highest modulus materials on the surfaces followed by successively decreasing modulus layers to redistribute and dissipate stress and deformation. More generally, civil engineers incorporate highly heterogeneous geological materials in construction such as foundations, slopes, and retaining walls. The design procedures include stress and deformation design/analysis for load transfer of point loads laterally and vertically through the layers as uniformly distributed loads. As an example, Table 2.2 outlines the often-used methods and theories by the civil engineers' communities that may be relevant to the biomaterials research community when understating the stress transfer mechanisms exhibited by layered and hierarchically graded composites (Mallick and

ElKorchi 2009; Huang 1993; Yoder and Witczak 1975; Timoshenko and Lessels 1925; Lambe and Whitman 1969; Terzaghi 1943; Das 1990, 1994; AASHTO 1993; Ashish et al. 2011; Brill 1998; Bull and Singh 1990; Chou 1997; Hammons 1997; Hammons and Ioannides 1997; Ioannides and Korovesis 1990; UFC 03-260-02 2001; Westergaard 1925).

Figure 2.10. Illustration of nanoindentation measured elastic modulus and hardness for gar fish scale (Allison et al. 2013).

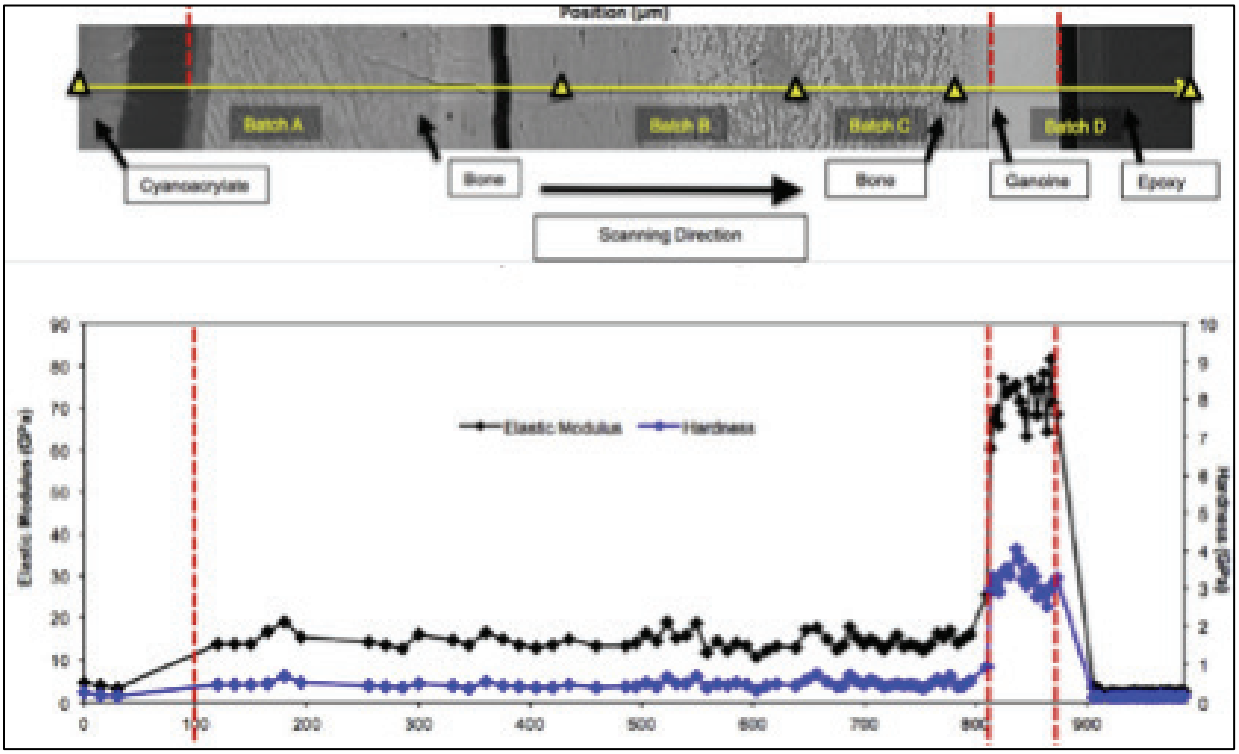

Upon further inspection, both birchir and gar ganoine layers have similar moduli and are effective in redistributing the microindentation point load through the layers' interfacial zones for the immediate underlying layers. The uniqueness of the gar fish scale is the ganoine-bone layers have a modulus mismatch, which acts to effectively transfer load across the interface, allowing the layered composite to remain undamaged when at the similar microindentation load levels, Table 2.3 (Chandler et al. 2014).

Figure 2.11. Microindentation simulation contours of stress, plastic strain and pressure fields of a birchir scale via multilayered finite element analysis (FEA) simulations. In "a"–"c," finite element analysis predictions of von Mises stress field, S22 (normal stress on the plane perpendicular to the 2 axis), S11 (normal stress on the plane perpendicular to the 1 axis) and pressure at a maximum depth when fully loaded, and S23 (shear stress on the plane perpendicular to the 3 axis acting in the 2 direction), S33 (normal stress on the plane perpendicular to the 3 axis) and plastic equivalent strain after fully unloaded for three models: all ganoine (a), discrete (b) and gradient (c) models for 1-N-maximum-load indentation (Bruet et al. 2008).

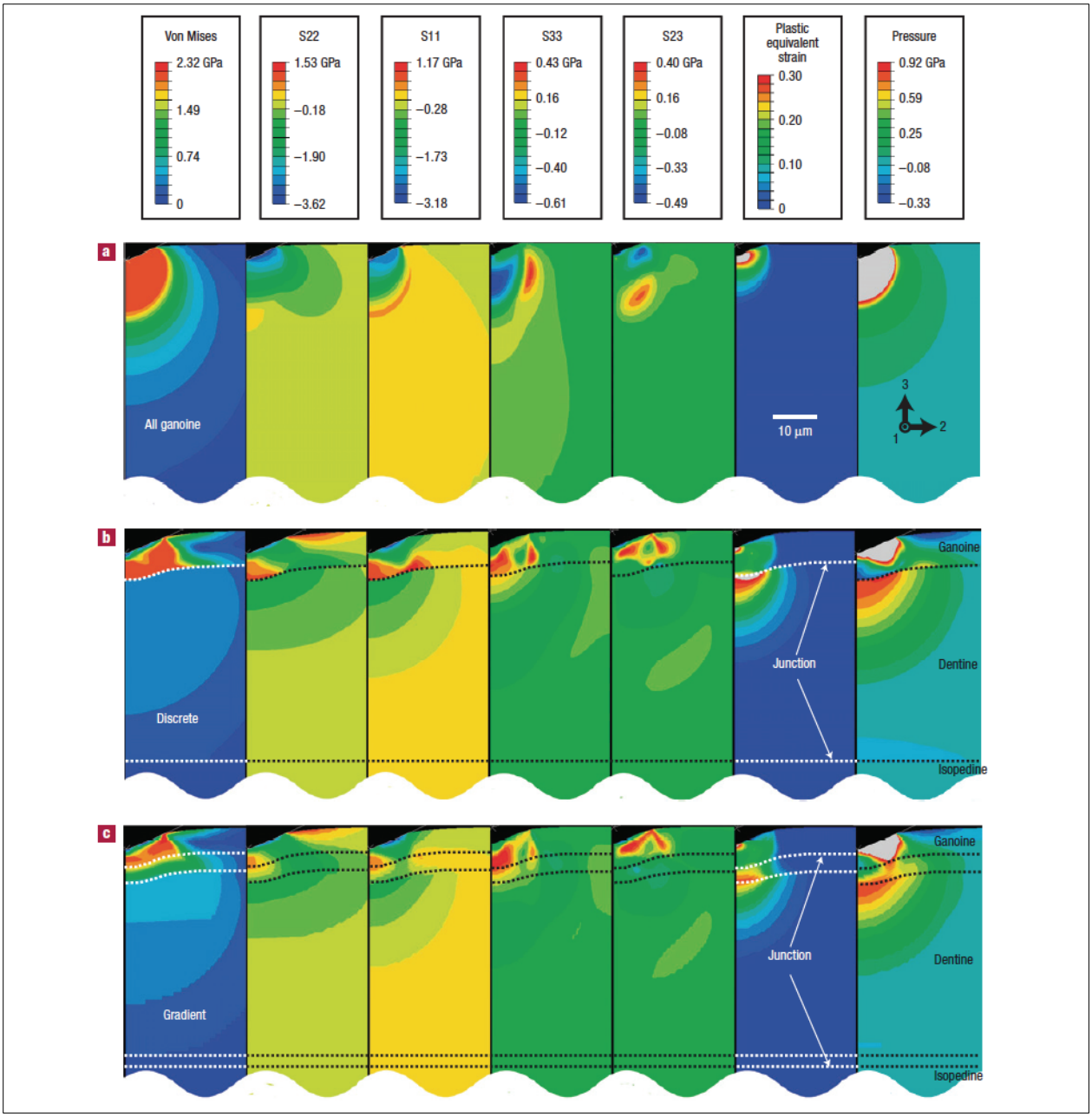

Figure 2.12. Microindentation simulation contours of stress, plastic strain and pressure fields of a gar scale via multilayered FEA simulations. When the indentation force is 10-N. (a) von Mises stress, (b) maximum principal stress, (c) effective plastic strain (Chandler et al. 2014).

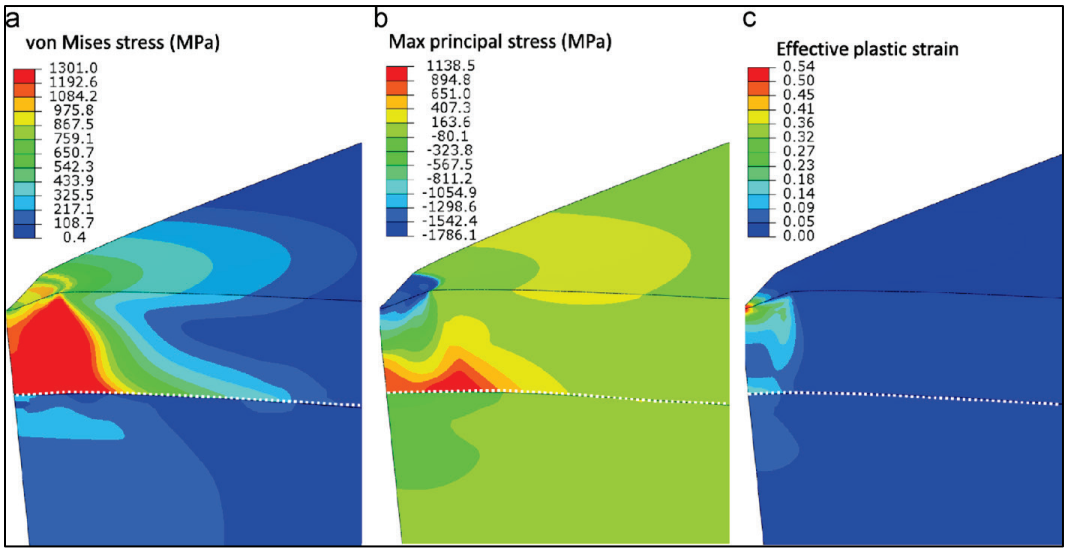

Table 2.2. Example methods for understanding load transfer in highly heterogeneous geological materials used in civil engineered structures (Huang 1993; Yoder and Witczak 1975; Timoshenko and Lessels 1925; Lambe and Whitman 1969; Terzaghi 1943; Das 1990, 1994; AASHTO 1993; UFC 03-260-02 2001; Westergaard 1925).

	Theories	Applications
Design/Analysis Methods		
CBR Pavement Design	• Boussinesq approximation • Layered Elastic	Stress distribution in soils and flexible pavements
AASHTO Pavement Design	• Boussinesq approximation • Layered Elastic • Westergaard analysis	Load transfer and stress distribution in flexible/rigid pavements
Foundation Design	• Terzaghi's	Shear deformation determination near soil surface
Retaining Wall Design	• Rankin • Coulomb's	Lateral/vertical earth pressure determination at soil depths

Table 2.3. Microindentation experimental observations for birchir and gar scales, under different load levels (Chandler et al. 2014).

	Microindentation Loads (N)		
	≈ 0.5	≈2.0	≈10.0
Fish Type			
Birchir	No cracking	Ring cracking at the edge of the indentation imprint	Already damaged
Alligator Gar	No cracking	No cracking	Ring cracking at the inside and outside of indentation imprint, interface cracking at the ganoine–bone junction, vertical cracking in ganoine layer

In manmade systems, one of the most critical aspects when designing composites is to prevent de-bonding/delamination of layers and at inter-facial transition zones (ITZ) of dissimilar materials. The modulus mismatch for the dissimilar materials leads to de-bonding/delamination at the ITZ causing premature shear failure. Therefore, the source of delamination resistance in ganoid fish scales is particularly attractive for additional research.

2.4.2 Role of material hierarchy in fish scale and other biomineralized composites

The formation/growth processes/functions may differ across the wide variety of biomineralized composites (e.g., fish, bone, tooth). Uniquely, the secret to nature's superior performing composite structures appears to be attributed to the materials hierarchy. Many biocomposites are complex structures that have arisen from millions of years of evolution, maintaining relatively simple chemical composition at ambient conditions, while modifying its physical geometrical structure (Bruet 2008). Naturally occurring biomineralized composite structures rely upon their hierarchical structure, rather than different composition, to provide exceptional mechanical properties such as high stiffness, toughness, and crack resistance. Remarkably, stiffness and toughness are examples of mutually exclusive properties for lightweight manufactured materials (Ritchie 2011).

The toughness of the functionalized constituents making up the biocomposite systems is several magnitudes greater than that of the individual component materials. As an example, illustrated in Figure 2.13 is the hierarchical structure of collagen, which scans over different material

length scales, from nano to macro. The macroscopic mechanical material behavior is controlled by the interplay of properties throughout various scales (Buehler 2007). Recent studies have shown that the desirable engineering properties of exceptional flexural stiffness, toughness, and adhesion are readily found in flaw-tolerant biomaterials (Gao et al. 2004).

The exoskeleton of fish scales has a hierarchical biocomposite structure, which is thin, lightweight, and durable. Nature has chemically/geometrically engineered the exoskeleton fish hierarchal structure to include bulk properties of strength and ductility that are several orders of magnitude higher than those found within the discrete structural units of hydrated collagen fibers and hydroxyapatite minerals. Note that the use of these weak constituent materials is a limitation imposed on biological systems by the ambient water temperature and requirement for soluble minerals. Typically, the inorganic phase of hard hydroxyapatite mineral matrix is interfaced with embedded polymer-like, soft organic collagen fibers' reinforcement phase. The discrete molecular units of hydroxyapatite crystals and bundled collagen fibers form a structural unit at the characteristic length scale of approximately one micron (Ochsner and Ahmed 2011; Nudelman et al. 2010). Independently these phases are weak but, when combined in the appropriate volume fractions, they form an extremely high-strength, high-toughness biocomposite system that is also lightweight (Barthelat and Espinosa 2007).

2.4.3 Challenges of measuring chemical composition, structural arrangement, and mechanical attributes within materials hierarchy from experimental laboratory methods

Recently, researchers have set forth the goal to analyze/design/prototype composite structures that have been inspired by nature (Bruet et al. 2008; Song et al. 2010). Nature has used self-assembly to meticulously form its complex structure (Chung et al. 2011; Sarikaya et al. 1999). The limited constituent's nature uses in the formation of robust hierarchical structures is one of the features of nature that has gained researchers' attention. To be able to meet the researchers' goals, the biocomposite system must first be reverse engineered. Reverse engineering can help with the understanding of how, what are the inherent chemical, morphological, and mechanical attributes that can lead to such enhanced performance and multi-functionality.

Figure 2.13. Overview of hierarchical structure of collagen, which scans over different material length, scales, from nano to macro (Buehler 2007).

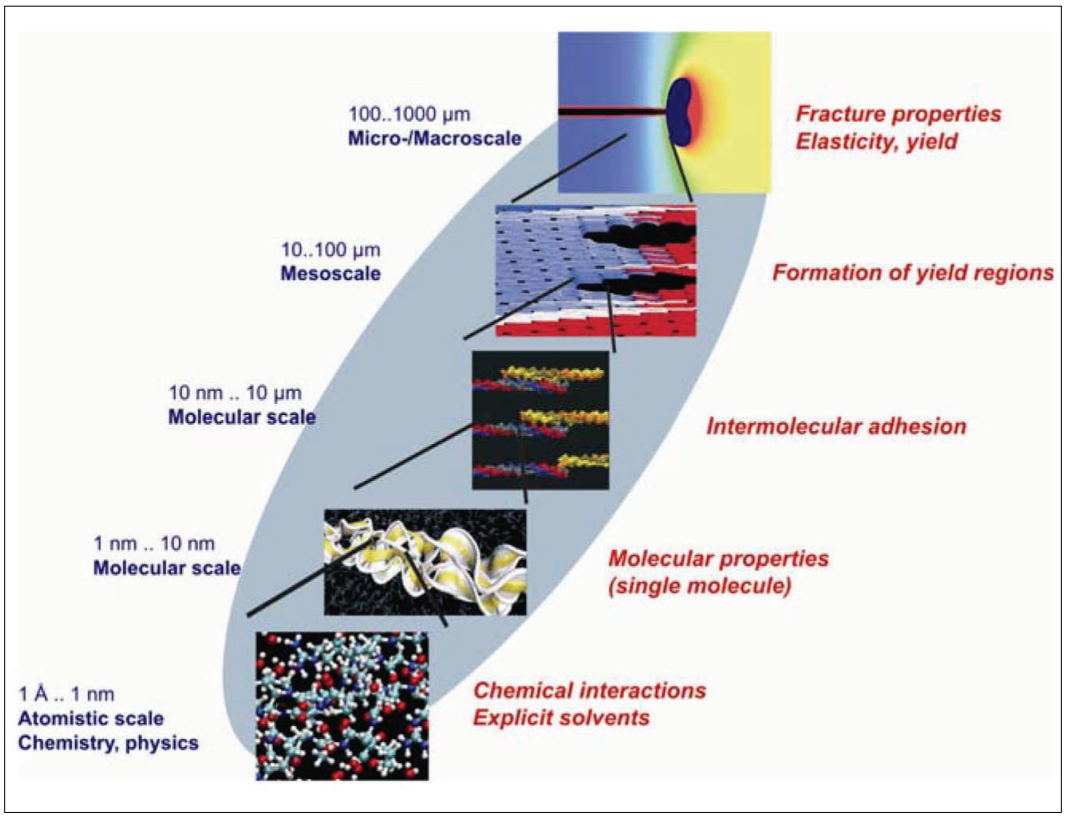

However, using laboratory experimental methods to probe the material hierarchy of biomineralized composites is challenging. The challenges are due to three aspects of multi-scale investigation. Firstly, even though researchers understand that several hierarchical levels exist in the composite material, it is not obvious how the structure spans across many orders of magnitude of spatial scales (Aizenberg et al. 2005). Secondly, by not knowing how many hierarchical levels exist, determining which experimental methods are appropriate is difficult. What is clear is no single experiment will sufficiently elucidate the attributes for the materials' multi-length scale mixing, integration, and variation (Bauerlein et al. 2007). Lastly, because the soft and hard materials at each length scale in biomineralized composites exhibit gradual variation in material properties, the researcher is challenged with developing a robust experimental plan that may better aid in identifying the subtle attributes for relevant mechanisms observed at each length scale and across scales (Beniash 2011).

2.5 Biological composite materials summary

Biological materials are well-organized and exhibit superior property characteristics of lightweight, high strength, high toughness, and energy absorbency. Nature does not design structures. Rather, it adapts to achieve niche functionality using whatever materials are indigenous to the geographical location. The functionality is what dictates the formation of the structure. Biological organisms adapt to environmental changes by enhancing their functionality. Biomineralized composites have exhibited superior performance under extreme conditions. Examples of superior-performing advanced mineralized biological composites are bone, teeth, and exoskeleton fish scales. The characterization, interpretation of processes, and functionality of the more complex biomineralized systems such as nacre, bone, and tooth is difficult. The composites are advanced, because of hierarchical ordering, grading of properties, and multifunctionality. However, researchers are having difficulty explaining what the attributes are that lead to superior performance. By investigating less complex ganoid exoskeleton fish scale, there is a greater chance for designers to use "biomimicry" or "bioinspiration" for synthesizing, designing, and manufacturing superior performing advanced composites.

2.6 Overall state-of-knowledge summary

Advanced engineered composites have been successfully used in several applications with a wide range of materials. However, there are several limitations in the design and manufacturing of advanced engineered composites. Advanced composites are susceptible to delamination. In particular, designers are in need of multifunctional composite materials that can readily meet a variety of in-service requirements (e.g., mechanical, sensing, or repairing). Because of the impending need, designers are probing nature for solutions. By investigating the superior-performing, less complex fish scale, insights may be gained on how to best meet the engineer's needs.

The literature review has shown extensive research efforts have been performed to characterize fish scale. From literature it was found each layer, at the micron scale, has subtle variations in the placement of the hard and soft materials. The fish scale is made up of 90 percent hard (inorganic minerals) and 10 percent soft (polymer-like organic collagen fibers) by volume. However, knowledge is lacking on how nature integrates hard and soft materials at each length scale to form a layered composite that is

lightweight and has high strength with good fracture toughness but does not delaminate. Additionally, knowledge gaps exist because past researchers were limited: (a) equipment technology was not available adding to the difficulty in quantifying descriptions, isolating mechanisms and leading to interpretations of results being based on idealized cartoon illustrations, (b) no characterization standard protocol exists for probing the multiscale and the experimental methods used to operate at different wavelengths of energy and different physical principles, leading to difficulty obtaining coherent descriptions at given length scales from disparate data sets, and (c) the researcher did not anticipate the experimental results would be used to build, calibrate, and validate computational models, which led to some of the subtle details of the fish scale being overlooked. Therefore, more comprehensive investigations are needed to understand how nature incorporates similar hard and soft materials that have been optimized so that a layered delamination-resistant composite system may be produced.

The following Chapter 3 describes the details of experimental techniques employed in this current research effort. Also provided in the next chapter is a discussion as to what criteria were used to select the experimental methods. The selected methods are thought to provide the best opportunity for obtaining the type, variation and integration of materials, and mechanical properties that best describe the gar fish scale inherent qualities.

3 Experimental Design Methodology

3.1 Formulation of hypothesis (*H*)

The rationale for the experimental program is tied to the problems associated with testing the hypothesis. The difficulty with any hypothesis is that it is stated sufficiently precisely so that its nullification is possible through experiment (Wheeler and Ganji 2001). Accordingly, the hypothesis will be reviewed in some detail before describing the experimental program.

The hypothesis *(H)* is the fish scales are effective in resisting cracks, dissipating energy, and transferring loads across interfaces because of the grading of the composite layer properties. The purpose of *H* is to test if there is a significant difference in the material above, below, or between layers. In addition to using the experimental program to test *H*, the program must verify the following: (a) interfaces exists and (b) the layers are graded.

3.2 Purpose of experiments for testing hypothesis (*H*)

When deriving basic questions from a reverse engineering approach to ascertain the fish-scale characteristics, the questions should lead to the selection of experiments that can be used to provide evidence and test *H*. Moreover, the overarching purpose of the experiments is to answer the following fundamental questions:

1. How are natural nano-composite systems assembled?
2. How do the layer thickness and the functionalized gradient properties interact to achieve high toughness?
3. What are the design principles of natural armor systems?
4. How can these design principles be applied to the design of manmade engineered composite systems?

3.3 Questions developed from hypothesis (*H*)

A reverse engineering approach is used to test the hypothesis that fish scales are effective in resisting cracks, dissipating energy, and transferring loads across interfaces because of the grading of the composite layer properties. By using a reverse engineering approach, scientific questions can be developed that may be answered with experimental evidence and test *H*. If

the primary scientific questions are developed sufficiently, secondary questions will often arise. When both the primary and secondary scientific questions can be answered with experimental evidence sufficiently, the information can be used to develop scientific theories.

Scientific theories use many observations and have volumes of experimental evidence that can be applied to unrelated facts and new relationships. Also, theories are flexible enough to be modified if new data/evidence is introduced. Furthermore, if sufficient evidence has been gathered to develop theories, researchers can begin asking tertiary questions such as: (a) are the results repeatable, (b) are the results equipment-operator dependent, or (c) are the results predictable? Meaning they follow directly from primary and secondary results. If the tertiary questions can be answered with sufficient experimental evidence, scientific laws can be established. In this current investigation the primary, secondary, scientific, and ancillary questions that have been formed from *H* are as follows:

3.3.1 Primary scientific questions

1. The primary question is determining how the chemical and morphological nature of the layering and thickness of the interface may affect the mechanical response?
2. What is the chemical composition?
3. What is the structure?
4. Does the structure have layers?
5. Are structural layers identifiable; if so, how many?
6. Are the structural layers graded?
7. To what extent can mechanical measurements, chemical composition, and structural morphological measurements be used to understand load transfer across layered interfaces and energy dissipation throughout the layers?

3.3.2 Secondary scientific questions

1. If the structural layers are graded, to what extent?
2. Is the observed morphology the reason for the graded properties in the fish scale?
3. Is the measured chemical composition the reason for the graded properties in the fish scale?
4. Is the chemical composition and morphology interrelated; if so, to what extent?

5. Is the fish scale composite system's chemical composition and morphological hierarchically arranged?
6. If there is a hierarchal arrangement, to what extent are the mechanisms observable/measurable?
7. Does the hierarchal arrangement lead to the development of the graded structure?
8. What role does the hierarchal arrangement have in mechanical measurements, to what extent?

3.3.3 Ancillary questions

1. Are there routine analytical and experimental approaches that have been used in the past that are relevant to the questions asked; if so, can they readily be applied in this research effort?
2. What are the attributes and limitations for the known analytical and experimental approaches?
3. Are there alternative analytical and experimentally viable approaches if routine methods are not available?
4. Is there reasonable information found in literature that can be used to compare the measured results and/or can help fill identified knowledge gaps?
5. Does the design of experiments (DOE) provide sufficient overlap between analytical and experimental methods for supplemental comparison of the measured phenomena/mechanisms?
6. What is a reasonable data collection plan that provides sufficient information?
7. Does the DOE and data collection plan provide sufficient evidence to test H?
8. In addition to testing H, does the DOE provide contingencies for further investigation of new discoveries that have been deemed necessary to address critical knowledge gaps?
9. What is the return-on-investment (ROI) for conducting additional experiments? Are the additional experiments cost effective? Will the additional efforts advance the community of practice for experimentation and specimen preparation? Are the additional experiments critical for advancing the body of knowledge in biomaterials, biomimicry/bioinspired design, and manufacturing?

3.4 Selection of experiments for testing hypothesis (*H*)

3.4.1 Criteria for selecting experimental methods

Ideally, when selecting experimental methods for biological characterization, consideration should be given on how to best mimic in situ conditions that can allow the specimen to remain in a pristine, undamaged, and unaltered state. Often, the specimens are unavoidably damaged during preparation for experimentation. Thus, verification methods must be incorporated in experimental program that can help determine sources of uncertainty in the specimen, preparation, experimental equipment, and forensic analysis technique.

The following considerations were used in developing the criteria for selecting experimental methods: (a) What is thought to be known about the fish scale? (b) Which methods have been used previously to investigate fish scales or other similar biomineralized materials along with their attributes? (c) Which methods can be used to identify the fish scale's hierarchal structure? (d) Which methods can be used to speciate the fish scale biochemistry? (e) Which methods provide bulk versus local measurements? (f) Which methods provide overlap and can be used to confirm other methods?

1. Recall, as discussed in Chapter 2, knowledge of the fish scale formation processes is limited. However, past researchers have reported the sub-units of the fish scale are made up of apatite crystals and collagen fibers (Chen et al. 2011; Yang et al. 2012; Allison et al. 2013; Yang et al. 2013a, Yang et al. 2013b). In addition, since the sub-units are derived from soluble geological minerals, then there is a likelihood the minerals themselves have a known structural class in terms of crystallographic diffraction, thermal gravimetric signature, x-ray, and electron patterns (Yang et al. 2013b). Furthermore, previous research has shown the biomineralized scales to exhibit property grading with very little change in composition so the sub-units may also have identifiable packing arrangements, grain shape, grain size distributions, and unique grain orientations at interfaces throughout the hierarchal levels (Chen et al. 2011; Allison et al. 2013; Yang et al. 2013a; Yang et al. 2013b).
2. (2.-6.) Table 3.1 lists 28 experimental characterization methods that have been commonly used to investigate the structural, chemical, and mechanical attributes of fish scales or other similar biomineralized

materials (Lee et al. 2011; Torres et al. 2008; Tai et al. 2005; Bruet et al. 2008; Yang et al. 2013b; Garrano et al. 2012; Landis 1995; Ikoma et al. 2003; Lin et al. 2011; Song et al. 2010; Chang and Chen 2013; Liu et al. 2008; Cuy et al. 2002; Waite and Broomell 2012; Bozec et al. 2005; Zhang et al. 2008; Klosowski et al. 2015; McNally et al. 2013; Rho and Pharr 1999; Bertassoni and Swain 2012; and Rodriguez-Florez et al. 2013). Furthermore, Table 3.1 provides a systematic means to critically evaluate experimental methods that may be useful in interpreting the structural, chemical, and mechanical processes when descending the hierarchical scales of highly complex heterogeneous composite materials.

Below are the critical aspects the experimental methods should address:

1. Structural Determination Considerations

- Usually microscopy techniques are used to elucidate physical features of materials. The methods should be able to provide details regarding the geometry in terms of weight, density distribution, feature size, orientation, surface texture, pores, pore connectivity, position, and assemblage junction points. The following methods that have been successfully used to identify the physical features of materials are: (1) unaided eye observation in visible light, (2) micro x-ray computed tomography (μm-XCT), (3) optical microscopy, (4) high magnification scanning electron microscopy (HR-SEM), (5) transmission electron microscopy (TEM), (6) scanning transmission electron microscopy-high angle annular dark field (STEM-HAADF), (7) atomic force microscopy (AFM), (8) surface profilometry, (9) mercury porosimetry, and (10) water absorption and desorption.
- Spectroscopy methods use analytic techniques to measure diffraction patterns or spectral wavelength scattering/absorption of materials. The measures are then compared to known standards and used for identifying the structural materials class. The following methods that have been successfully used to identify the structural patterns and spectral features of materials are: (1) microcomputed synchrotron x-ray diffraction (μm-XRD), (2) microcomputed synchrotron x-ray absorption near edge structure (μm-XANES), (3) fourier transform infrared spectroscopy (FTIR), (4) raman spectroscopy, (5) thermal gravimetric analysis (TGA), and (6) solid-state nuclear magnetic resonance (SS-NMR).

Table 3.1. DOE—Methods used for characterizing fish scale, bone, tooth, and other biomineralized composites.

Hierarchal Length Scale Measurable Range [>1] mm												
Characterization												
	Purpose						Phases			Measurement Type		
	Structural		Chemical		Mechanical							
Method	Class Deter	Family Speciat.	Class Deter.	Family Speciat.	Class Deter.	Family Speciat.	Cryst.	Prot.	Cryst. + Prot.	Global	Local	Reference
Unaided Eye Observation in Visible Light	No	No	No	No	No	No	No	No	No	Yes	No	N/A
Water Absorption and Desorption[1]	No	No	No	No	No	No	No	No	Yes	Yes	No	(Torres et al. 2008)
Drop Tower Impact	No	No	No	No	No	No	No	No	No	Yes	No	(Lee et al. 2011)
Uniaxial Compress	No	No	No	No	No	No	No	No	No	Yes	No	(Yang et al. 2013b)
Uniaxial Tension	No	No	No	No	No	No	No	No	No	Yes	No	(Garrano et al. 2012)
Hierarchal Length Scale Measurable Range [0.001-1] mm												
µm-XCT[2]	No	No	No	No	No	No	Yes	Yes	Yes	Yes	Yes	(Yang et al. 2013b)
FTIR	Yes	No	Yes	No	No	No	Yes	Yes	Yes	No	Yes	(Song et al. 2010)
Optical Microscopy[3]	No	No	No	No	No	No	No	No	No	Yes	Yes	(Song et al. 2010)
EMPA	Yes	No	Yes	No	No	No	Yes	No	No	No	Yes	(Cuy et al. 2002)
µm-XEDS	Yes	No	Yes	No	No	No	Yes	No	No	No	Yes	(Lin et al. 2011)
µm-XRD	Yes	No	Yes	No	No	No	Yes	No	No	Yes	No	(Song et al. 2010)
µm-XANES	Yes	Yes	Yes	Yes	No	No	Yes	No	No	Yes	Yes	(Waite and Broomell 2012)
µm-XRF	Yes	No	Yes	No	No	No	Yes	No	No	Yes	Yes	(Waite and Broomell 2012)
TGA[4]	Yes	No	Yes	No	No	No	Yes	No	No	Yes	No	(Liu et al. 2008)
HR-SEM[2]	No	No	No	No	No	No	Yes	Yes	Yes	Yes	Yes	(Yang et al. 2013b)

Characterization												
	Purpose						Phases			Measurement Type		
	Structural		Chemical		Mechanical							
Method	Class Deter	Family Speciat.	Class Deter.	Family Speciat.	Class Deter.	Family Speciat.	Cryst.	Prot.	Cryst. + Prot.	Global	Local	Reference
Vickers Microindentation	No	No	No	No	No	No	No	No	No	Yes	No	(Bruet 2008)
Surface Profilometry[5]	No	No	No	No	No	No	No	No	No	No	Yes	(Song et al. 2010)
Mercury Porosimetry[6]	No	No	No	No	No	No	No	No	No	Yes	Yes	(Song et al. 2010)
SS-NMR	Yes	Yes	Yes	Yes	No	No	Yes	Yes	Yes	Yes	No	(Waite and Broomell 2012)
Raman Spectroscopy	Yes	Yes	Yes	Yes	No	No	Yes	Yes	Yes	No	Yes	(Waite and Broomell 2012)
µm-Uniaxial Comp.	No	No	No	No	No	No	No	No	Yes	No	Yes	(Zhang et al. 2008)
Hierarchal Length Scale Measurable Range [0.3-1] µm												
HR-SEM[2]	No	No	No	No	No	No	Yes	Yes	Yes	Yes	Yes	(Bruet 2008)
TEM[3]	No	No	No	No	No	No	Yes	Yes	Yes	Yes	Yes	(Garrano et al. 2012)
Hierarchal Length Scale Measurable Range [1-300] nm												
Nanoindentation	No	No	No	No	No	No	No	No	Yes	No	Yes	(Bruet 2008)
Atomic Force Microscopy[3]	No	No	No	No	No	No	Yes	Yes	Yes	No	Yes	(Bozec et al. 2005)
TEM[2]	No	No	No	No	No	No	Yes	Yes	Yes	Yes	Yes	(Garrano et al. 2012)
STEM- HAADF[7]	No	No	No	No	No	No	Yes	Yes	Yes	No	Yes	(McNally et al. 2013)
STEM-EELS[7]	No	No	No	No	No	No	Yes	Yes	Yes	No	Yes	(Klosowski et al. 2015)

[1]Measure permeability of bulk structure.
[2]Provides structural arrangement of surface and internal structure.
[3]Provides structural arrangement and texture of structure surface.
[4]Provides structural and chemical content.
[5]Provides structural surface texture only.
[6]Provides mapping of pore structure in bulk system.
[7]Provides high-magnification view of structural orientation of crystal and proteins.

2. Chemical Determination Considerations

- Typically analytical spectroscopy techniques are used to discern elemental composition of materials. The spectroscopy methods should be capable of identifying between minerals/metals elemental composition. In addition, the experimental methods should be able to spatially resolve, using either stand-alone spectroscopy methods or can be coupled with microscopy techniques to map the elemental distribution. The following methods that have been successfully used to identify the chemical/elemental composition of materials are: (1) microcomputed x-ray energy-dispersive spectroscopy (μm-XEDS), (2) electron microprobe analyzer (EMPA), (3) microcomputed synchrotron x-ray fluorescence (μm-XRF), and (4) scanning transmission electron microscopy- Electron Energy Loss Spectroscopy (STEM-EELS).
- The experimental methods should also be capable of deciphering between inorganics/organics, classify/speciate family and classes of chemical compounds and molecules. The following methods provide overlap/confirmation and can be used to determine structural characteristics and also speciate the compounds and molecules in the system: (1) microcomputed synchrotron x-ray diffraction (μm-XRD), (2) microcomputed synchrotron x-ray absorption near edge structure (μm-XANES), (3) fourier transform infrared spectroscopy (FTIR), (4) raman spectroscopy, (5) thermal gravimetric analysis (TGA), (6) solid-state nuclear magnetic resonance (SS-NMR).

3. Mechanical Property Determination Considerations

- Experimental mechanical methods should be capable of providing a profile analysis of strength, toughness, and hardness that is representative of the structural composition. The methods should consider the effects of bulk irregular geometrical shape, local property grading, and antistrophic structural reinforcement. The following mechanical methods have been used to measure materials response, when externally loaded: (1) Vickers microindentation, (2) micropillar uniaxial compression (μm-UC), and (3) nanoindentation.
- In addition, the experimental measures should provide the means for spatially correlated spectroscopy and microscopy methods that help resolve the structural characteristics and chemical composition. The following mechanical method that has been successfully used to map

mechanical response to structural characteristics and chemical composition is nanoindentation.
- Experimental mechanical methods should also consider measurements that can lead to the design and manufacturing of materials. Often the mechanical experiments that consider both analysis and design for manufacturing purposes provides an index for the average measured bulk response. Useful mechanical measurement techniques are: (1) drop tower impact (DTI), (2) uniaxial compression (UC), and (3) uniaxial tension (UT).

3.4.2 Down selection of experimental methods for testing hypothesis (H)

The previous section outlined the criteria for selecting experimental methods for meeting the requirements for testing *H*. The selection criteria were applied to Table 3.1. Upon applying the criteria, some of the experimental characterization methods were reclassified as contingent supplemental methods while others were completely removed from the DOE plan.

Experimental methods that have been either designated as contingent supplemental methods or eliminated from the DOE plan are provided below.

1. Raman spectroscopy has been designated as contingent supplemental structural/chemical speciation methods. Raman spectroscopy or data sets of similar structural and chemical characteristics will be employed only if FTIR cannot adequately identify the constituents in the fish scale.
2. The following mechanical characterization methods eliminated from the DOE plan were: DTI, UC, μm-UC, and UT. The methods were eliminated because they will provide only an indexed average of bulk mechanical response. Furthermore, sample preparation would require removal of materials to meet the appropriate geometrical aspect ratio standards. Altering the inherent geometry of the specimen will provide mechanical results that would not be representative of the fish scale and negates the beneficial attributes gained from the composite structure.

Also eliminated from the DOE plan was the Vickers microindentation. Since the specimen has a non-uniform thickness, applying uniform external loading is not possible without major modification to the experimental

specimen mounting procedure. Along with procedure modification, finite element analysis (FEA) will need to be conducted to understand the non-linear mechanical response caused by the non-uniform loading distribution. Moreover, to effectively obtain useful information from FEA the exact specimen geometry, material property identification/distribution, indenter geometry, and appropriate material model selected must be known while simultaneously accounting for the numerical instabilities/ inaccuracies due to mesh development.

Additionally considered, when conducting forensic analysis for post-failure mechanism identification, there is not a reasonable method to section the specimen without causing further damage. Consequently, sectioning the specimen for the forensic investigation will more than likely mask the damage caused by external loading. Thus, the mechanical characterization methods that were eliminated from the DOE plan are less likely to provide sufficient information of how the structural arrangement and chemical composition affect the mechanical response or insight to what is attributing to the fish-scale delamination resistance.

3. The remaining experimental methods removed from the DOE plan were surface profilometry, AFM, mercury porosimetry, water absorption, and desorption measurements. Additionally, eliminated from the DOE were the topographical measurements obtained from surface profilometry and AFM, which are redundant measurements that can be obtained from HR-SEM and TEM. Unlike HR-SEM and TEM, surface profilometry and AFM cannot be readily coupled to other characterization methods used for structural/chemical class identification and family speciation.

In regard to water absorption/desorption methods, they will provide information only for bulk density. The measurements cannot quantify solid and pore volume fractions nor provide information regarding the pore geometry and size distribution for the structure. Unlike the water absorption/desorption characterization technique, mercury porosimetry measurements do well in spatially resolving pore geometry and pore size distribution for surface pores. Surface pores are voids that occur on the external face of the structure, have limited penetration depth, but do not proliferate through the entire structure. Unfortunately, the mercury porosimetry method lacks the capability to identify internal pores and pore connectivity. Pore connectivity identification is used to quantify the

permeability of the structure. If surface pores, internal pores, and/or connected pores are present in the structure neither pore measurement methods can adequately describe the functional role they play in transporting fluids for growth, energy dissipation, structural and mechanical property grading in the biomineralized fish scale composite.

3.5 Relevance of selected experimental methods for characterizing materials hierarchies

The remaining experiments are thought to be the best suited for testing *H*. Additionally, when combined, the remaining methods can be used to provide information at descending levels of the fish scale's hierarchy. The selection of experimental methods to ascertain what's structurally, chemically, and mechanically relevant for the discovery/identification of mechanisms necessary for hypothesis testing is forever challenging. Still problematic will be the interpretation of results obtained from the physical measurements. To reduce the variability in data interpretation, the experiments were conducted in dry state. As shown in Figure 3.1, an illustration I developed shows when descending hierarchical length scales from high to low of highly complex heterogeneous composite materials, the uncertainty of results increases. The uncertainty is attributed to increasing unknown variables affecting measurements of chemical, structural, and mechanical process. Therefore, the interpretation of results from individual experiments can become very subjective. The selected experiments have been combined in such a way that they can provide empirical evidence and for the most part eliminate subjectivity. Empirical evidence will lead to conclusions that are objectively determined.

3.6 Description of experimental methods used for testing hypothesis (*H*)

The experimental methods commissioned by this research provide a systematic top-down approach, which can be used to probe the length scales. Most of the techniques are either based on visible light, infrared, electron, or x-ray diffraction/absorbance. As shown in Figure 3.2, when the electromagnetic spectral wavelength decreases, the wavelength's signal frequency increases (The Electromagnetic Spectrum 2015). The increase in signal frequency increases heat generation (Callister and Rethwisch 2008; Kim 2013; Coates 2000; Gunther 2013; Willmott 2011; Leng 2008; Williams and Carter 2009; Henderson et al. 2014).

Figure 3.1. Illustration of increasing uncertainty due to increasing unknown variables affecting measurements of chemical, structural and mechanical process when descending hierarchical scales of highly complex heterogeneous composite materials.

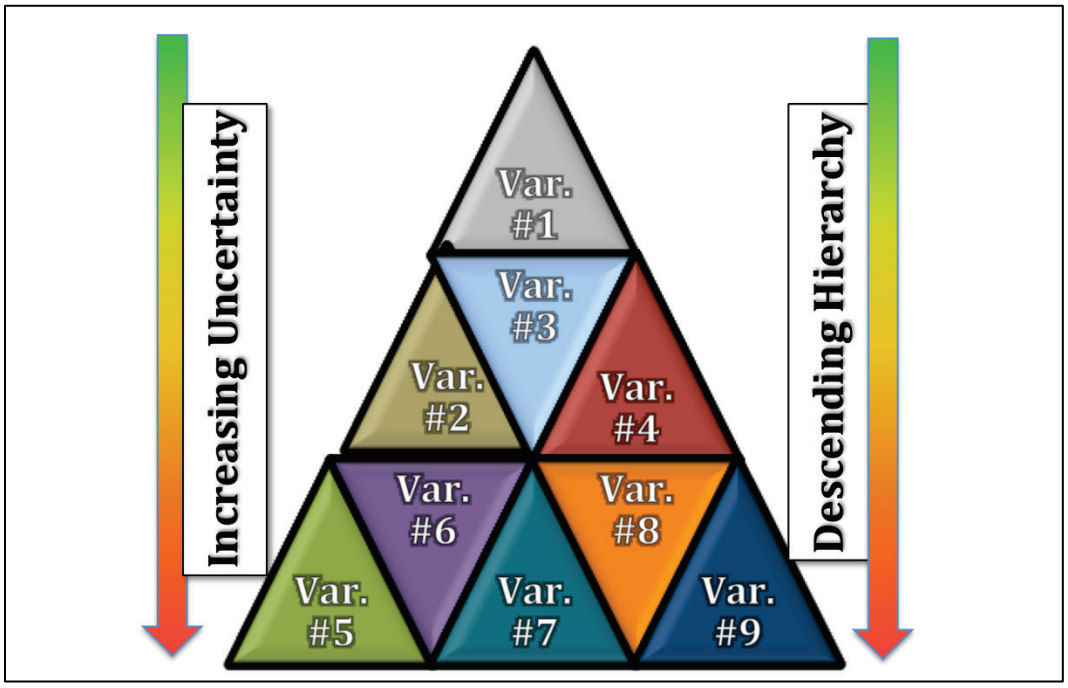

Figure 3.2. Illustration of electromagnetic spectral wavelength ranges (The Electromagnetic Spectrum 2015).

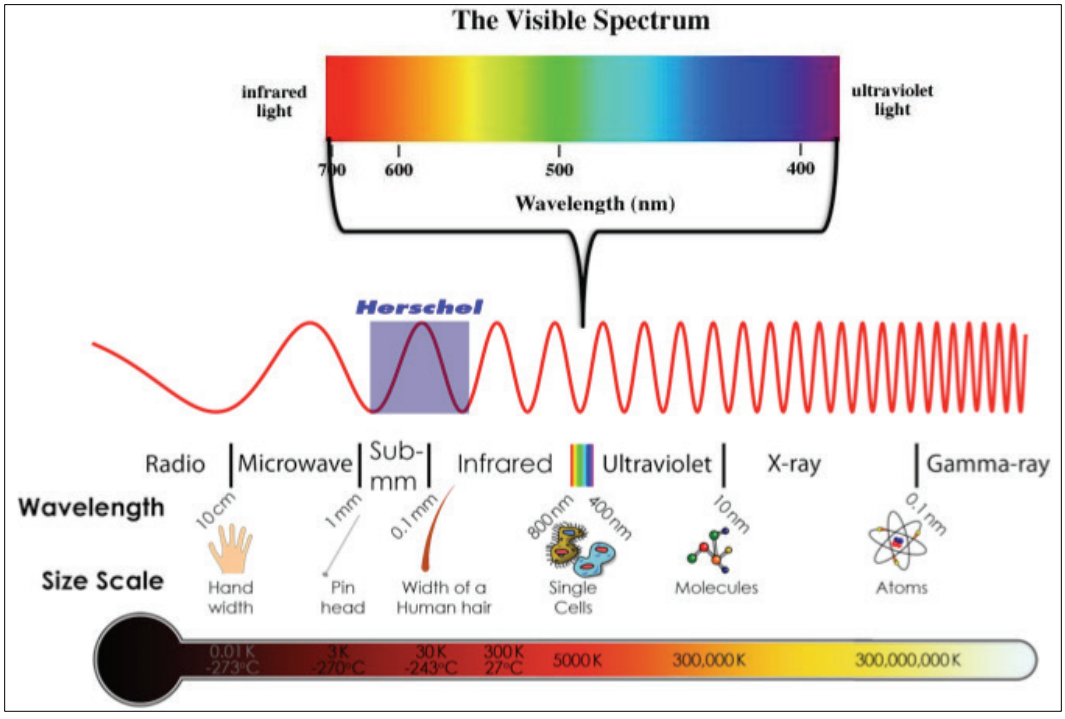

As a result, careful/detailed specimen preparation methods are used to minimize heat damage caused by x-rays and electrons, such as mineral recrystallization and excessive cracking due to drying (Kim 2013; Coates 2000; Gunther 2013; Willmott 2011; Leng 2008; Williams and Carter 2009; Henderson et al. 2014). Furthermore, careful specimen preparation helps minimize the variables when making observations along the various length scales. Provided below is a summary description of methods and sample preparation techniques.

3.7 Summary of experimental methods

3.7.1 Unaided eye observations (measurements taken at length scale [>1] mm)

Unaided eye observations can provide a sense of the specimen's size, shape, and texture. Specimens are viewed in visible light without the aid of a microscope. The eye observations are useful for deciding which length scale-based experimental measurements and required specimen preparation techniques may be useful for characterizing the fish scale.

3.7.2 Nanoindentation (measurements taken at length scale [1-1000] nm)

Nanoindentation is a mechanical characterization method that can be used to measure the near-surface local average elastic modulus and hardness of biological materials (Oyen 2011; Cuy et al. 2002; Waite and Broomell 2012; Balooch et al. 2004; Rho and Pharr 1999; Tai et al. 2005; Pharr et al. 2009; Pharr et al. 2010; Rho et al. 2002). Nanoindentation is used to map the mechanical properties across the fish scale and observe the evolution of mechanical properties across the interface. The experimental protocol uses dynamic indentation during the test to characterize the evolution of mechanical properties as the indenter tip penetrates into the surface of the sample; the indentation technique is further described in Oliver and Pharr's pioneering work (Oliver and Pharr 1992; Oliver and Pharr 2004).

3.7.3 Thermo-gravimetric analysis (TGA) (measurements taken at length scale [N/A])

Thermo-gravimetric analysis (TGA) uses heat to force reactions and physical changes in materials. The experimental method provides quantitative measurement of mass change in materials associated with transition and thermal degradation. The measurements allow rapid and

precise determination of weight losses due to moisture or loss of crystal water. TGA records change in mass from dehydration, decomposition, and oxidation of a sample with time and temperature. Characteristic thermogravimetric curves are given for specific materials and chemical compounds due to unique sequence from physicochemical reactions occurring over specific temperature ranges and heating rates (Leng 2008).

3.7.4 Optical microscopy (measurements taken at length scale [1-1000] µm)

The optical microscope uses visible light and a system of lenses to magnify images of small samples. Since microscope optics are static, different magnification objective lens are used to focus at different focal depths. In addition, visible light-sensitive cameras are usually used to capture the image from the optical microscope; however, the image's resolution is limited to the wavelength of visible light (Leng 2008).

3.7.5 Solid-state nuclear magnetic resonance (SS-NMR) spectroscopy (measurements taken at length scale [1-1000] µm)

The Solid-State Nuclear Magnetic Resonance (SS-NMR) spectroscopy method can be used to identify/speciate the organic chemical-structural phases in fish scales. SS-NMR spectroscopy is used to determine the resonance frequency that causes the nuclear spin state in solid media. In solid media with little or no mobility (e.g., crystals, powders, large membrane vesicles, molecular aggregates), anisotropic interactions have a substantial influence on the nuclear spin state. In this context, "nuclear spin" is defined as the magnetic state of the nuclei when the electromagnetic radiation is absorbed and re-emitted. The technique works by inducing the alignment of nuclear spins. Nuclear spin alignment is achieved by placing the specimen in a strong homogenous magnetic field and then exciting the chemical structure's nucleus by using computer-controlled resonance frequency (RF) manipulation (Gunther 2013; Henderson et al. 2014).

3.7.6 Raman spectroscopy (measurements taken at length scale [1-1000] µm)

Raman spectroscopy uses a laser beam to irradiate a spot on the specimen. The scattered radiation produced by the Raman provides information about the molecular vibrational and rotational energies. The energies depend on the particular atoms or ions that comprise the molecule, the chemical bonds

connecting them, the symmetry of their molecule structure, and the physico-chemical environment where they reside. The analytical technique is often used to identify/speciate either mineral or organic phases in materials (Coates 2000; Leng 2008; Henderson et al. 2014).

3.7.7 Fourier transform infrared spectroscopy (FTIR) (measurements taken at length scale [1-1000] µm)

Fourier Transform Infrared Spectroscopy (FTIR), sometimes complementary to Raman spectroscopy, is an analytical technique often used to identify/speciate either mineral or organic phases in materials. It provides information about the chemical bonding and molecular structure. The operating principle for FTIR is based on the fact that bonds and groups of bonds vibrate at characteristic frequencies that are slightly higher than what's typically used in Raman spectroscopy. A molecule that is exposed to infrared rays absorbs infrared energy at frequencies that are characteristic to that molecule. During FTIR analysis, a spot on the specimen is subjected to a modulated IR beam. The specimen's transmittance and reflectance of the infrared rays at different frequencies is translated into an IR absorption plot consisting of reverse peaks. The resulting FTIR spectral pattern is then analyzed and matched with known signatures of identified materials in the FTIR library. The FTIR measurements can be used to identify unknown materials present in a specimen when coupled with EMPA (Cuy et al. 2002; Coates 2000; Leng 2008; Henderson et al. 2014).

3.7.8 High resolution scanning electron microscopy (HR-SEM) (measurements taken at length scale [1-1000] µm)

High Resolution Scanning Electron Microscopy (HR-SEM) uses an electron probe that is scanned across the sample, producing secondary and back-scattered electrons that can be detected and recorded as an image. The penetration depth is generally less than one micron, so the images produced are of the sample surface. The backscattering of electrons increases with increasing atomic number so that imaging with this method can produce images of heavier elements (Leng 2008).

3.7.9 Microcomputed X-ray energy-dispersive spectroscopy (µm-XEDS) (measurements taken at length scale [1-1000] µm)

Microcomputed X-ray Energy-Dispersive Spectroscopy (µm-XEDS) makes use of the X-ray spectrum emitted by a solid sample bombarded with a

focused beam of electrons to obtain a chemical analysis. Mapping is most commonly used to produce 2-D elemental distribution images within a sample. Images are collected from x-ray intensities that are measured by counting photons. Commonly μm-XEDS devices are coupled to either HR-SEM or TEM equipment. Usually, in conjunction with microscopy investigation, μm-XEDS is conducted to measure the individual elements in the material at the micron scale. The individual elemental distribution maps can be used for both quantitative/qualitative assessments if calibrated with material control standards (Nieto and Livi 2013).

3.7.10 Electron microprobe analyzer (EMPA) (measurements taken at length scale [1-1000] μm)

Electron Microprobe Analyzer (EMPA) is an analytical technique often used to identify/speciate elemental constituents. EMPA can provide information to the degree of impurity with respect to chemical composition of single particles. When coupled with TEM, spatial mapping of elements is possible. EMPA can also be used to examine the inorganic/organic interface and determine chemical variation from the micron to nanometer scale (Cuy et al. 2002).

3.7.11 Transmission electron microscopy (TEM) (measurements taken at length scale [1-1000] nm)

Transmission electron microscopy (TEM) is a microscopy technique in which a beam of electrons is transmitted through a thin specimen. Generally a specimen must be thinner than one micron to obtain a useful image. TEM provides information through the thickness of an electron-transparent specimen (Leng 2008; Williams and Carter 2009; Henderson et al. 2014; Nieto and Livi 2013).

3.7.12 Scanning transmission electron microscopy (STEM) (measurements taken at length scale [1-1000] nm)

Scanning transmission electron microscopy (STEM) is a type of TEM. In TEM electron beam is spread to image thin sections. However, for STEM the electron beam is focused into a narrow spot, which is scanned over the specimen in a raster pattern. The rastering of the beam across the sample makes STEM suitable for coupling spectroscopy and microscopy analysis techniques, such as EELS, and HAADF. The EELS and HAADF spectral signals can be obtained simultaneously, allowing direct correlation of

image and quantitative data. When a hi-angle detector is used with STEM, it is possible to form atomic magnification images where the contrast is directly related to the elemental atomic number (z-contrast image). STEM has been used to image biological materials using dark-field microscopy. Dark-field microscopy is used to show high contrast images in heterogeneous biological samples without requiring staining (Leng 2008; Williams and Carter 2009; Henderson et al. 2014; Nieto and Livi 2013).

3.7.13 Electron energy loss spectroscopy (EELS) (measurements taken at length scale [1-1000] nm)

Electron energy loss spectroscopy (EELS) is a technique that provides elemental information on a nanometer scale when coupled with STEM. The energy of the incident electrons is altered as they pass through the sample. These energy loss spectra can be characterized using EELS to provide elemental identification. Because EELS provides improved spatial magnification (down to 1 nm), the energy magnification (<1 eV for EELS) technique is capable of measuring lower atomic number elements (e.g., H, O, Na, Mg, P, Ca). In addition, the low-angle inelastically scattered electrons used in EELS compliments the high-angle scattered electrons in HAADF images by allowing both signals to be acquired simultaneously (Leng 2008; Henderson et al. 2014; Nieto and Livi 2013).

3.7.14 High-angle annular dark-field (HAADF) (measurements taken at length scale [1-1000] nm)

High-Angle Annular Dark-Field (HAADF) is used to show atomic number contrast for high scattering angles of the electrons. The purpose of measurement is to determine local thickness of a specimen. When STEM is combined with both EELS and HAADF, the scattered electrons can be used to discern structural and elemental composition from discrete spectral interfaces at the lowest nanometer scale, such as those measured in hydroxyapatite + collagen boundaries (Leng 2008; Nieto and Livi 2013; Carlino and Grillo 2006).

3.7.15 Micro X-ray computed tomography (μm-XCT) (measurements taken at length scale [1-1000] μm)

Micro X-ray Computed Tomography (μm-XCT) is a nondestructive technique that uses x-ray spectra to visualize the interior of objects. The μm-XCT scans can be used to resolve fine cross-sectional details. The thin

two-dimensional scans are reconstructed using computed tomography, to form three-dimensional volumes. With the μm-XCT, reconstructed volumes can be imaged with a voxel magnification down to micron range (Song et al. 2010; Allison et al. 2013, 2014; Yang et al. 2013b; Chang and Chen 2013).

3.7.16 Synchrotron x-ray methods (μm-XRD/μm-XANES/μm-XRF-CT) (measurements taken at length scale [1-1000] μm)

The next three experimental methods involve the use of x-rays. As opposed to using bench top spectroscopy techniques exclusively, synchrotron x-ray methods were also included. Since Synchrotron uses much stronger energy to produce x-rays, the methods can be used to identify and sufficiently spatially map structural and elemental composition that could not otherwise be obtained from μm-XEDS, and EMPA. Additionally, by combining Synchrotron x-ray with the μm-XEDS and EMPA spectroscopy methods, most of the periodic elements that are common to biomineralized composites may be measured. Thus the differing energy range levels for each complimentary technique provides some overlapping information that can be used for confirmation.

Synchrotron X-rays are electromagnetic radiation that is emitted when charged particles are accelerated radially. Synchrotron radiation is produced when accelerated electrons pass radially through magnetic fields. The radiation has a characteristic polarization and the frequencies generated can range over the entire electromagnetic spectrum. As a result of the wide range electromagnetic spectrum a variety of synchrotron x-ray measurements can be made. The current research used microcomputed x-ray diffraction (μm-XRD), absorption near edge structure (μm-XANES), and florescence (μm-XRF) synchrotron based methods to determine the structural and elemental composition for the fish scale (Willmott 2011; Kennedy et al. 2012).

Synchrotron μm-X-ray Diffraction, μm-XANES, and μm-X-ray Fluorescence Mapping using μm-CT experiments were conducted on Beamlines X2B, X26A and X27A at the National Synchrotron Light Source at Brookhaven National Lab (NSLS) in Upton, NY. X-ray microprobes for the beamlines are designed to provide elemental distribution and speciation information for heterogeneous solid samples. The beamlines are powerful because they couple a number of analytical techniques thus providing

information about complex samples that cannot be achieved using any other tool.

µm-XRF mapping is most commonly used to produce 2-D elemental distribution images within a sample. Images are collected from many angles by rotating the specimen through small, evenly spaced, angular increments between 0 and 180 deg. The number of images needed is proportional to the width of the specimen. These individual 2-D images are then reconstructed into a 3-D image. A magnification of [3~5] microns is achievable. Elemental correlations and changes in sample composition on the micron scale can be monitored using µm-XRF. Once the elemental composition of the sample is determined, µm-XANES and µm-XRD are collected on the same specimen to aid in identifying any major compounds present within the material.

µm-XRD is not element specific and provides information about any crystalline or well-structured compounds within a sample. µm-XRD is excellent at identifying minerals (e.g., carbonates, phosphates, silicates) within a completed matrix on a micron-level scale. The techniques were used to monitor changes in chemical or mineral composition moving across the cross section of the scale (>10 micron step intervals). Because the sections within the fish scale differ in chemical composition, the transition boundary between these sections could be monitored using these tools.

µm-XANES is an element specific technique that provides chemical information about oxidation state and the environment surrounding the element (how and to what it is bound, and how tightly it is bound). µm-XANES was used to identify Ca compounds within the gar scales. Changes in Ca complexion from the outermost layer to the inner boney section of the scale were monitored.

3.8 Summary of sample preparation methods

3.8.1 Animal care guidelines and specimen preservation

Prior to conducting any studies using animals, regardless whether the subjects are living or deceased, permission must be granted by the appropriate wildlife and safety management authority. Permission was obtained by providing written animal care guidelines to the proper authority. The research discussed in this report was conducted at ERDC

under the federal government-approved animal care guidelines listed under #EL-6009-2011-5. The ERDC's approved animal care guidelines encompass the National Institutes of Health (NIH) Guide for Care and Use of Laboratory Animals. The ERDC specimens were immersed in a phosphate-buffered saline (PBS) solution. The PBS solution was used to maintain the fish scale's full hydration state during storage.

3.8.2 Initial sample preparation

The scales were dissected from the middle region of the alligator gar fish and with its epidermis skin layer intact, Figure 3.3. After procurement, scales were further sectioned into individual fish scales. Next, the epidermis soft-tissue layer was removed using a razor blade. The scales were then sonicated in deionized water to remove any remaining soft-tissue particles and mucus. The cleaned scales, shown in Figure 3.3, were then placed in fresh PBS to prevent cross contamination and stored for future specimen preparation and characterization. The details are provided below for methods used to prepare specimen for experimental characterization, unless further explained, in Chapter 4 during data analysis and presentation of experimental results.

3.8.3 Unaided eye observations, optical microscope, and HR-SEM sample preparation

Since the purpose of the unaided eye observations and optical microscope were to provide a sense of the specimen's size, shape, and texture, no further sample preparation was needed after the scales were freshly cleaned.

Figure 3.3. Freshly cleaned scales dissected from middle region of alligator gar fish.

3.8.4 Cross-sectional analysis using optical microscope, nanoindentation and FTIR sample preparation

Individual fish scales were mounted in 38-mm inner diameter molds. The stiff medium optically transparent epoxy, product name EPO-TEK™ 301-2, which consists of a two-component resin and hardener, was used to mount the sample. The samples were allowed to cure in ambient conditions at an average temperature [25±5]°C. The samples were de-molded after they had cured for a minimum of 72 hr. To expose the interior fish scale layer(s) for experimental characterization and to meet the recommended specimen height by equipment vendor a, Buehler Isomet™ 2000 model cut-off precision diamond-bladed saw cut was made across the short axis "A" at near the midline of the sample (Figure 3.4)

Figure 3.4. Cross section of µm-XCT images of alligator gar scale depicting the short-axis "A" transverse section examined in this study by optical microscope, nanoindentation and FTIR techniques (Images courtesy of the U.S. Army's Engineer Research and Development Center [ERDC]-Geotechnical and Structures Laboratory [GSL] located in Vicksburg, MS).

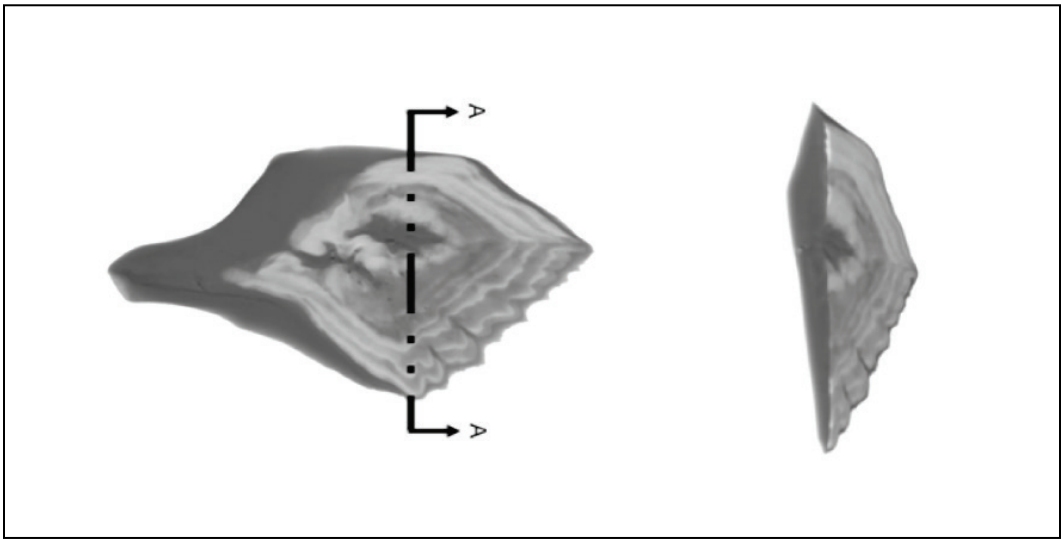

After cutting, the sample was sonicated in water for 15 min to remove any loose fragments and residual traces of cutting lubricant. The specimens were manually polished, with slight modification of the procedure described in textbook reference *Materials Characterization: Introduction to Microscopic and Spectroscopic Methods* by Leng, on a Buehler Handi-met™ I Strip Grinder, sequential from coarse to fine by using #240, 320, 400, and 800-silicon carbide grit paper (Leng 2008). In all grinding steps water was used as the lubricant. Before proceeding to the next smaller size grit, the sample was placed under a microscope to determine if scratches were all unidirectional. Unidirectional scratches were achieved by rotating the specimen clockwise one-quarter turn after every 50 forward hand strokes until four-quarter rotations had been completed. Following the 800-silicon carbide grit polishing, fine polishing using 1- and 0.03-micron Alumina water-based suspensions on a Buehler Ecomett™ II mechanical rotating polisher was conducted. The samples' cross sections were polished until the uniform unidirectional scratch width was less than 3 nanometers. Finally, the specimens were oven-dried at 25 deg Celsius for 24 hr. The samples were dehydrated to ensure consistent measurements were taken.

3.8.5 μm-XCT sample preparation

Specimens were initially cleaned and dried as described above in Section 3.8.2. After cleaning the specimens were mounted to a holder using standard double-sided tape. No further preparation was needed.

3.8.6 Cross-sectional analysis using TEM, STEM, EELS, HAADF, μm-XEDS and EMPA, sample preparation

First follow the same sample preparation methods explained in the "Cross-Sectional Analysis Using Optical Microscope, Nanoindentation and FTIR Techniques" Section 3.8.4, with the exception that the specimens were mounted in a 25-mm inner diameter mold. The purpose for using a smaller specimen is to minimize outgassing effects, caused by the excited electrons heating the epoxy and/or biological materials. Excessive outgassing can cause distortions when electron-based measurements are taken. After the specimens have been oven-dried, the specimens were then ion milled, using a PIPS™ II - Precision Ion Polishing System, at cryo-temperature. Ion milling was used to cut the short-axis "A" transverse slices of whole specimens that are each [~10-nm] uniformly thick. Finally, to minimize ion charging, overheating, and recrystallization, the samples were carbon coated.

3.8.7 FIB sample preparation

Focused ion beam-prepared specimens can provide serial thin x-sections [~10 – 30 nm] for site-specific μm-CT images that can better resolve geometrical features at the surface, near surface. Specimens were initially cleaned and dried as previously described. Since every specimen reacts differently during the local milling, there is no specific guidance for preparing FIB specimens. The suggested practice used was the application of a palladium surface coating to minimize ion charging, overheating, and recrystallization. Also used was a "wedge" sectioning technique (Nalla et al. 2005; Jantou et al. 2009; Grandfield et al. 2010; Grandfield and Engqvist 2012; McNally et al. 2012; Resnikov et al. 2014; Kizilyaprak et al. 2014).

3.8.8 TGA sample preparation

Freshly cleaned scales are oven-dried at 25°C for 24 hr. Wire cutters were then used to cut the whole fish scale into smaller pieces. The smaller pieces were placed into several weigh pans. The weigh pans were filled until each had a minimum weight of 50 mg. The weight average of the

pans was used to determine the overall TGA value. The temperature range used was [35°C to 1550°C] with a heating rate of 10°C/min as recommended by Liao et al. (1999).

3.8.9 SS-NMR spectroscopy sample preparation

Freshly cleaned scales were oven-dried at 25°C for 24 hr. Individual specimens were prepared by using a mortar and pestle to pulverize them into powder form. Approximately 50 mg by weight of powder was then packed into a 4-mm zirconium rotor. For the fish scales, analysis was conducted via solid-state 400-MHz NMR and spun at what is termed the "magic angle" within the magnetic field at speeds ranging from 5 to 12 kHz to eliminate spectral artifacts such as spinning side bands (How To Make A NMR Sample 2015).

3.8.10 Synchrotron x-ray methods (μm-XRD/μm-XANES/μm-XRF-CT) sample preparation

Freshly cleaned scales were oven-dried at 25°C for 24 hr. Synchrotron x-ray analysis samples were prepared by slicing serial thin cut sections from whole intact scales using a diamond-tip knife attached to an ultramicrotome device. The cut sections were each approximately [3 to 5 μm] thick. Each serial section was mounted on separate Mylar™ films.

3.9 Overall experimental design methodology summary

The experimental design methodology was developed to provide a systematic top-down approach, which can be used to probe the length scales. The outcome of the primary questions raised from the hypothesis *(H)* may lead to the development of secondary and ancillary questions as research progresses. The questions will be addressed based on the predefined research scope previously discussed in Chapter 1 and DOE strategy outlined earlier in Chapter 3.

The experimental characterization starts with the largest length scale as knowledge is learned but further questions may be raised. Shown in Figure 3.5 are locations probed and the experimental techniques used to examine the fish scale's hierarchy. As the successive length scales are examined some research questions are answered while others are raised. The process stated above will continue until the lowest measurable length scale has been examined. The individual data sets will be analyzed first

based on the discrete length scales and then assembled. When combining the experiments, they can fill knowledge gaps that may not be possible from individual experiments alone. In addition, some of the experiments provided overlap and serve as confirmation for the others.

Figure 3.5. Locations probed and the experimental techniques used to examine the fish scales hierarchy.

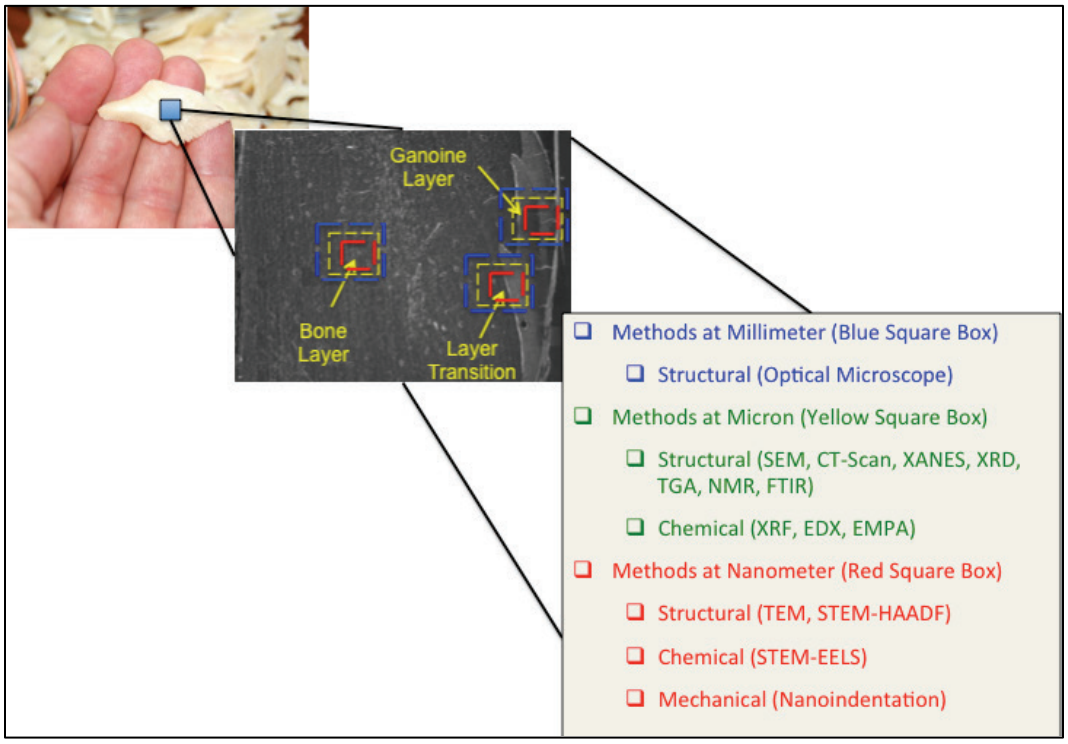

The combined experiments used to characterize each length scales will ultimately lead to the identification of mechanisms. The identification of mechanisms will also lead to new discoveries that inherently describe the attribute that governs the fish scale hierarchy mechanical response as a function of chemical composition and structural arrangement.

After resolving the data relevance the experiments will be used to test the hypothesis *(H)*. If the hypothesis is true, then an appropriate DOE methodology has been established by this overall research effort. In addition to testing *(H)*, the research findings will be used to establish a suggested framework and requirements for incorporating bioinspired design. The attributes of alligator gar's biomineralized exoskeleton fish scales can be used to develop nature-inspired advanced superior performing composite prototypes. Chapters 4 and 5 will present and discuss results to address questions developed from hypothesis *(H)*. Recommendations will also

include pertinent concepts that have been identified because of this research effort. Also provided will be a recommended strategy for manufacturing and prototyping model systems.

4 Results

Presented in Chapter 4 are the experimental results that are used to discuss the questions developed from hypothesis *(H)*. The presentation of results begins with the largest length scale and continues until the lowest measurable length scale has been explained. After the individual results have been discussed, they will be assembled to determine what may be the attribute(s) that govern the fish scale hierarchy mechanical response as a function of chemical composition and structural arrangement.

Where possible, two weight classes for the alligator gar fish were examined. Since the exact ages of the fish could not readily be determined by the ERDC researchers, acquired scales are classified by fish weight. The first set of alligator gar fish scales were procured from one fish that fell in the weight range of 1 to 30 lb. The second set of alligator gar fish scales were procured from one fish that fell in the weight range of 31 to 70 lb. The scales used in this study were obtained from alligator small and medium fish that weighed 2.5 and 38 lb, respectively. Both sets of scales were harvested from the middle region of the fish scale's body as illustrated in Figure 3.3. The purpose for examining two distinct fish weight classes was to infer how the mechanical, structural, and chemical properties evolve as the fish grows.

4.1 Investigation of length scale [>1] mm

Unaided eye observations. The fish scales were first visually inspected using unaided eye observations. Shown in Figure 4.1 are whole small and medium unpolished biomineralized fish scales. From observation the scales have long and short axes. The scales' shape appears to have subtle curvature around its perimeter that converges at the vertices to form sharp points similar to arrowheads. The curved perimeter of the scales is thinner on the edge and overlap when connected to other scales with sharper fibers as previously described in Chapter 2 and shown in Figure 2.6.

The small scale seems to grow more in the long-axis direction. In addition, the small scale looks and feels smooth on top while the bottom side of the scale seems to have a depression containing pits on the surface (Figure 4.2). The bottom side of the scale is nearest the face that is attached to the fish's body. As the small scale grows to the medium size, the top surface appears and feels as if there is a crown forming or a subtle ledge near its center. Yet,

the pitted area remains present as the fish scale grows. The exact purpose and function of the depressed pitted area is not known; however, the depressed region is somewhat concave. One possibility why nature maintains the aspect ratio throughout the growth process for the concave geometry is the scales can form-fit the fish's body shape assisting with insulation and maneuverability through water, similar to a deep-sea diver wearing a wet suit (Bartol et al. 2003). The questions raised from unaided eye observations were (a) what are the fine details of the surface textures when viewed at the next lower length scale, and (b) does the surface texture percolate outward from the scales' internal structure.

Figure 4.1 Whole biomineralized small and medium alligator gar fish scales.

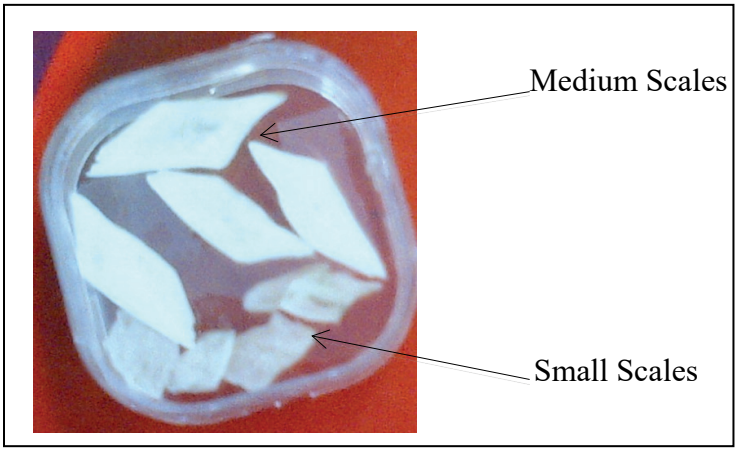

Figure 4.2. Medium size biomineralized fish scale with concave depression containing pits on the bottom side of the alligator gar scale.

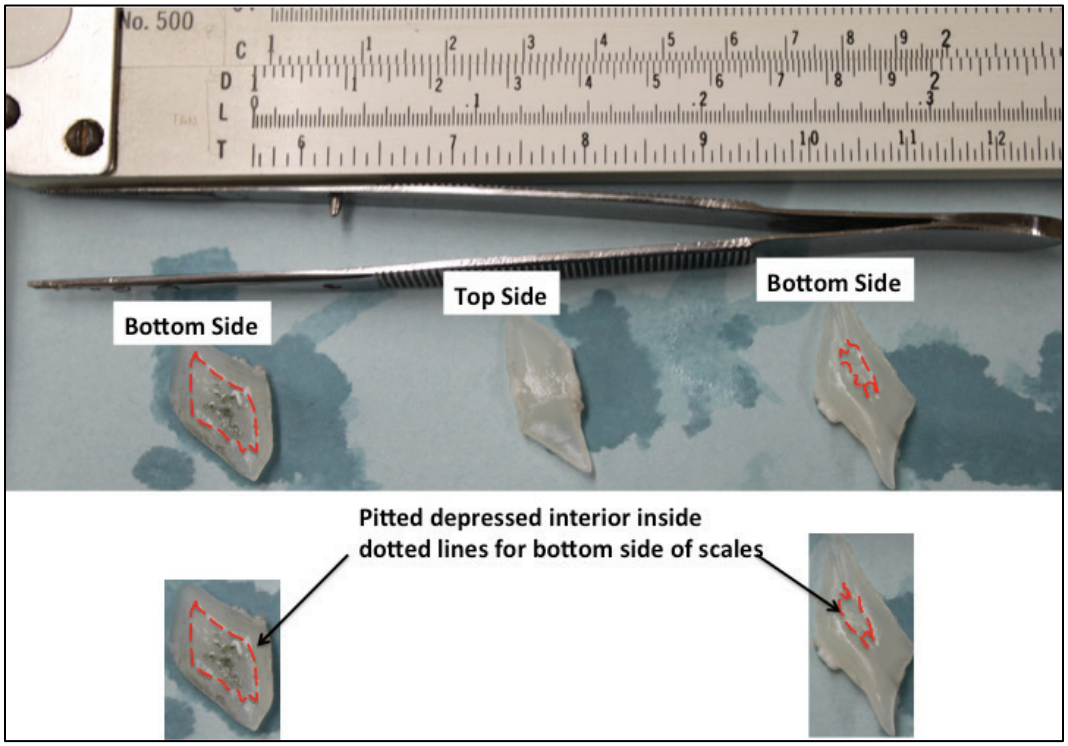

4.2 Investigation of length scale [1-1000] µm

4.2.1 HR-SEM observations

To investigate the questions (a) and (b) raised during the investigation of length scale >1 mm, further observations were made at the 1-1000 µm length scale. Only the medium scale surface topology was investigated, using a JOEL™ HR-SEM, since the geometry and textures were more pronounced than the small scale when inspected by the naked eye in visible light. The HR-SEM images were able to show surface details at higher magnification. In Figure 4.3, the top of the medium alligator gar scale at 1-mm magnification clearly shows a non-smooth and non-level surface. The specimen appears to have at least two distinct texture regions, as highlighted by the dotted lines, along the surface. The backscattered gray-scale surface image indicates that at least two regions that have differing material densities. There is a smoother surface for Region 2 when compared to Region 1. However, the surface of Region 2 shows a gradual surface textural transition from Region 1 to Region 2.

Also observed in Region 1 are circular features that are uniform in size inside the black circles. On the outer edge of the circle features is a crack

propagating linearly. Similarly, the specimen has two cracks running parallel near the edges of the circular feature in Region 1. The specimen has yet to be loaded or polished so the cracking may be due to shrinking caused by drying. In addition, the cracks are consistently appearing near the edges of the circular formations as if there is a zone of discontinuity for the material.

Region 2 has a smoother topology that is more or less defect free and sloping/transitioning downward and away from Region 1. Unlike Region 1, the surfaces of Region 2 do not show cracks. Further examination of the surface is needed to understand the details of cracking occurring near the circular feature.

Figure 4.3. Top surface of medium size gar fish scale at 1-mm magnification using HR-SEM backscatter mode.

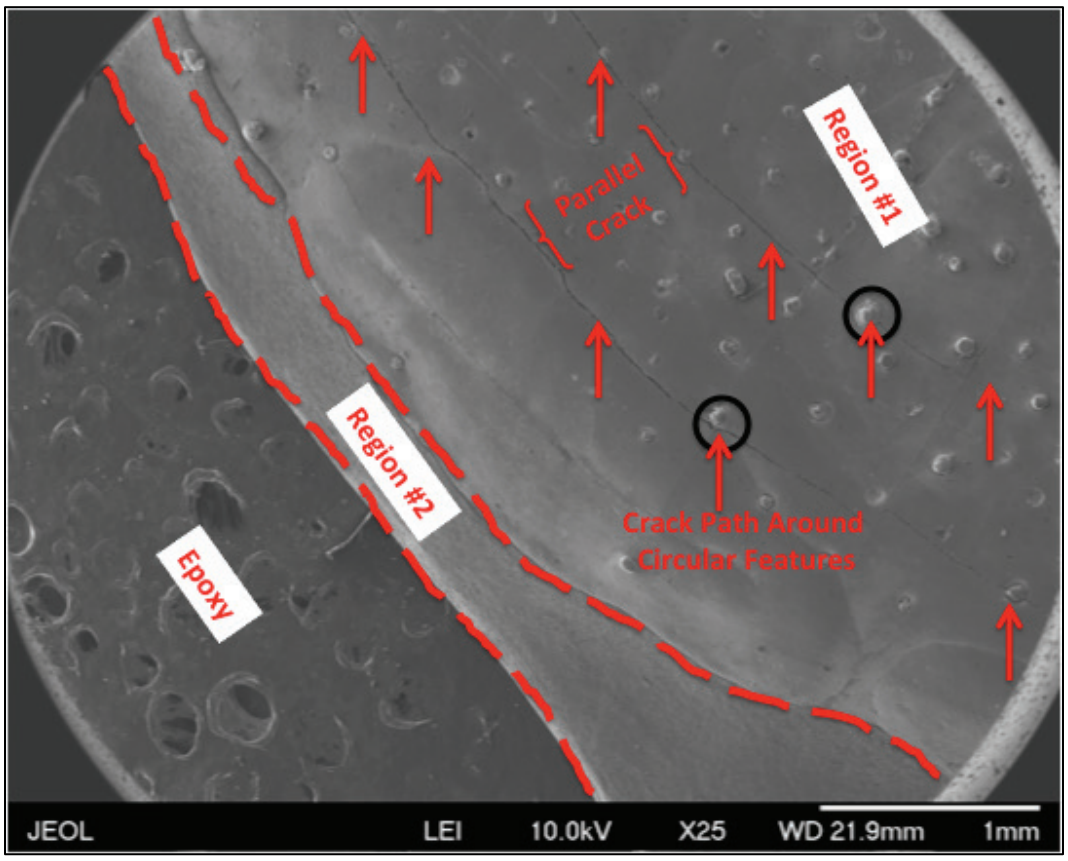

To further investigate the fine details of the circular feature, finer HR-SEM images were taken at the higher magnifications of 100 microns in Figure 4.4 and 10 microns, shown in Figures 4.5 and 4.6. Shown in Figure 4.4 is the top surface of medium size gar fish scale at 100-micron magnification. There are several features that are observed at the finer magnification. For

instance, when viewing the surface Regions 1 and 2 at their interface, barbs are propagating out of the surface. The barbs are equally spaced and hook over toward the Region 1 direction. Another important discovery illustrated in Figure 4.4 is the barbs are hollow.

Figure 4.4. Top surface of medium size gar fish scale at 100-micron magnification using HR-SEM backscatter mode.

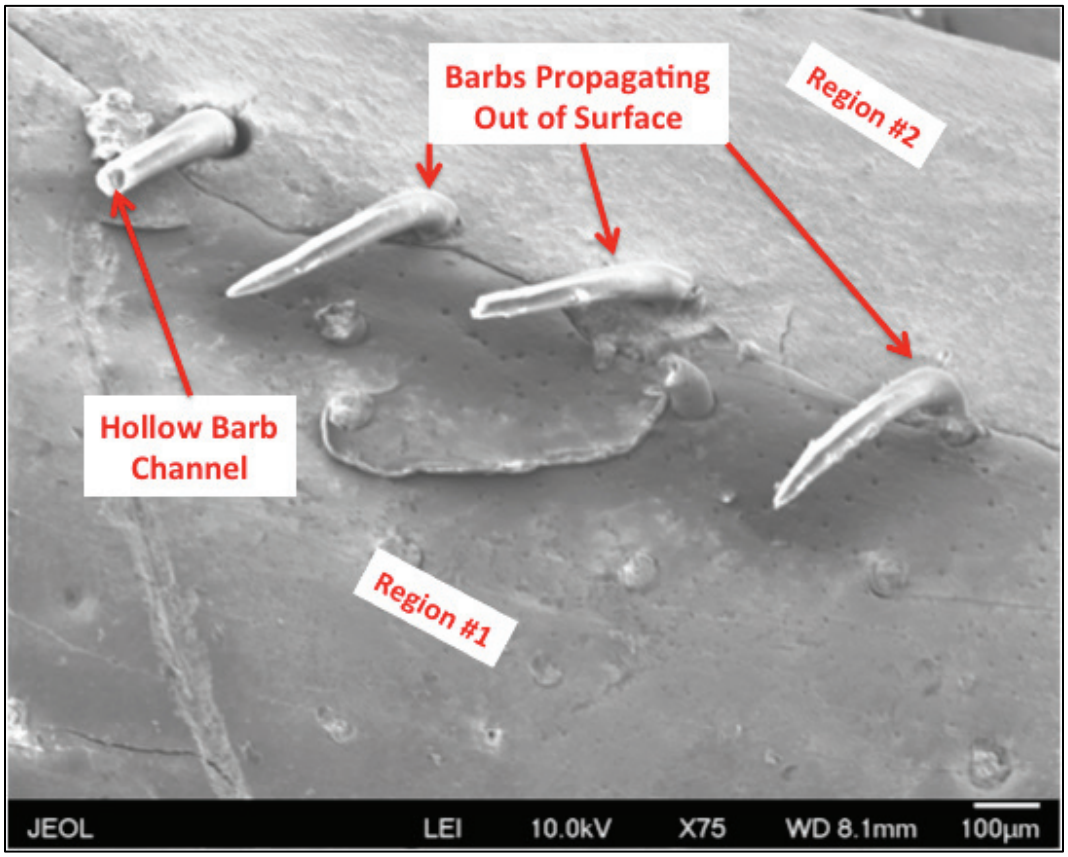

At the 10-micron magnification the hollow barbs appear to be transport channels that are self-contained and serve some unknown function, Figure 4.5. On the surface of the fish scale are bumps/pores similar to the human skin which hair fibers grow from. Here the fibers may have been used to attach the soft tissue to the surface. Furthermore, what appeared as circles at the 1-mm range there are actually remnants of the hollow barb's base. The researcher believes these are only remnants left, because during cleaning the scales' surface most of the barbs were unknowingly scraped off.

In Figure 4.6, also at the 10-micron magnification, are surface damage sites for the areas where the barbs were scraped off. Notice the barb channel area has become detached from the surrounding materials. The

surrounding area has cracked. Crack paths seem to follow along the detached area and surface imperfections.

The unanswered question (b) raised during the investigation of length scale >1 mm of whether the surface texture percolates outward from the scales internal structure is still unknown and cannot be answered from surface observations alone. The additional questions now raised during the investigation of length scale 0.001-1 mm are: (c) Do the layers exist through the thickness of the fish scale? (d) Do the hollow barbs observed at the surface extend through the entire thickness of the fish scales' internal structure?

Figure 4.5. Top surface of medium size gar fish scale at 10-micron magnification showing damage site around hollow barb base using HR-SEM backscatter mode.

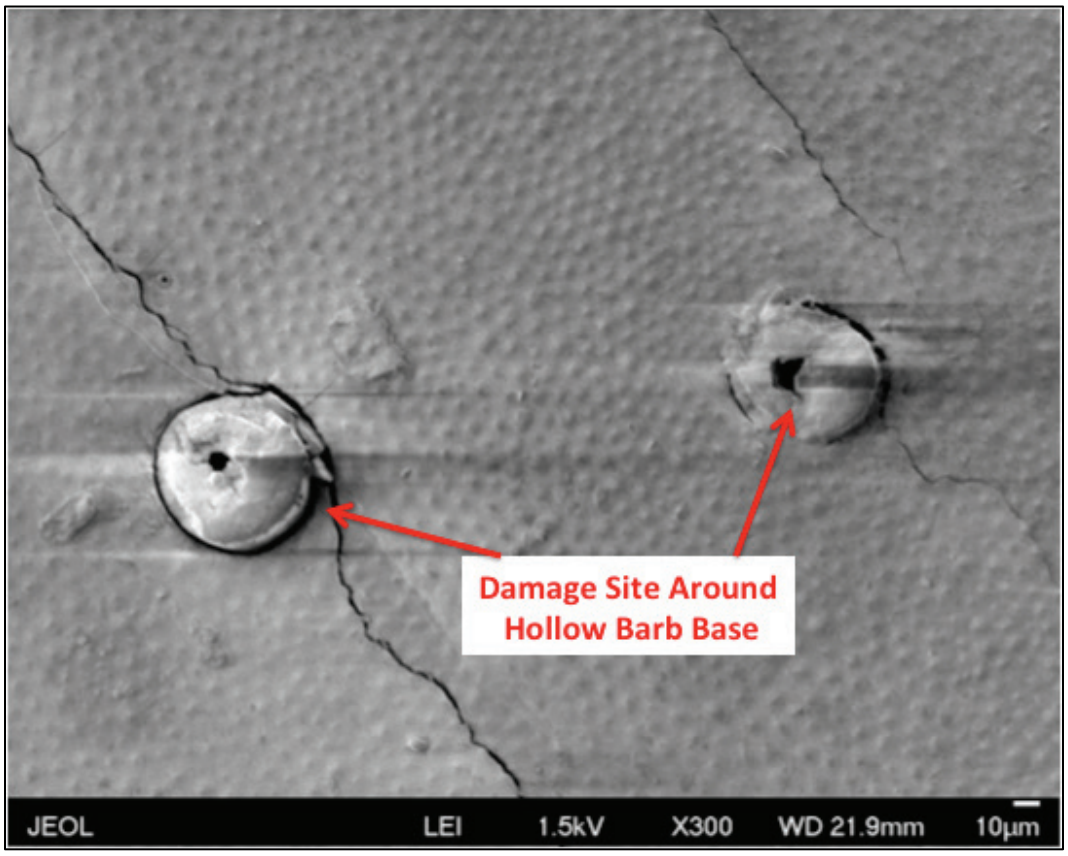

Figure 4.6. Top surface of medium size gar fish scale at 10-micron magnification showing crack paths tied to surface imperfections using HR-SEM backscatter mode.

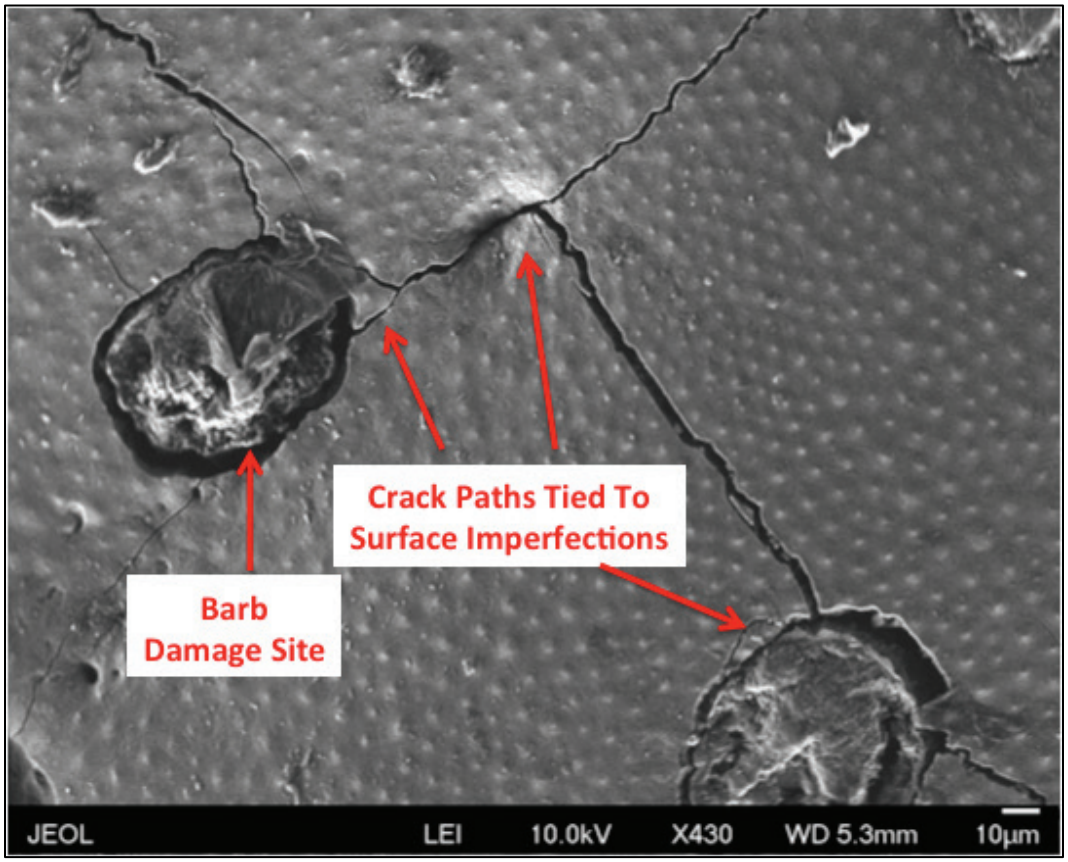

To be able to determine if the internal structure contributes to the surface layering, texturing, and cracking, both fractured and polished cross sections surface were imaged using HR-SEM. The fish scale specimen was fractured by using two sets of needle-nose pliers to apply sufficient manual force to break the specimen. The direction of the applied force was selected based on previous literature that showed hardness decreased with depth along with collagen fiber content increased with depth across the short axis (Allison et al. 2013). Therefore, to better capture images that contain fibers that may be pulled out during fracture, the concave external forces were applied upward (weakest direction) using the needle-nose pliers as shown in Figure 4.7.

After breaking the fish scale, the fracture surface images were taken. Figure 4.8 shows the overall facture surface at 1 mm in the HR-SEM. There are two distinct layers identified by backscattered gray-scale in the cross section. The answer to question (c), formed by the hypothesis is yes, layers do exist. Likewise, the layers are present through the thickness of

the fish scale. Additionally, Layer 1 is a lighter gray than the darker gray shown in Layer 2. The lighter gray image is an indication Layer 1 has a higher material density than Layer 2. Similarly the gray-scale fracture surface appears to correspond to the gray-scale surface images seen in Figure 4.3. Also, in Figure 4.8, the backscattered image shows Layer 2 is much thicker than Layer 1. Layer 2's fracture surface starts at the edge of the inner surface and stops at the dotted red line. Layer 1 is the shown to be inside the red dotted line and does not have a uniform thickness. Within Layer 1, the layer is thinnest near the center of the outer surface and progressively becomes thicker at the edges of the outer surface.

Figure 4.7. Schematic of applied force and direction used to fracture fish scale specimen.

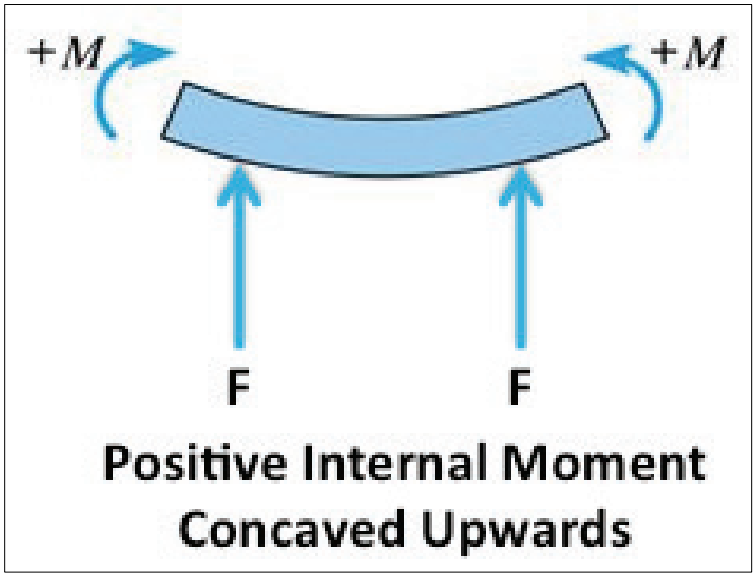

Figure 4.8. Overall facture surface at 1-mm magnification using HR-SEM backscatter mode.

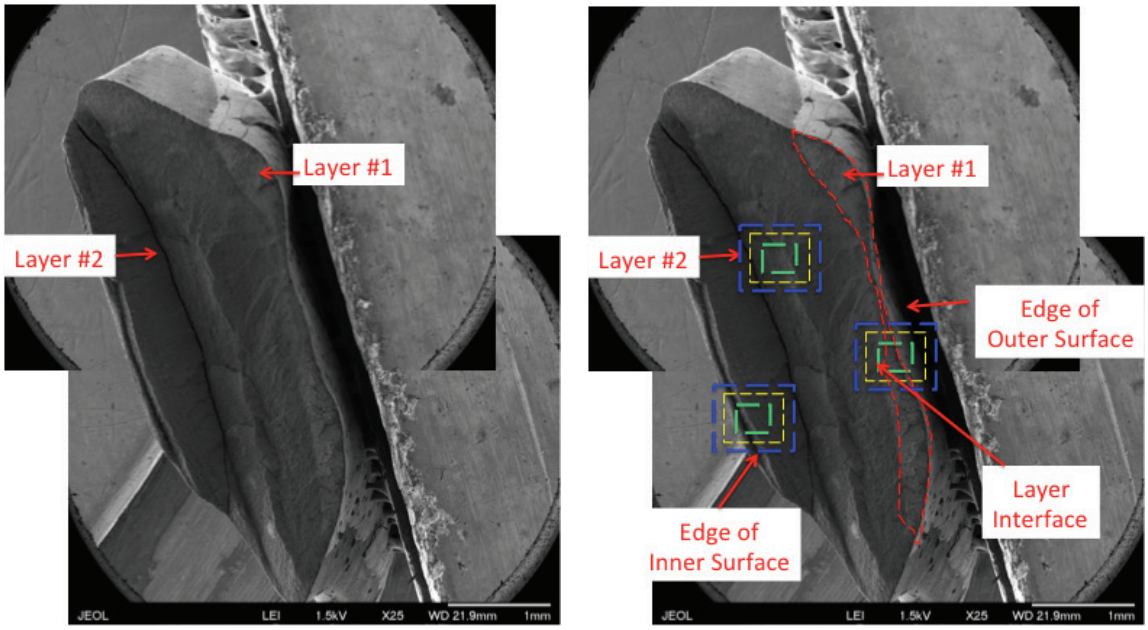

Next, the inner layer fracture surfaces were investigated for Layer 1, Layer Interface (ITZ), and Layer 2 at finer magnifications. The blue, yellow, and green dotted boxes, in Figure 4.8, identify investigated sites. The blue, yellow, and green dotted boxes represent 100-, 10-, and 1-micron magnification levels, respectively.

At 100-micron magnification, Figure 4.9 enhances the linear cracking found in the ITZ. The linear (parent) crack path, outlined by the yellow-dashed line, in the ITZ seems to be continuous along the interface of Layers 1 and 2. Since there does not appear to be branch (child) cracking emanating from the linear (parent) crack, then cracking does not seem to be related to mechanical interface shearing. Instead the parent crack is likely occurring due to environmental dehydration, leading to debonding of the layers. Debonding is an indication of a change in structural arrangement and/or chemical composition.

Figure 4.9. Cross section for fracture surface at a 100-micron magnification using HR-SEM backscatter mode.

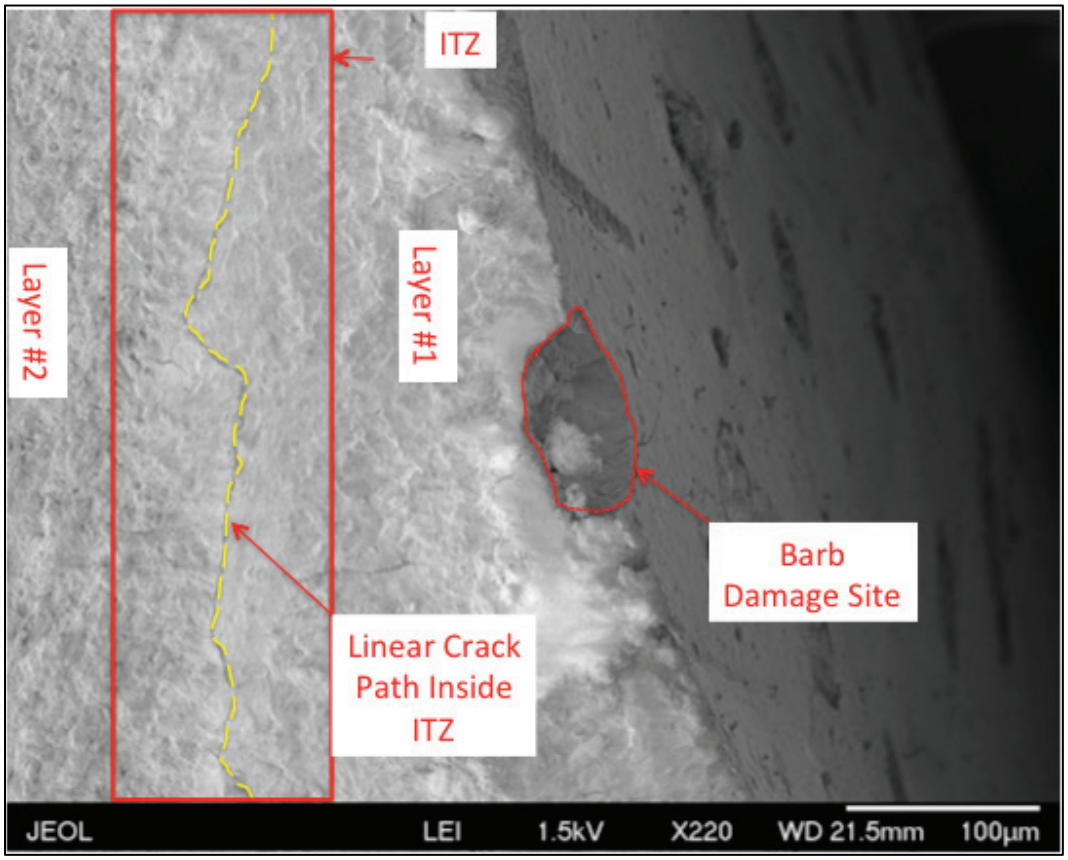

When observing the fractured cross-sectioned barb damage site at a 50-micron magnification, displayed in Figure 4.10, for the surface damaged areas in Figures 4.6 and 4.9 at 1 mm and 100 microns, respectively, the higher fidelity image provides no evidence the barb is embedded nor does a hollow region exist directly below the surface of Layer 1. Nor do cracks seem to penetrate far below the surface. Also shown by the fracture surface for Layer 1 side of interface is a texture that appears to be dense/compact with very few pores. At 10 microns, Figure 4.11, the fracture surface for Layer 1 side of interface illustrates a roughened, unleveled surface texture. At the even more refined 1-micron magnification, Figure 4.12 displays the fracture pattern lineated by the red dotted arrows for the roughened topology.

Figure 4.10. Cross section of the barb damage site at a 50-micron magnification using HR-SEM backscatter mode for Layer 1.

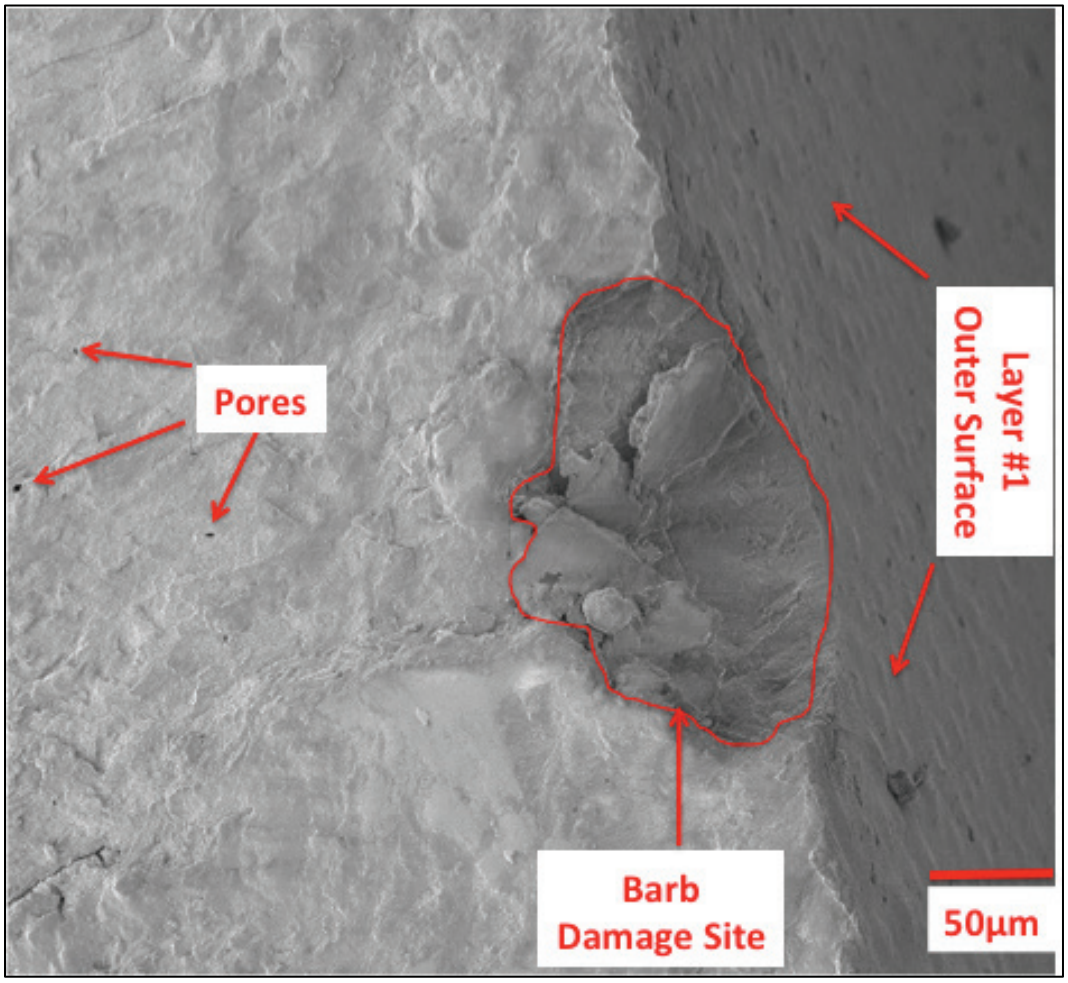

Immediately adjacent to the ITZ is Layer 2, Figure 4.13, illustrating the fracture surface that does not appear to be densely compact as found in Layer 1. The pore volume increased when approaching the innermost edge of the fish scale. In addition, the surface contains several identifiable pore structures that are visible at the 100-micron magnification. The image shows there are several pore sites having a varying distribution of sizes.

Additionally, some of the pore sites seem to be connected. Also shown was that connected pore sites can form pore channel structures. Upon further investigation, at the 1-micron range, the pore channel was found to have a fibrous interior, Figure 4.14.

Figure 4.11. Cross section for roughened fracture surface at a 10-micron magnification using HR-SEM backscatter mode for Layer 1.

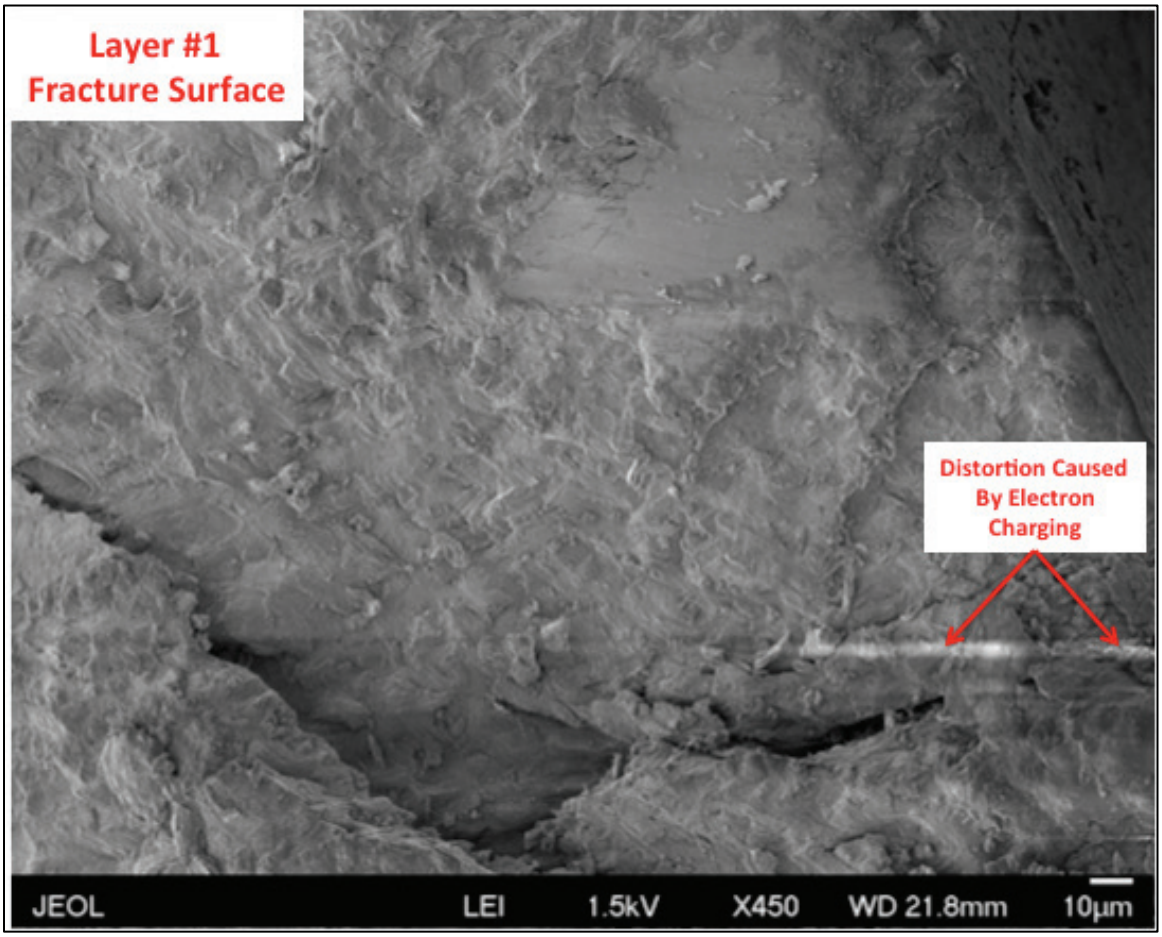

The innermost edge of the fish scale was next examined. Shown in Figure 4.14 is a vastly different structural arrangement than what was observed in Layer 1 and the ITZ. At 10-micron magnification the image shows a loosely compacted surface, Figure 4.15. Furthermore, the pullout of fibers shows they were previously embedded in the loosely compacted solid phase prior to fracturing the surface. At the finer 1-micron magnification, Figure 4.16 elucidates the hierarchical fibrous structure. Collections of individual fibrils are woven to form individual fiber strands. The individual fiber strands become entwined to form fibrous bundles. By observation, the solid fractions appear to be individual minerals that are much smaller than individual fibers.

Figure 4.12. Cross section showing surface, delineated by red dotted arrows, at 1-micron magnification using HR-SEM backscatter mode for Layer 1's roughened fracture surface.

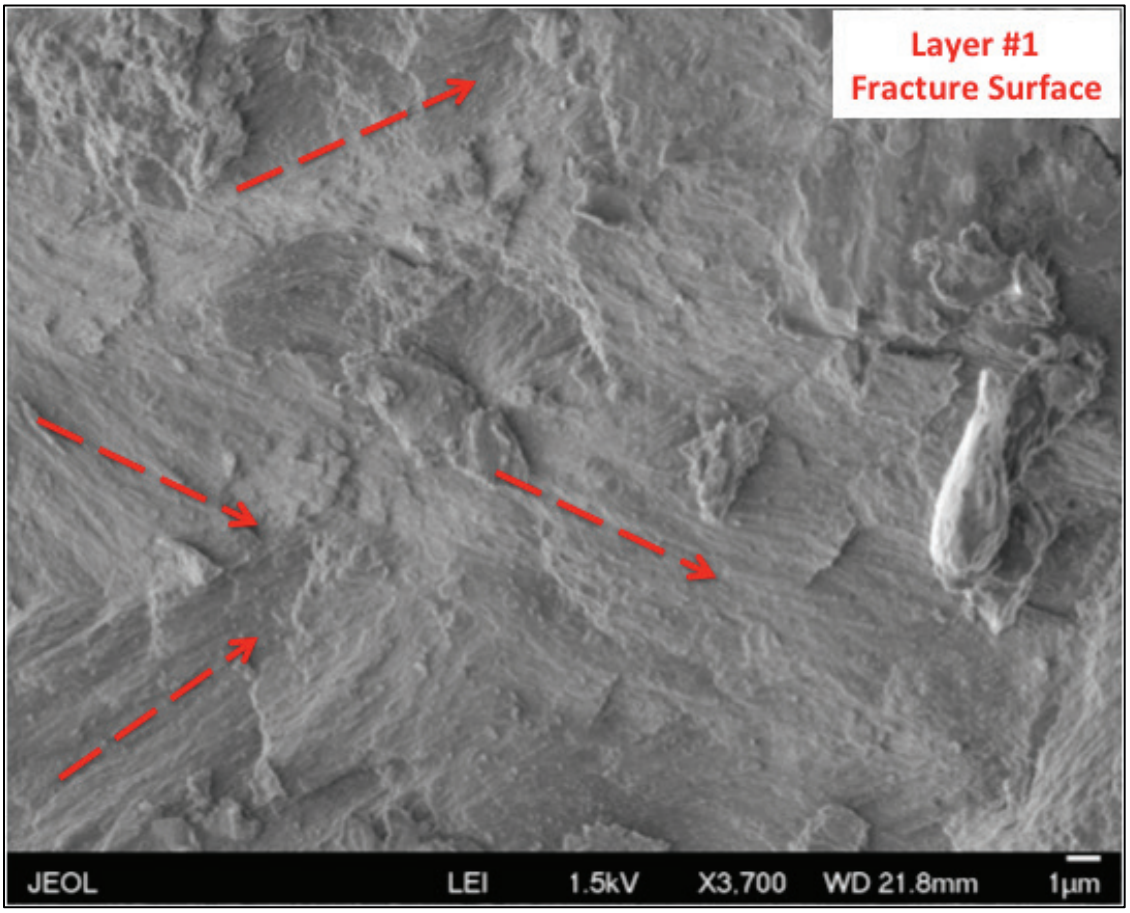

So far the research has presented and discussed the structure for the fish scales' fracture surface. Next, HR-SEM will be used to elucidate the structural details for both the small and medium polished cross sections. There are distinct differences and similarities for the two fish scale sizes, shown in Figure 4.17, at 200-micron magnification.

There are few differences in the small and medium scales. However as the fish grow, the scale seems to be prone to more defects/damage. The HR-SEM image for the medium scale shows cavities (also known as tubules or canals), outlined by the red dotted circles, and is present near the center of the scale. Also observed was that the outermost dense-layer fractured and flaking occurred. Further analysis will be discussed later in Chapter 4 that helps determine if differences in the two scales are caused by a change in chemical, structural, and/or mechanical properties.

Figure 4.13. Cross section of fracture surface immediately adjacent to ITZ using HR-SEM backscatter mode at 100-micron magnification.

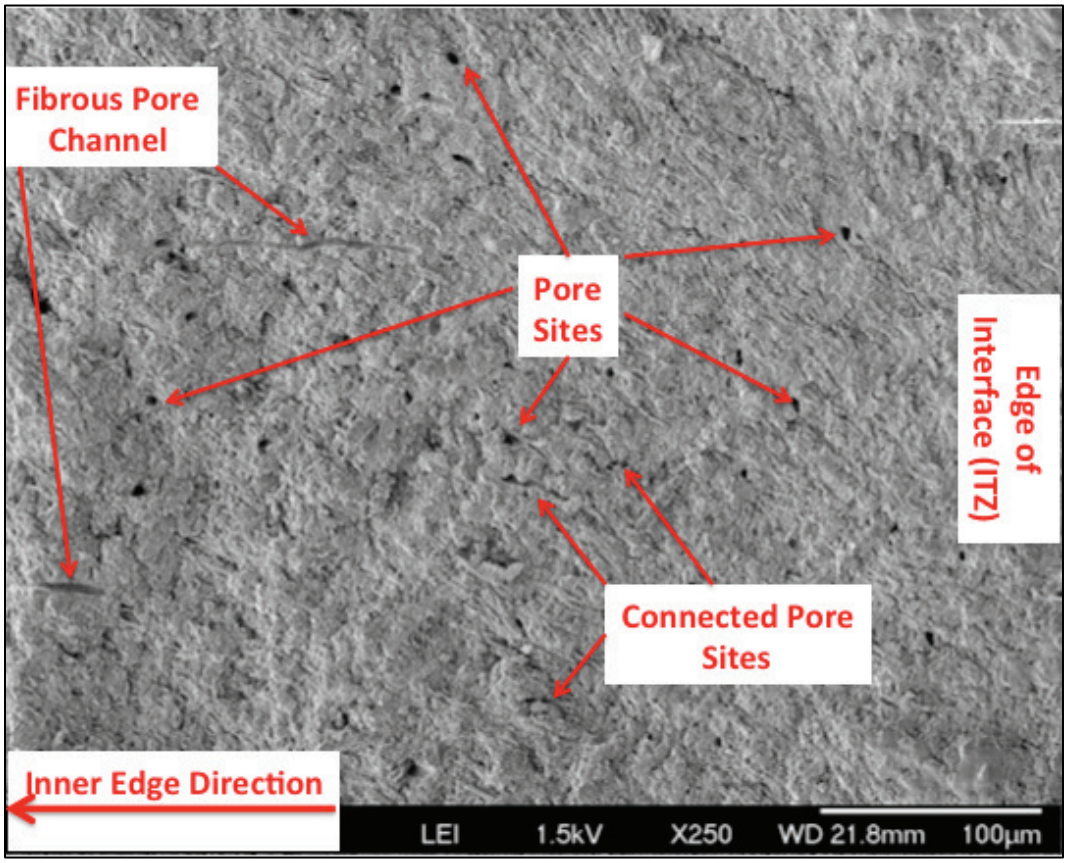

The fish both have dense exterior layer thickness, which appear to grow proportionally with the underlying layer. The outer layer does not extend to the edge of the scale. Furthermore, the layer is thicker at the edge and gradually becomes thinner toward the center of the layer. At the center of the dense layer there is a noticeable depression. The exterior layer appears to provide little to no coverage for the underlying layer at the depression zone. The dense layer is connected to the underlying layer by what seems to be a sawtooth geometrical interlocking interface. In addition, the interface seems to be mainly bonded by mechanical means, rather than chemically, because of sawtooth geometries, Figure 4.17. Since sawtooth geometries are used to secure the layers' interfaces, the layers are not discreetly bonded like layers in engineered laminates. Within the sawtooth regions the material overlaps and is embedded at various depths within each layer to form periodic "repeating" bonded connections. The sawtooth connections perhaps provide enhanced shear resistance at the interface when the full hydration state is maintained and helps inhibit debonding.

Figure 4.14. Cross section of fracture surface showing a fibrous interior for the pore channel, using HR-SEM backscatter mode, at 1-micron magnification.

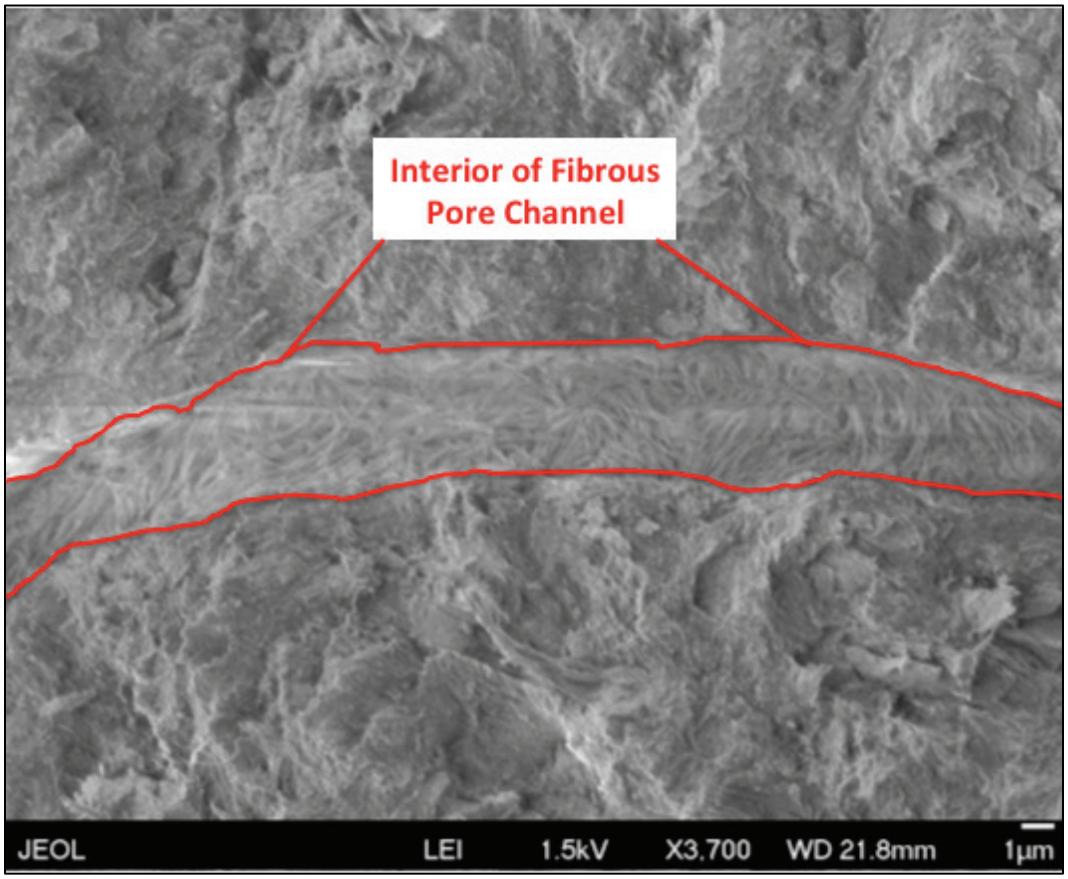

Evidence for mechanical bonding is shown in the medium fish scale. At the interface for the medium fish scale there is some indication shrinkage cracking has occurred. More than likely, shrinkage cracking was caused by sample preparation. The image for the medium fish scale shows the two layers have separated, however, they maintain the sawtooth shape at the junction sites.

As illustrated in Figure 4.18, for the small and medium scales, the enhanced image highlights linear cracks occuring through the short axis of the dense layer. The lateral spacing between the cracks seems to be directly proportional to the change in thickness. In the images as the layer thickens, the lateral spacing between cracks widens.

Figure 4.17 also shows repeating contrasting gray-scale concentric rings occurring throughout. The highlighted layers, in Figure 4.19, show contrasting rings that tend to follow the contours of the scale. Upon zooming into the denser outer layer, Figure 4.20, the image shows an increase in contrast. Each sub-layer has a bright bottom and darker top.

Figure 4.15. Cross section of inner fracture surface elucidating mineral-fiber structure, using HR-SEM backscatter mode, at 10-micron magnification.

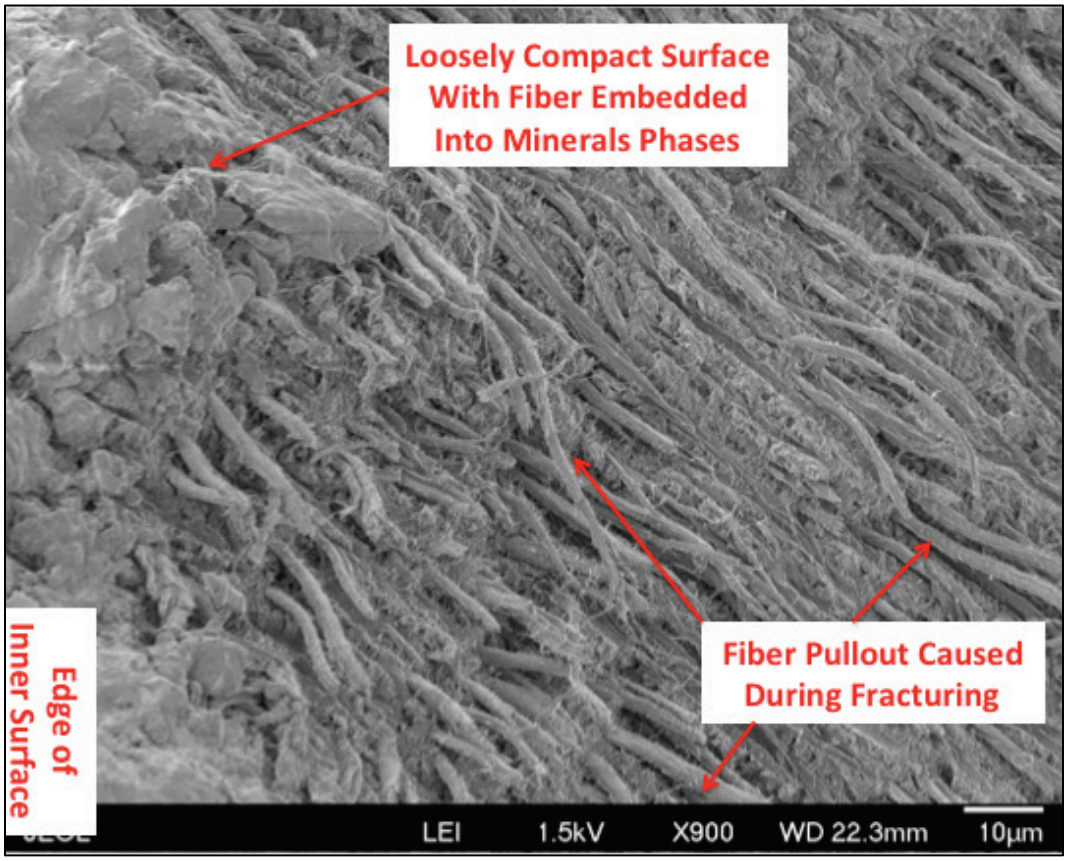

Each sub-layer grades from a dense underside to a less dense upper layer. Each sub-layer ends in a rasp shape.

The contrast in the image indicates there is high likelihood that density is changing within the layers. The contrasts revealed by HR-SEM enhanced backscatter image for the medium fish scale, shown in Figure 4.21, indicates within the ITZ (yellow-dashed lines) at the center top of scale is the oldest. Both layers become less dense (younger) further away from top center.

The significance of gray-scale contrasting provides more evidence the density likely changes with age. The change in density and the repeating contours provide an indication the scale's composition and structure may be evolving with growth. To obtain greater knowledge of how the scales are evolving during growth, further optical microscopy, µm-XCT, structural, and chemical analysis was conducted at the micron level.

Figure 4.16. Cross section of inner fracture surface elucidating mineral-fiber structure, using HR-SEM backscatter mode, at 1-micron magnification.

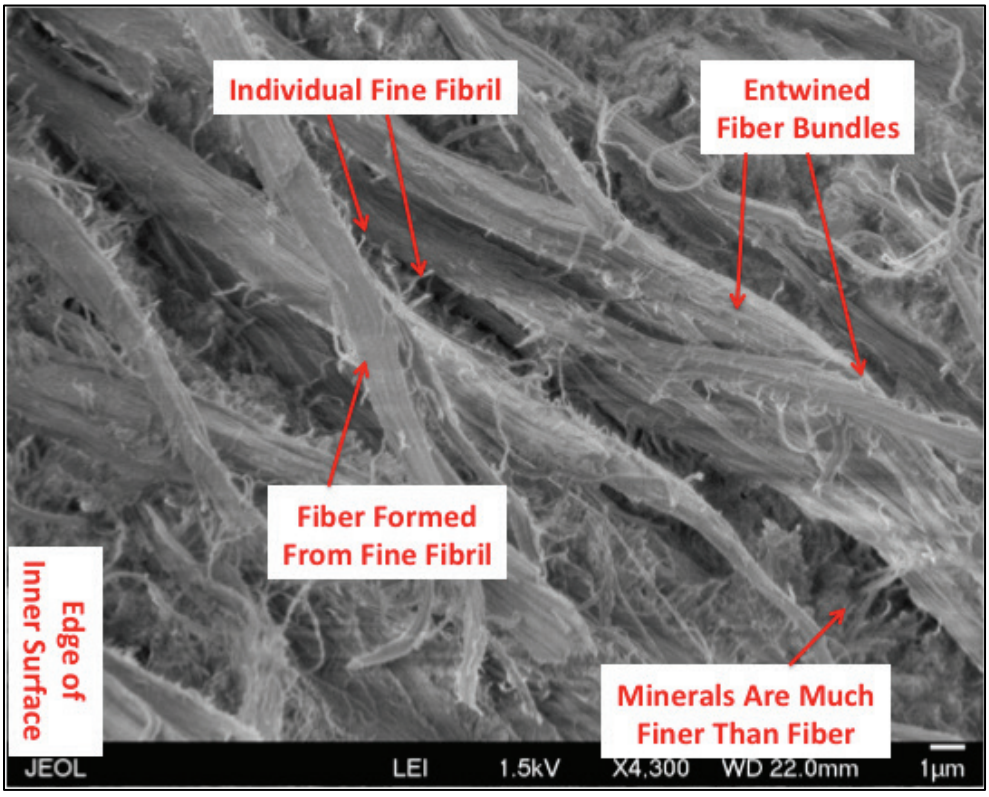

Figure 4.17. Cross section for small and medium polished fish scale surfaces at a 200-micron magnification using HR-SEM backscatter mode.

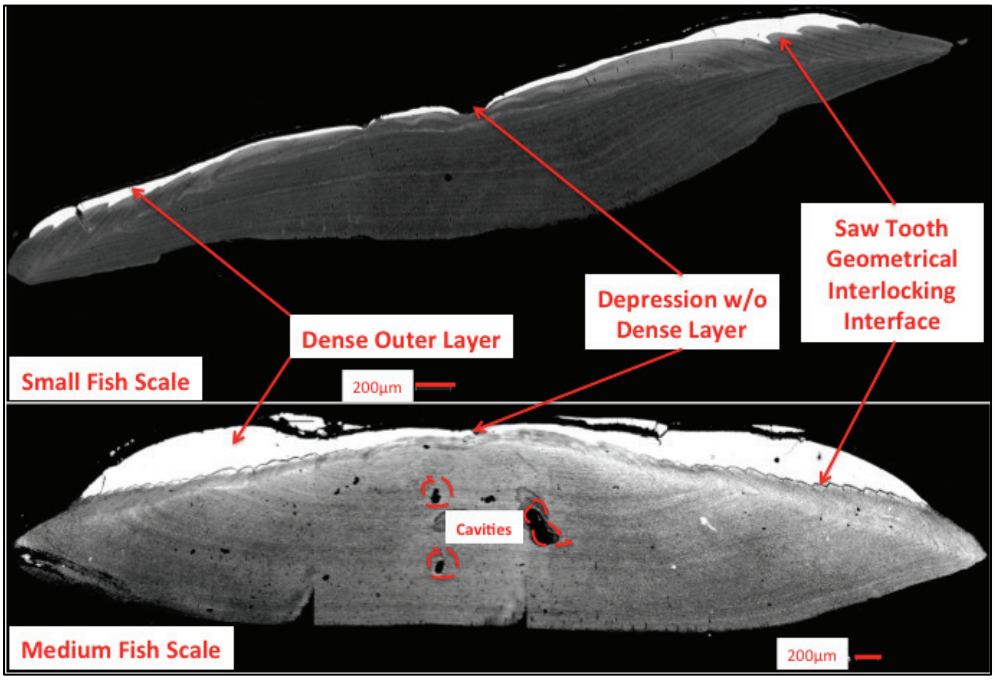

Figure 4.18. Enhanced HR-SEM backscatter image at 200-micron magnification, for small and medium scales, highlighting linear cracks occurring through the short axis for dense layer.

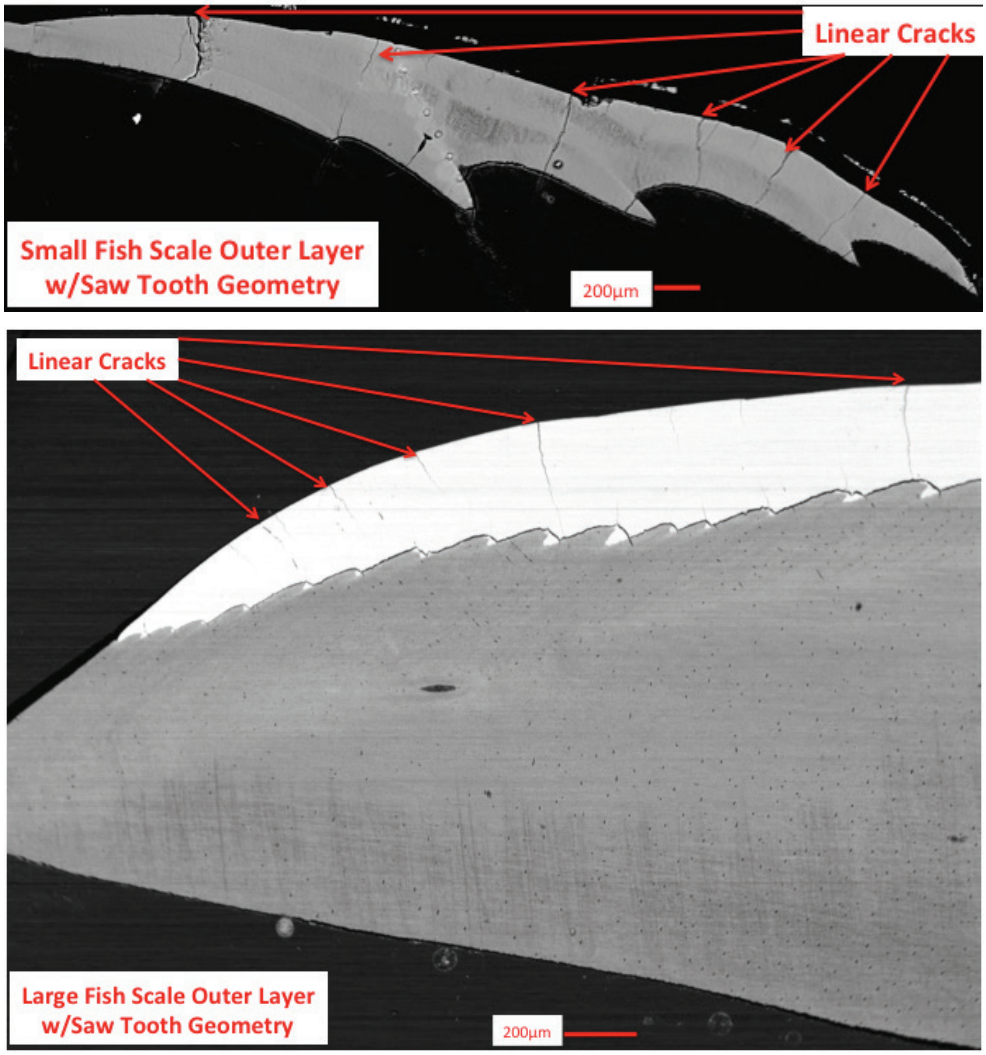

Figure 4.19. Enhanced HR-SEM backscatter image at 500-microns magnification, for small fish, highlighting the gray-scale concentric rings occurring throughout scales layers.

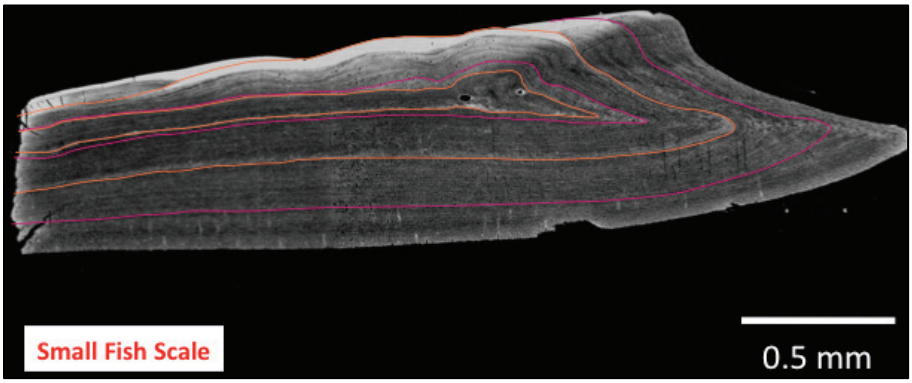

Figure 4.20. Enhanced HR-SEM backscatter image at 200-micron magnification, for small fish, highlighting the gray-scale sub-layers occurring within the denser outer layer.

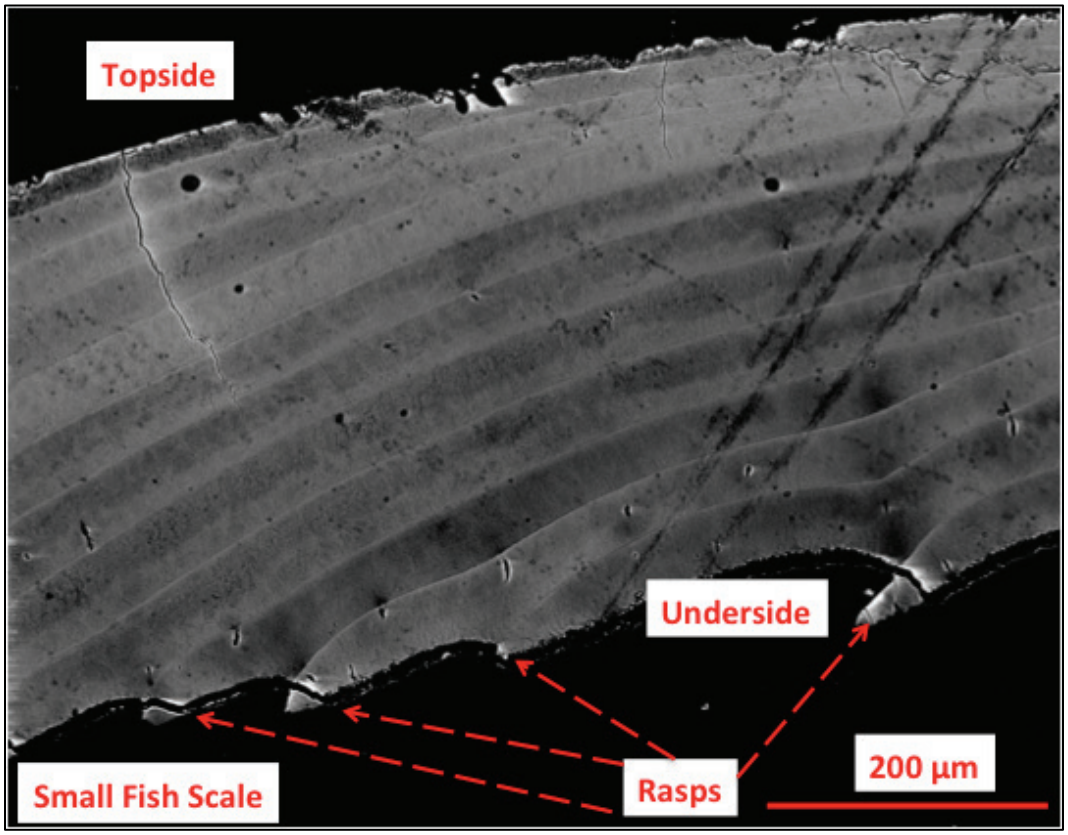

Figure 4.21. Enhanced HR-SEM backscatter gray-scale image, at 200-microns, highlighting the growth initiation and direction for the medium fish scale layers.

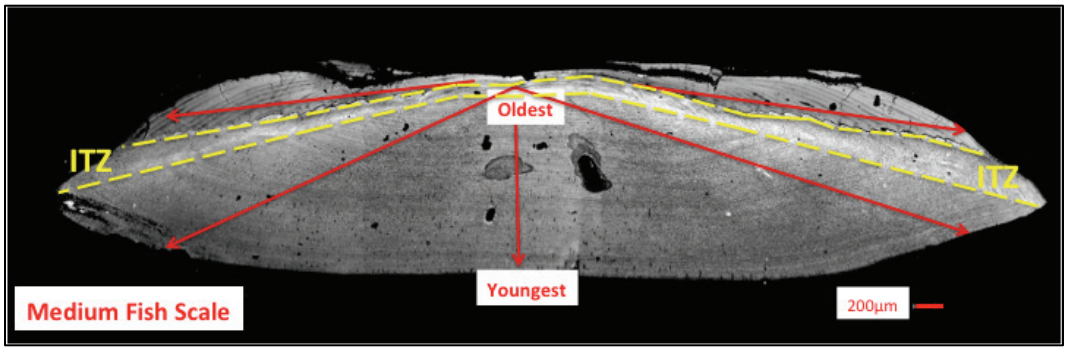

The questions that arose with no definitive answers: (e) Why does the lateral spacing between cracks widen as the layer becomes thicker (No Answer)? (f) Also, what may be the reason for linear cracking occurring within the layer of what appears to be like materials (Stress Release Due To Drying)? Both of these questions are addressed in the next sections.

4.2.2 Optical microscopy observation

A Carl-Zeiss Imager Z1m ™ optical light microscope was used to measure average layer thickness for the small and medium size scales. Shown in Figure 4.22, is the average thickness in the small fish scale for Layer 1 and Layer 2, which are 44.87 and 287.59 microns, respectively. Additionally in Figure 4.23 is the average thickness in the medium fish scale for Layer 1 and Layer 2, which are 1575.40 and 11804.40 microns, respectively. The nominal ratio for *Layer 1 Thickness-to-Total Scale Thickness* for the small and medium fish scales are 13.3 and 15.6 percent, respectively. The ratio was used to show how the individual layers for the fish scale tend to grow. As the fish scale grows, the ratio indicates the layer thicknesses remain constant.

Figure 4.22. Optical microscopy image showing the average layer thickness for small fish scale.

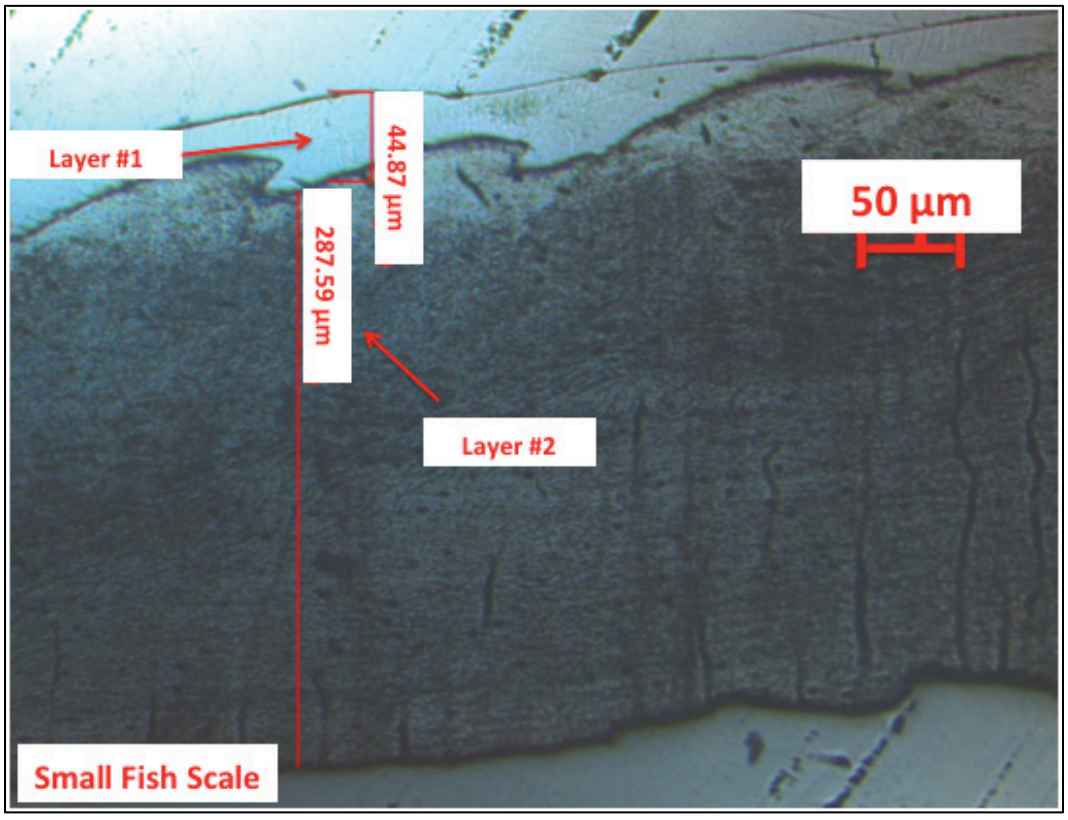

Figure 4.23. Optical microscopy image showing the average layer thickness for medium fish scale.

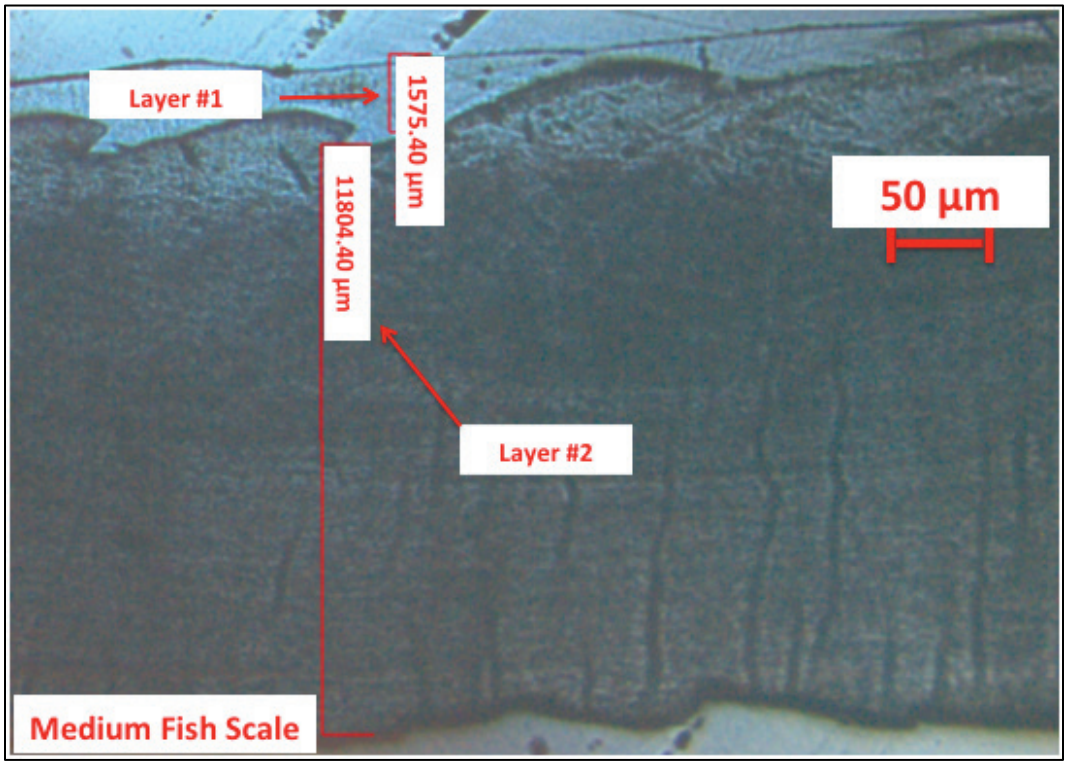

4.2.1 µm-XCT observations

Displayed in Figure 4.24 is the µm-XCT image for a medium-size fish scale. The reconstructed three-dimensional image volume for the whole intact scale provides verification there exists a dense outer Layer 1 that does not fully cover the underlying Layer 2. Inside the dotted red line shows the scale does not have a uniform thickness indicated by concave sloping surface occurring toward the center.

The reconstructed three-dimensional scale was digitally sliced at the bottom of Layer 1 near the interface, Figure 4.25, to show ridges that were formed. The ridges are analogues to the grooves seen in Tupperware™ storage container lids. The grooves point in opposite directions going down and outward, indicated by the red dotted arrows, from the scales' center. The saw-tooth rasps observed in HR-SEM and optical microscope cross-section images, for Figures 4.17, 4.22, and 4.23, are formed from the ridges. The µm-XCT image also confirms the interface uses geometry to form a mechanical bond when anchoring Layer 1 to the underlying Layer 2. At the center of the scale, indicated by the blue interior, is the hollow area. The hollow area corresponds to the pitted area previously

discussed for Figure 4.2 and the non-uniform thickness seen in the μm-XCT image for Figure 4.25. Still uncertain is reason for cracking, crack spacing, and how the ridges form. Perhaps the ridges represent growth rings as individual sub-layers, which were previously discussed in HR-SEM cross-section image, Figure 4.19.

Figure 4.24. Reconstructed 3-D volume μm-XCT image for a medium-size whole intact fish scale.

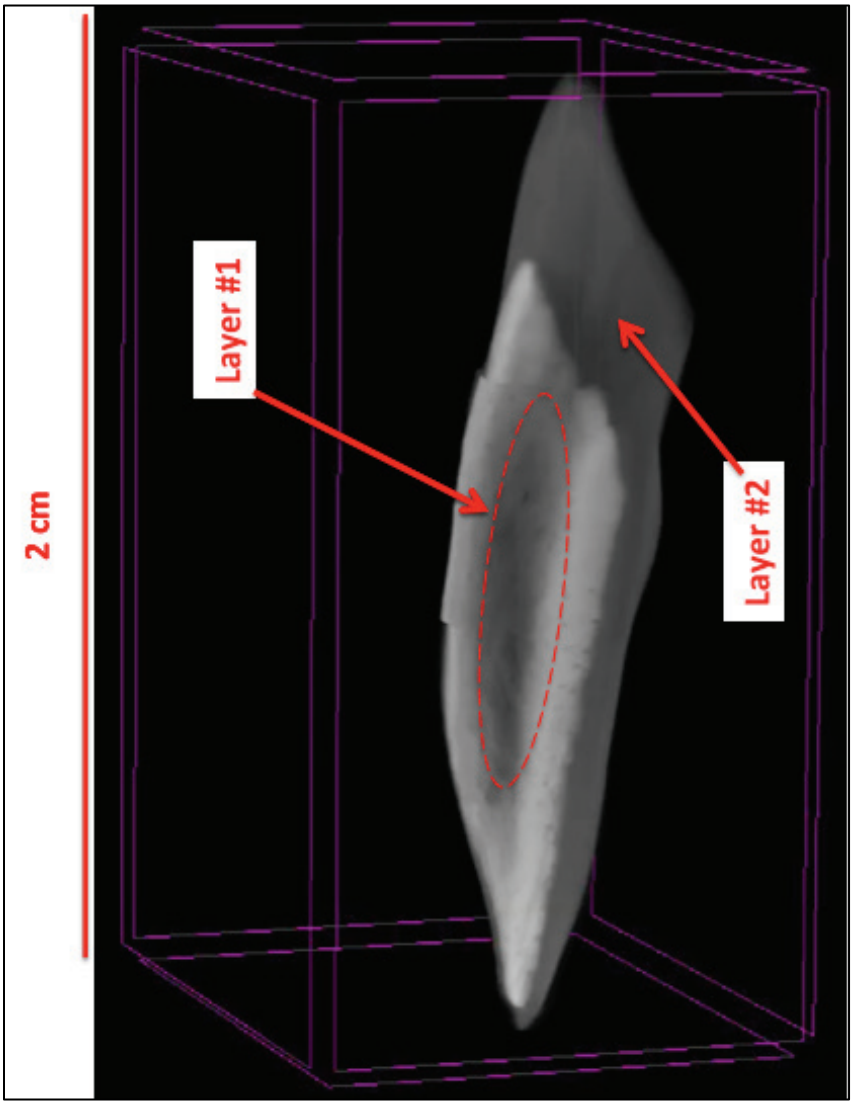

Figure 4.25. Reconstructed fish scale image from 3-D µm-XCT volume at the bottom of Layer 1 near the interface, where ridges are formed.

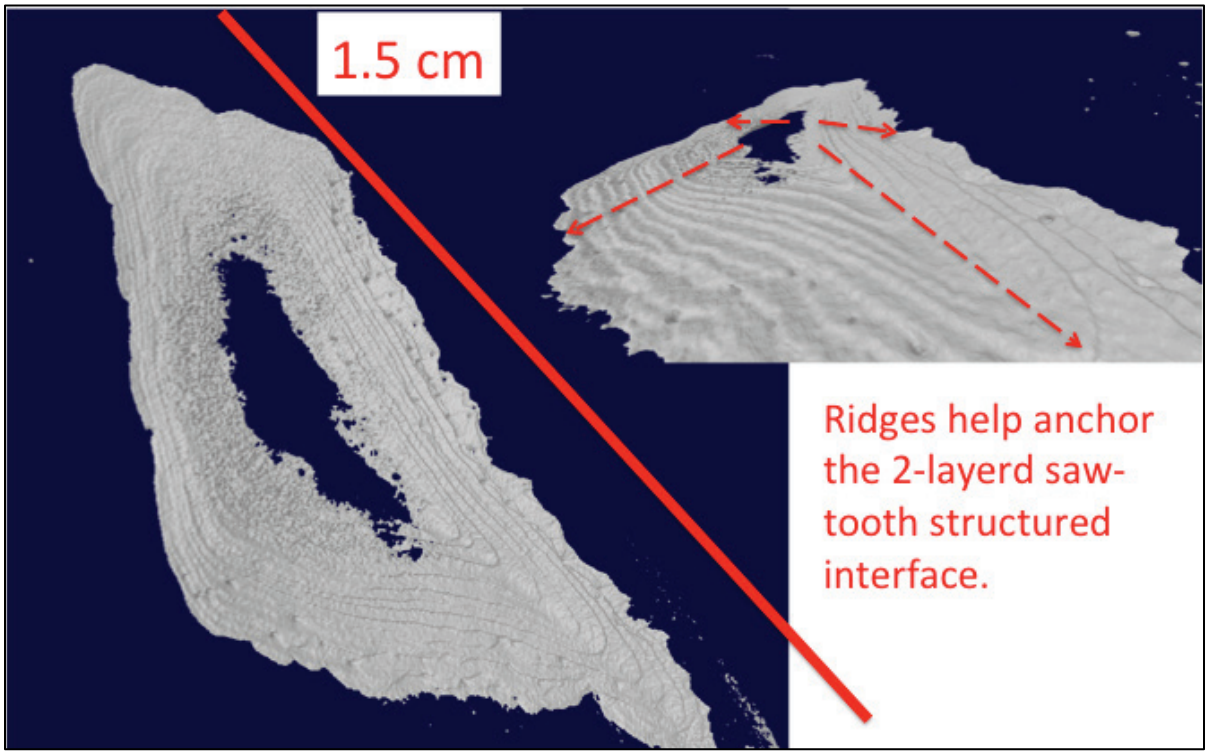

So far the results have discussed how the structural layers are assembled geometrically at micron level. The remaining sections will discuss the use of analytical techniques for identifying the chemical composition and elemental distribution that are measured at the 1-1,000 µm length scale. The information was used to determine what are components that make up the fish scale's structure.

4.2.2 Synchrotron x-ray analysis (µm-XRF- CT/µm-XANES/µm-XRD)

Synchrotron µm-XRF-CT, µm-XRD, and µm-XANES microprobe analysis was conducted to determine the elemental distribution and provide speciation information for heterogeneous solid fish scale. The analysis was performed at beamline X26A, X27A, and X2B at the National Synchrotron Light Source at Brookhaven National Laboratory in Upton, NY. At the time of this research beamline X27A was the only synchrotron x-ray energy source in the United States calibrated uniquely for the x-ray properties of calcium. Previously, researchers have shown calcium, by percent dry weight, is one of the main elements that is responsible for the degree of mineralization in bone, tooth, and even fish scales (Currey 1999; Mann 2001; Ochsner and Ahmed 2011; Olszta et al. 2007; Fratzl et al. 1991;

Boskey 1991, 2007; Canton and Tucker 2009; Sahi and Schoonen 2006; Jantou-Morris et al. 2010; Schonborner et al. 1981; Weiner et al. 1999; Ratner et al. 2013; Shapiro et al. 2014).

Two-dimensional elemental distribution images were produced from the five-micron-thick serial sliced scale sections for the small and medium fish only, using μm-XCT mapping. The beam size on the sample was approximately 7 μm × 10 μm using Rh-coated Kirkpatrick-Baez focusing optics. X-rays were selected using a water-cooled, channel-cut Si (111) monochromator. Changes in elemental compositions for the serial sections were monitored using μm-XRF and correlations were made between elemental composition and location. Once the elemental composition was determined, the same specimens were then analyzed, using μm-XANES and μm-XRD analytical techniques to aid in identifying any major compounds present within the biomineralized fish scale.

The μm-XRF data were collected at energies either 4100 electron volt (eV), 11,000 eV, or 13,000 eV using a four-channel Silicon drift detector. To maximize the detection for the light element of calcium μm-XRF data were collected at 4,100 eV. The same sample was scanned a second time at a higher energy (11,000 or 13,000 eV) to collect data on the trace elements present in the samples. For the current investigation bio/geo chemistry trace element interpretations were used. Specifically, to be considered a trace element for a given energy range, a chemical element has an average concentration that is less than 1,000 parts per million (ppm) of a material's composition and is usually measured in counts per arbitrary unit (Albarede 2003; Reinhardt 2001; Rakovan et al. 2008). Each individual atomic count represents a single x-ray photon entering the energy detector (Faust et al. 1998; Levinson et al. 2001; Leng 2008; Willmott 2011).

The μm-XRF multi-channel analyzer plot (MCA), shown in Figure 4.26,elucidate the elements that fluoresce in the 3,000--10,000 eV energy range. The energy peaks were used to identify the periodic elements. Each element has known x-ray properties. The x-ray properties were identified using Lawrence Berkeley National Laboratory's website that provides a downloadable PDF document titled "X-RAY DATA BOOKLET," which contains information for all elements (X-RAY DATA BOOKLET, 2015). The "Ka" and "Kb" are shell emission lines in electron volts that were compared to those listed in the x-ray properties of elements found in the "X-RAY DATA BOOKLET."

Figure 4.26. Synchrotron µm-XRF multi-channel analyzer plot showing periodic elements that fluoresce in the 3,000-10,000 eV energy range, for the small fish scale.

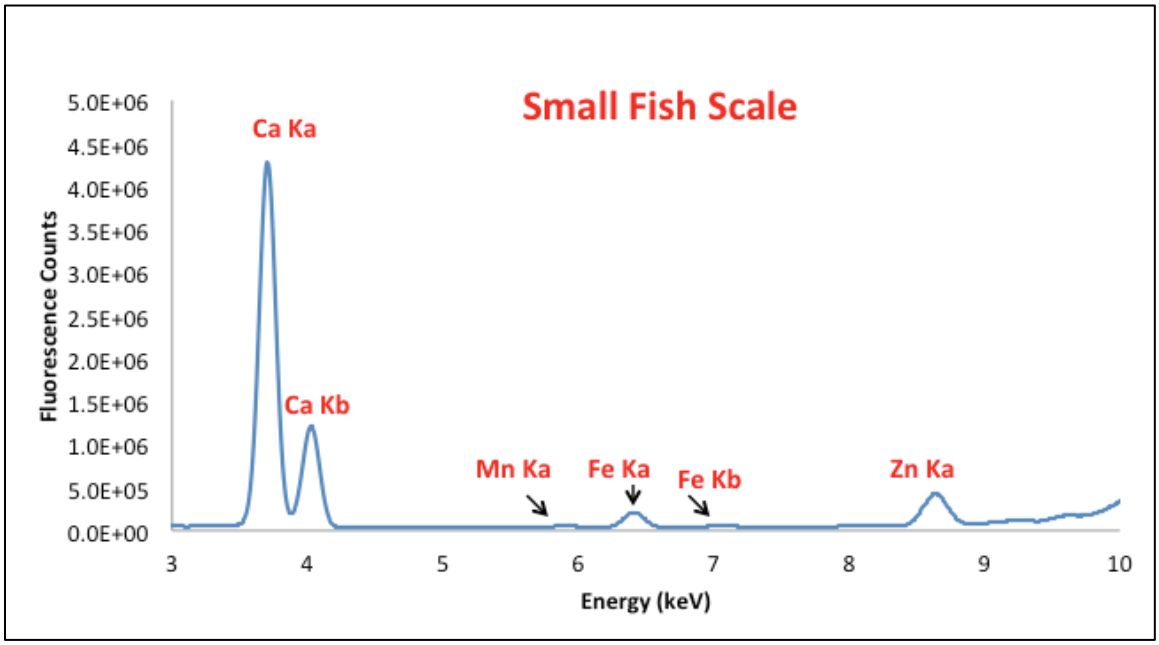

The MCA-plot identified calcium and zinc as the main elements found in the small fish scale. The trace elements found were iron and manganese. Observed in Figure 4.27 are the µm-XCT elemental two-dimensional distribution maps for Ca and Zn. The warmer colors (red/yellow) indicate areas of higher concentration. The Ca and Zn distribution appear in the concentric ring as sub-layers throughout the scale. The darker yellow area on Ca map indicates an increase in Ca concentration. When comparing the light white region to the synchrotron µm-XCT two-dimensional density map, Figure 4.28, to the yellow region in the µm-XRF calcium maps, Figure 4.27, the area is most likely the densest for the fish scale. Since the medium scale was much denser, the ultramicrotomy technique caused crinkling of the specimen during preparation. The µm-XRF measurements and maps obtained from the damaged specimens provided results that were inconclusive, Figure 4.29.

Figure 4.27. Synchrotron μm-XCT 2-D elemental distribution maps for Ca and Zn for the small fish scale.

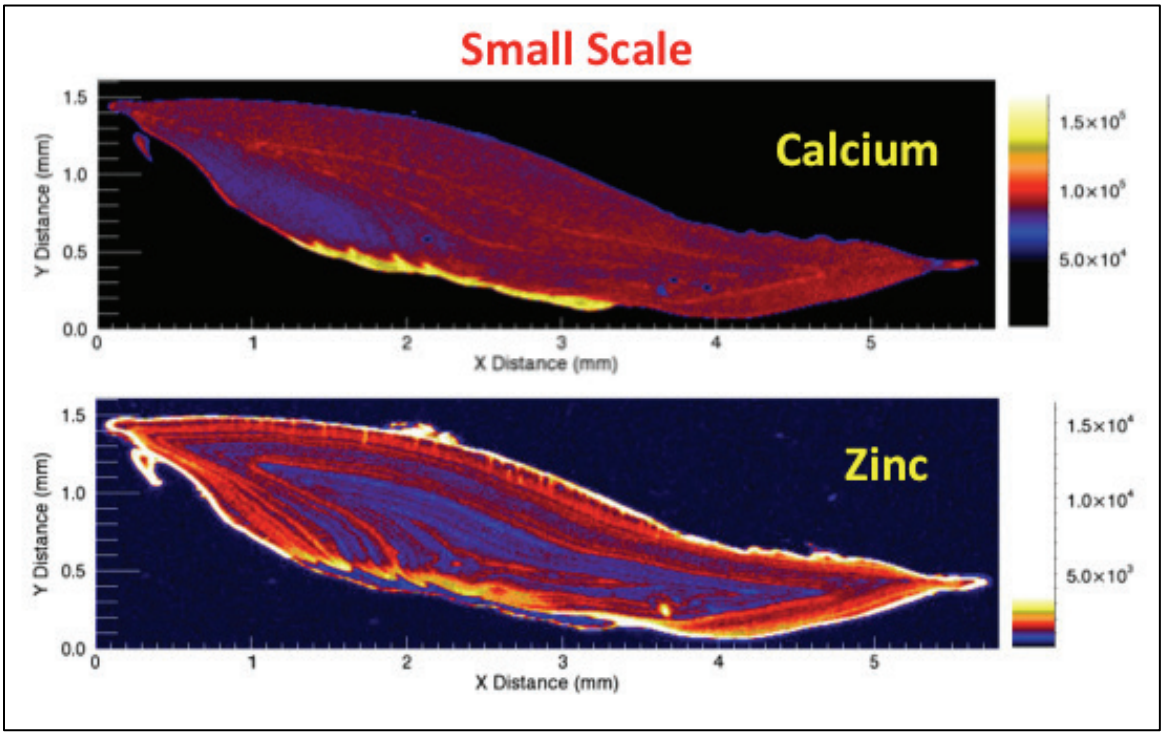

Figure 4.28. Synchrotron µm-XCT 2-D density map for the small fish scale.

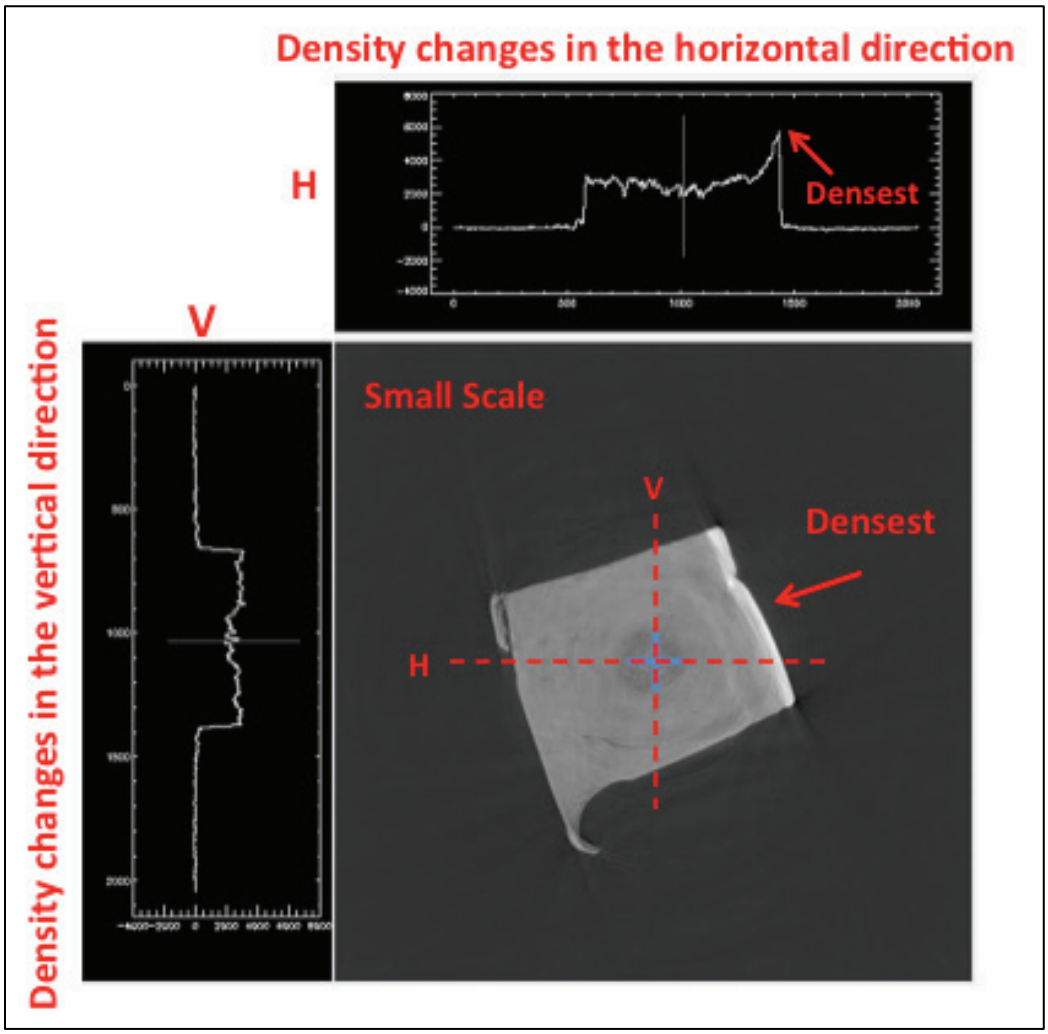

The µm-XANES spectroscopy was next collected for both the small and medium biomineralized scale for mineral speciation. The beamline was calibrated to 4,038 eV for calcium µm-XANES/XRF analysis and to 9,659 eV for Zinc µm-XANES/XRF analysis using standard metal compounds (X-RAY DATA BOOKLET, 2015). µm-XANES data were processed using a combination of the X27A data software and Athena software packages.

Figure 4.29. Synchrotron µm-XCT 2-D elemental distribution maps for Ca and Zn for the medium fish scale.

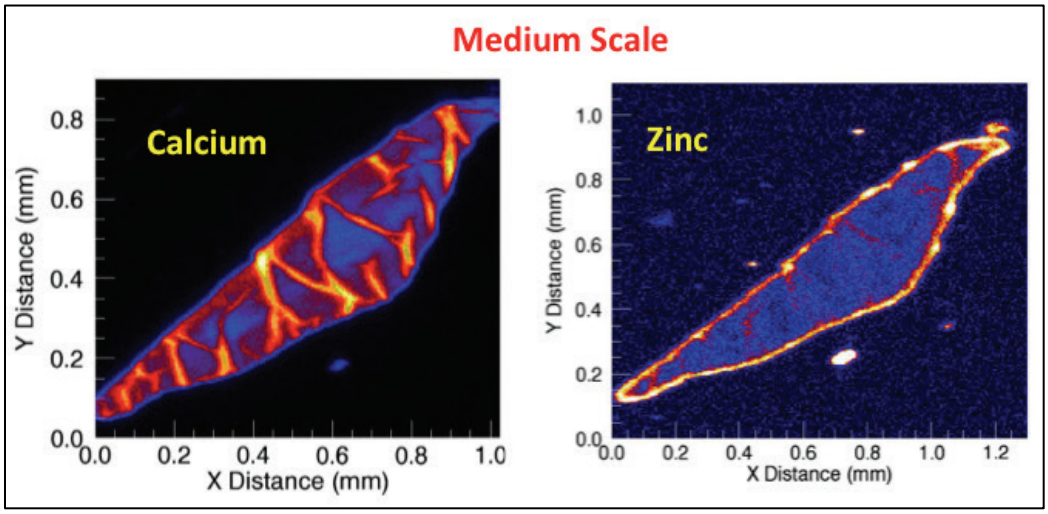

In Figure 4.30, µm-XANES spectroscopy is used to compare the collected experimental fish scale data to known Ca standards for energy absorbance. Calcium µm-XANES was used as a fingerprinting technique to determine the form of Ca in the fish scale. On the left are µm-XANES scans of only Ca standards-notice the differences between these compounds-this is critical when looking at µm-XANES plots. On the right are µm-XANES collected on a larger and smaller fish scale-note the similar structure-indicating that there is little difference in Ca speciation between the scales as they age.

The energy absorbance spectra, in Figure 4.31, are nearly identical to the bio-apatite (mouse bone) minerals as opposed to the pure inorganic Ca minerals. The comparison further indicated that Alligator gar fish scale is composed of a biogenic Ca-Phosphate mineral. Additionally, the amorphous Ca-phosphate mineral is a better fit than the pure apatite; therefore, the inorganic portion of the scale may be composed of amorphous Ca-phosphate.

When comparing fish scale µm-XANES data to known bio-apatite (mouse bone) and Zn-standards, Figure 4.32, an interesting trend was observed for the Zn. Zinc is distributed throughout the fish scale-it appeared to correlate closely with the Ca levels. The Zn XANES also indicates that the Zn in the Alligator Gar scale is much more closely related to Zn found in bio-minerals than pure inorganic phases. Chemistry suggests that Zn could replace Ca in the Ca-phosphate structure (Mucalo 2015). The role Zn plays in biomineralized bio-apatite is not well-understood.

Figure 4.30. Synchrotron μm-XANES spectroscopy plots for comparing the collected experimental fish scale data to known Ca standards.

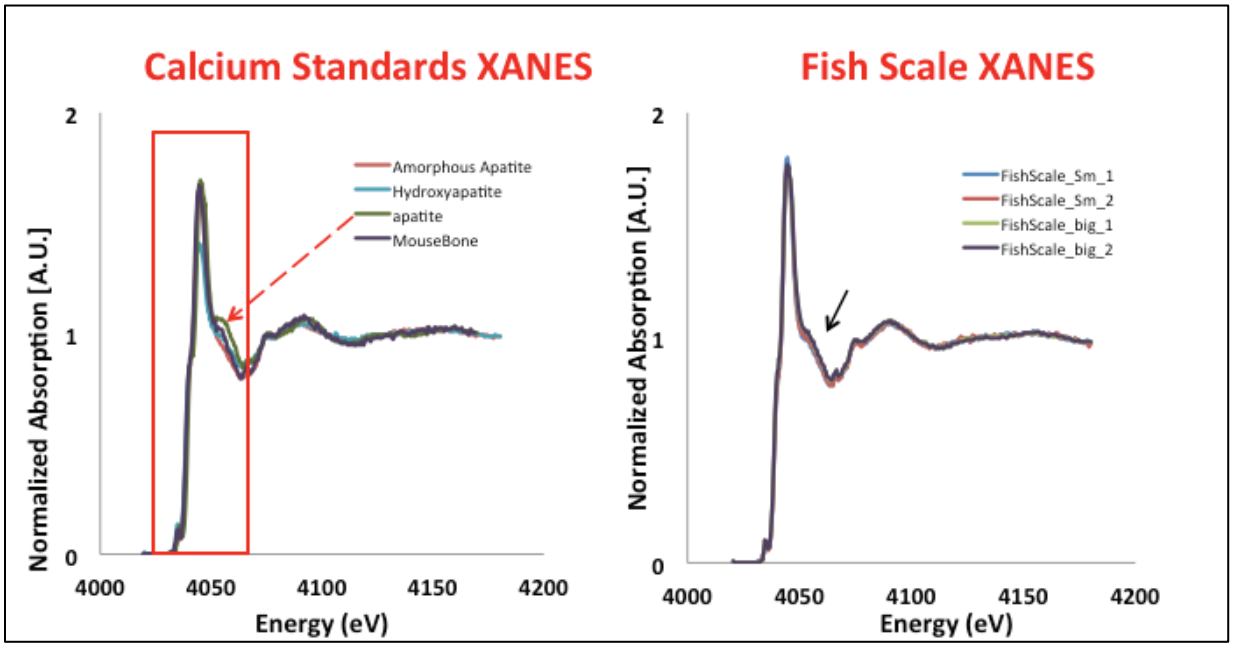

Figure 4.31. Synchrotron μm-XANES spectroscopy plots for comparing the collected experimental fish scale data to known apatite and bio-apatite (mouse bone) standards.

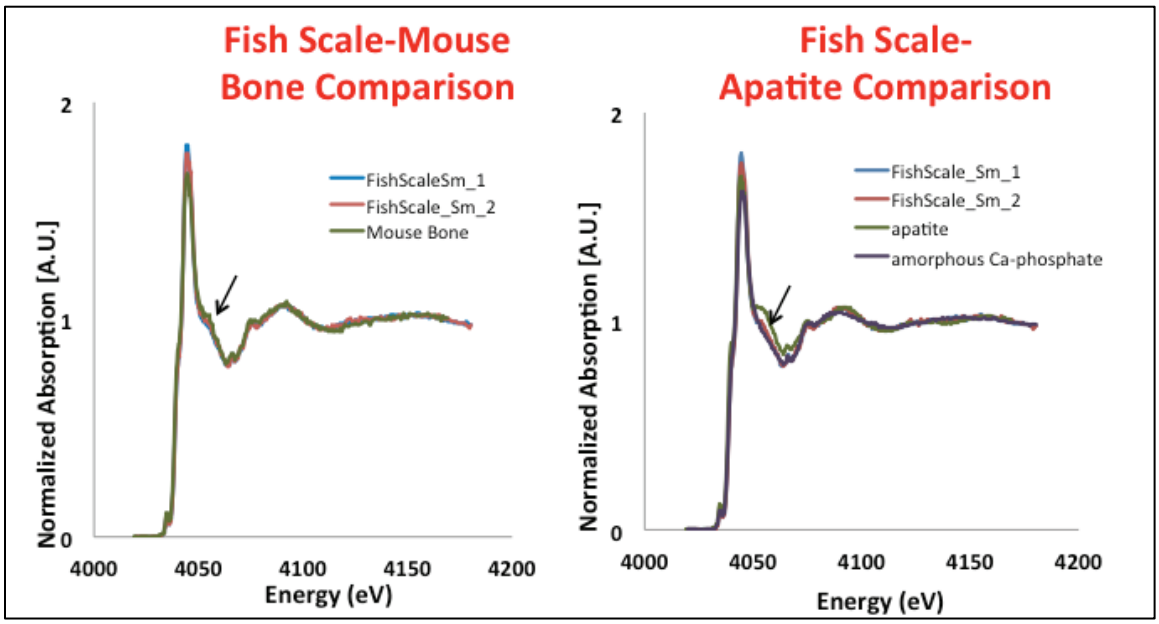

Figure 4.32. Synchrotron µm-XANES spectroscopy plots for comparing the collected experimental fish scale data to known bio-apatite (mouse bone) and Zn standards.

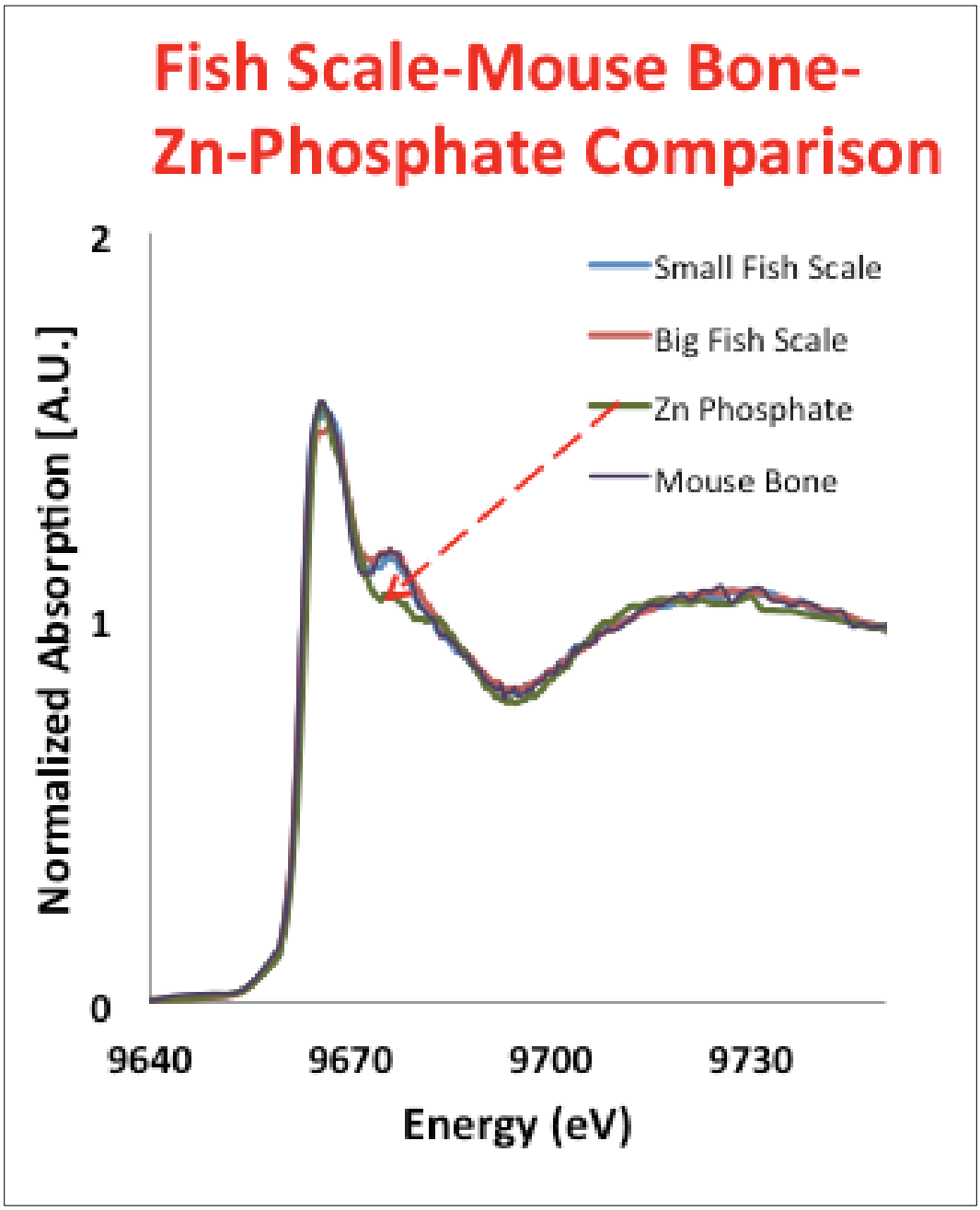

After completing synchrotron µm-XANES measurements the µm-XRD data were collected at 0.7093λ with aluminum oxide (α-Al_2O_3) and silver behenate ($AgC_{22}H_{43}O_2$) as calibration standards. Data were fit using Fit2D™ and Match!™ software packages. Once collected the µm-XRD spectra for the fish scale was compared to four-mineral types: Hydroxylapatite-(Carbonate), Apatite-Human Dental, Apatite-(F), and Apatite-(MnF). Provided in Figure 4.33 are the crystallographic structures along with

calculated stoichiometry for the relative quantities of reactants and products in chemical-reacted apatite minerals used for comparison (Wilson et al. 1999; Fleet et al. 2004; Hughes et al. 1989, 1991). As an aside, usually present in all matter is carbon, but it is difficult to measure so the reacted oxidation state is normally assumed in stoichiometric calculations.

Figure 4.33. Crystallographic structures and calculated stoichiometry for apatite minerals used in fish scale XRD comparisons (Wilson et al. 1999; Fleet et al. 2004; Hughes et al. 1989, 1991).

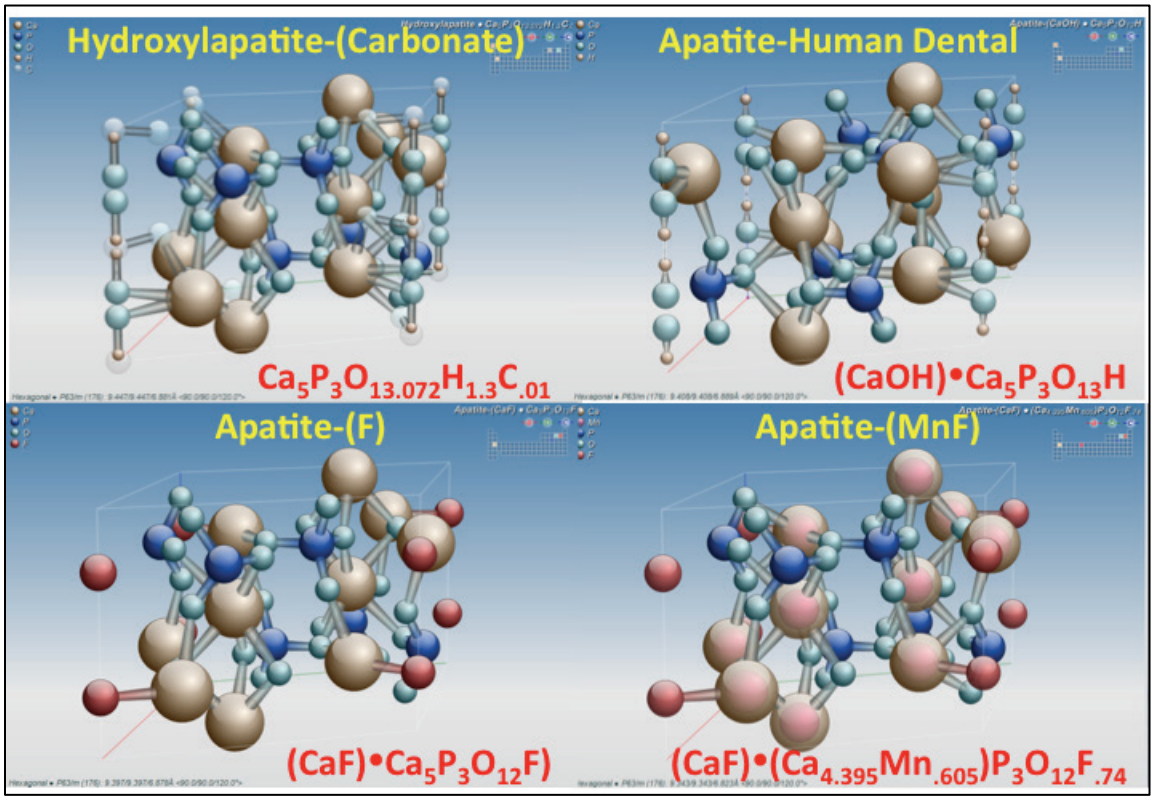

The mineral phase speciation for the small fish scale structure was proven to be an apatite-based mineral (Figure 4.34). In general, there were no discernible differences for the varying apatite structures shown by the comparison. Equally, the apatite minerals with elemental substitutions (Carbonate, Ca, F, and Mn) retain a similar pattern. Meanwhile, the µm-XRD crystallographic comparison with other apatites illuminated the P and F periodic elements in the fish scale structure. Recall, µm-XRF mapped the presence of Ca, Zn, Mn, and Fe elements. Since synchrotron x-ray experimental methods could be coupled, they were able to show distribution and speciation for major and trace elements for the fish scale structure. Data were not collected for the medium fish scale because µm-XRD experiment showed there was very little variation in apatite structures.

Figure 4.34. Synchrotron µm-XRD spectra for the small fish scale compared to several known varying apatite crystallographic structures.

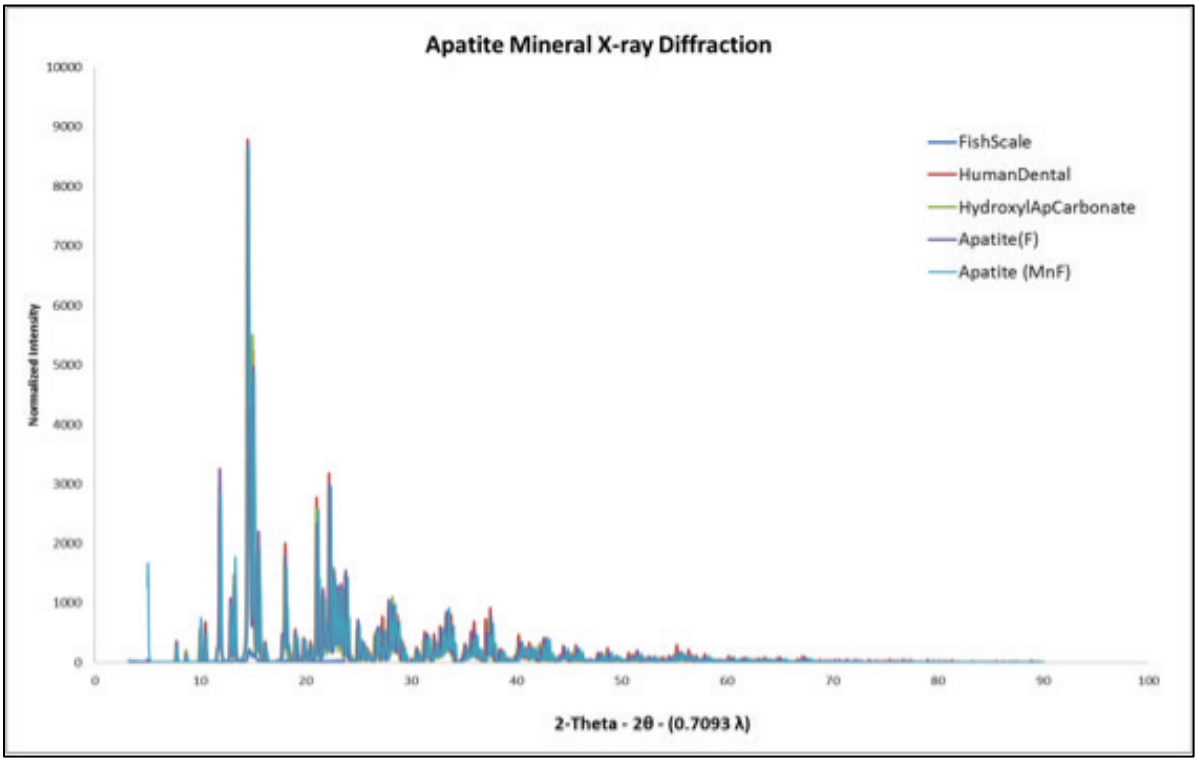

4.2.3 TGA

Phase changes and decomposition of apatite structure was studied by means of thermal gravimetric analysis. The TGA experimental technique measures total mineral and organic contents, including carbonated mineral and non-collagenous proteins, providing additional insight into bulk composition. Thermal response depends on the heating rate, amount of sample, and phase purity (Haines 1995; Bigi et al. 1997; Bahrololoom et al. 2009 Markovic et al. 2004).

Prior to TGA, the fish scales were wiped with filter paper to absorb the excess water on the scale surface. The experiment was conducted for both the small and medium scales. The initial mass for the small and medium fish scales were 55.3 and 46.3 mg, respectively. The samples were heated in alumina (Al_2O_3) crucibles. Using a Netzch™ system the scanning temperature range was from 35 to 1,550°C with a heating rate of 10°K/min, balance flow of 20 mL/min and a sample flow of 50 mL/min of ultra-purity N_2.

The results for TGA, shown in Figure 4.35, indicate there are three thermally identifiable processes. Water (free and physi-sorbed) loss due to evaporation occurs between 35 and 250°C. Calcination of the carbonated hydroxyapatite biomineral phase resulting from thermal decomposition and subsequent loss of chemically bound H_2O ($2HPO_4^{-2} \rightarrow P_2O_7^{-4} + H_2O$ [gas]) and CO_2 ($P_2O_7^{-4} + CO_3^{-2} \rightarrow 2PO_4^{-3} + CO_2$ [gas]) occurs between 250 and 1,000°C. During calcination, the decomposition of collagen and combustion of the residual organic components occurs between 250 to 450°C and removal of carbonate ions from the inorganic phase between 450 and 1,000°C.

Figure 4.35. Thermal gravimetric analysis for the small and medium fish scales.

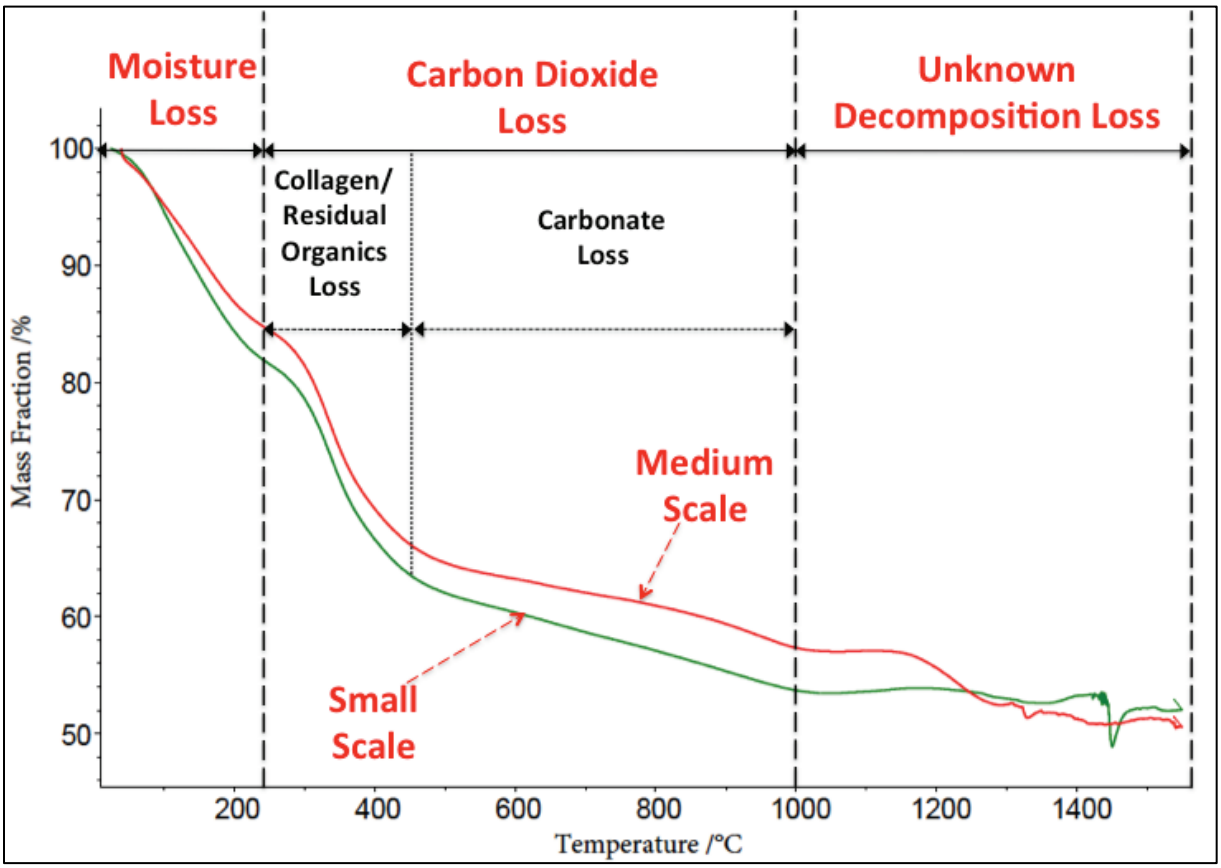

The assumption made from μm-XRD crystallographic comparison was that the chemical composition of the fish scale structure produces a carbonated bio-apatite structure (B-Ap); thus, the decomposition beyond 1,000°C is uncertain. The uncertainty is due to lacking full knowledge of the starting composition. As earlier discussed, trace elements measured at a given energy state depend on their measurable molar concentrations

being below 1000 ppm; therefore, all elements in the structure may not be detectable.

Previous research has described carbonate is liable in apatite-based minerals and can be substituted with cations and anions (Tonsuaadu et al. 2012). Depending on the element type and molar concentration used to modify the atomic structure, the carbonate may either produce apatites that range from thermally unstable to highly stable molecules. Ion exchange has been explained to occur more freely in calcium-based bio-apatites with Al, Si, Cl, Na, Mg, Zn, P, Mn, F, Fe, and K periodic elements (Fleet 2015; Liou et al. 2004; Mathew and Takagi 2001; Young 1974). Also provided in this dissertation is evidence, obtained from TGA, that can be used to postulate how calcium carbonate allows nature to substitute elements based on availability and can evolve as needed to maintain a stable biomineralized structure.

Additionally, TGA was able to support the assumption made for the carbonate presence because of the reported temperature range for mass loss, so the difference in the small and medium fish scale results can be elucidated. For biological materials that have composite layers with graded calcium concentrations that cause a density distribution, the rate of calcination will vary. As shown in teeth, which are akin to fish scales, there exists an outer denser layer with higher calcium concentrations than the underlying layer (Nieto and Livi 2013). Unlike the teeth, but similar to bone, the fish scale layers become denser with growth/age thereby requiring elevated temperatures to calcine the medium scales when compared with the small scales.

4.2.4 SS-NMR analysis

Solid-state nuclear magnetic resonance was used to investigate the organic phase contained in the biomineralized fish scale structure. The organic phase is the proteinaceous fibrous components that are assembled from amino acid groups. The molecular structure for the amino acid group is defined by bond length, angles, and orientation of atoms. The resonant frequency for atoms can be used to identify/speciate the bound elemental constituents in the organic carbonate phase.

For heterogeneous structures, SS-NMR results are inherently anisotropic. The measured peaks are often broad, with substantial overlap among the different carbon functional groups. To overcome the ambiguous

overlapping for the carbon groups, “selective” Cross-Polarization (CP) techniques were used to dephase some groups over others. The following five SS-NMR one-dimensional cross-polarization techniques, “(a)-(e),” were used to amplify the carbon compounds: (a) Total Carbon Speciation (CP-TOSS) can be used to determine the carbon group type, (b) Dipolar De-phasing (CP-DD) can be used to identify “unprotonated” and “mobile” carbon segments, such as quaternary carbons and rotating CH_3 groups respectively, (c) Chemical Shift Anisotropy (CP-CSA) can be used to search specifically for sp^3-orbital-hybridized carbons, (d) Dipolar De-phasing Difference (CP-DDD) can be used to find explicitly the protonated carbons, and (e) Carbon-Hybridized (CP-CH) can be used to select only sp^2-orbital-hybridized carbon groups while de-phasing all other groups.

The SS-NMR experiment was performed on the small fish scale only. The results from TGA showed both fish small and medium scales had similar organic thermal decomposition rates; therefore the chemical structure does not drastically change with age. The results from the one-dimensional SS-NMR spectra, shown in Figure 4.36, provide the biopolymeric composition for the small-mineralized fish scales.

The cross-polarization diagnostic examination of carbon nuclei, within the complex fish scale structure, shows strong evidence for carboxyl (COOH) groups within the samples, indicating the presence of organic acids. The spectra greater than 150 ppm were truncated due to substantial carbon overlapping. However, not shown at 172 ppm, a strong/narrow peak occurs that suggests the proteinaceous materials are formed from amino acids. Below 150-ppm CP-TOSS spectra resembles collagen. Also seen is a strong absorbance at 24 and 16 ppm indicating alkyl-bearing (nonpolar) fatty acids.

The CP-DD pulse spectra cannot efficiently dephase the “mobile” CH_3 groups within the samples. Yet, peaks at approximately 75 ppm suggest the carbon is associated with the hydroxy-proline amino acid group. Identical peaks appear as quaternary carbons and sp^3 quaternary carbons; however, the latter is scaled differently in plots labeled CP-DD. The CP-CH selection technique emphasizes absorbance between 40 and 70 ppm, indicating highly substituted sp^3-hybridized carbons with only one hydrogen atom. The relatively high chemical shift (>40 ppm) suggests that the substituents (single and double bonds) are largely oxygen, not nitrogen, to carbon.

Figure 4.36. SS-NMR 1-D spectra showing the biopolymeric composition for the mineralized small fish scale.

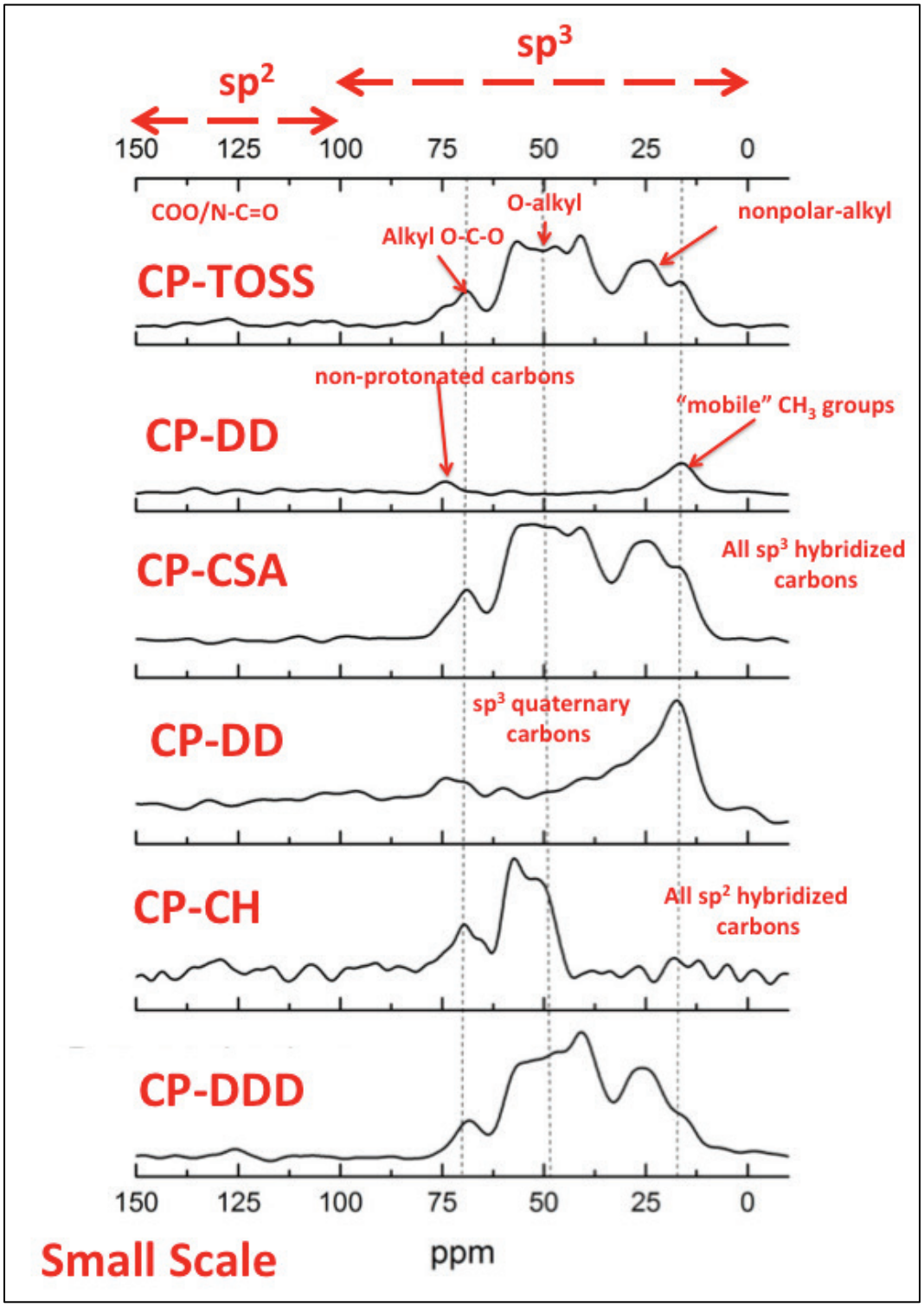

The widths of the absorbance bands suggest the organic material is relatively non-crystalline. There are a wide variety of organic molecule types, combination of amino acid residues, polysaccharides, and fatty acids. No aromatic compounds were found. However, the SS-NMR instrument could not produce a sufficiently higher resonant frequency so uncertainty lies in whether any aromatic-bearing amino acids are present. Knowing the type of amino acids could specify the collagen type. Higher resonance frequencies are needed to better detect the presence of aromatic carbons, which usually can be seen at approximately 120 ppm. But because the hydroxyl-proline amino acid group could be identified, it is likely that Type-I collagen is present in the fish scale.

4.2.5 FTIR analysis

The FTIR analysis was used to further investigate the inorganic/organic molecular phase compounds. The mechanical behavior for carbonated bioapatites containing mineralized collagen fibers is a function of the atomic inter/intra atomic bonds strength for the (Chang and Tanaka 2002). The vibrational frequencies, produced by FTIR, excite the atomic bonds and were used to identify/speciate the different phase compounds. Spectral FTIR analysis also provided spatially resolved information regarding the chemical and structural composition of the fish scale.

The FTIR spectra for bioapatites are very complex, so researchers mainly focus on the phosphate, carbonate, and collagen bands (Grunenwald et al. 2014). Usually, the spectra from the amide functional groups are used to specify collagen types. Supplemental to the phosphate, carbonate, and collagen bands; the vibrational spectra for hydrocarbons (CH_X) and hydroxide (OH^-) compound classes are sometimes measured as well.

A Nicolet 6700 ™ FT-IR spectrometer interfaced with Continuum FTIR microscope equipped with a single bounce Attenuated Total Reflectance (ATR) attachment was used to collect FTIR spectra for the polished fish scale cross section. The ATR attachment included a germanium (Ge) internal reflection element (IRE) and mid-range spectra were collected between 750 and 4000 cm^{-1} with 4-cm^{-1} magnification, averaging 512 scans. Using the same justification provided during the SS-NMR results presentation in Section 4.2.5 on TGA only the small fish scale was examined. Spectra was collected on the outer layer and the less dense internal layer of the small fish scale, at seven line-scan locations, to determine differences between and within the layers.

The FTIR results, in Figure 4.37, for the small fish scale were compared to published research. Previous researchers compared ATR-FTIR spectra for the three reference materials of cortical bone, hydroxyapatite, and Type-I collagen (Figueiredo 2015). The pertinent chemical and structural details used for comparison were extracted from the 750 to 1,800-cm^{-1} spectral range, inside the red dotted rectangular box. The FTIR spectra for the fish scales' outer [Locations 1 through 5] and inner [Locations 6 and 7] layers identify the main functional groups present as amide, carboxylic, phosphate and carbonyl. Specifically, a strong absorbance band at ~1,000 cm^{-1} signifies phosphate (PO_4) stretching was occurring in both layers of the fish scale spectra. Also, distinctive absorption bands characteristic of carbonate substitution for phosphate in apatite were present at ~870, ~1,420, and ~1,450 cm^{-1} in both layers. The spectra of inner layer of the fish scales showed peaks at ~1,660, ~1,520, ~1,225 cm^{-1} denoting amide I, II, and III absorption bands common to Type-I collagen.

When comparing the compounds for fish scale to the three reference materials the ATR-FTIR spectra most closely resembles as an analogue to either the cortical bone or Type-I collagen structures. Generally speaking all spectra beyond 1,800 cm^{-1}, for fish scale, were nearly identical to cortical bone. Interestingly, the spectra collected in this study differed not only between the two layers but within the individual layers. Limited conclusions can be drawn for the quantity of individual compounds within different layers of the fish scale from FTIR data. However, the results suggest the carbonate (CO_3) present in the two layers might differ either in chemical composition or in concentration depending on location within the fish scale. Moreover, the carbonate phase might be either highly mineralized or amorphous and liable for anion substitution at lower degrees of mineralization (Chang and Tanaka 2002).

Figure 4.37. FTIR results for the small fish scale compared to that of cortical bone, hydroxyapatite, and Type-I collagen reference materials.

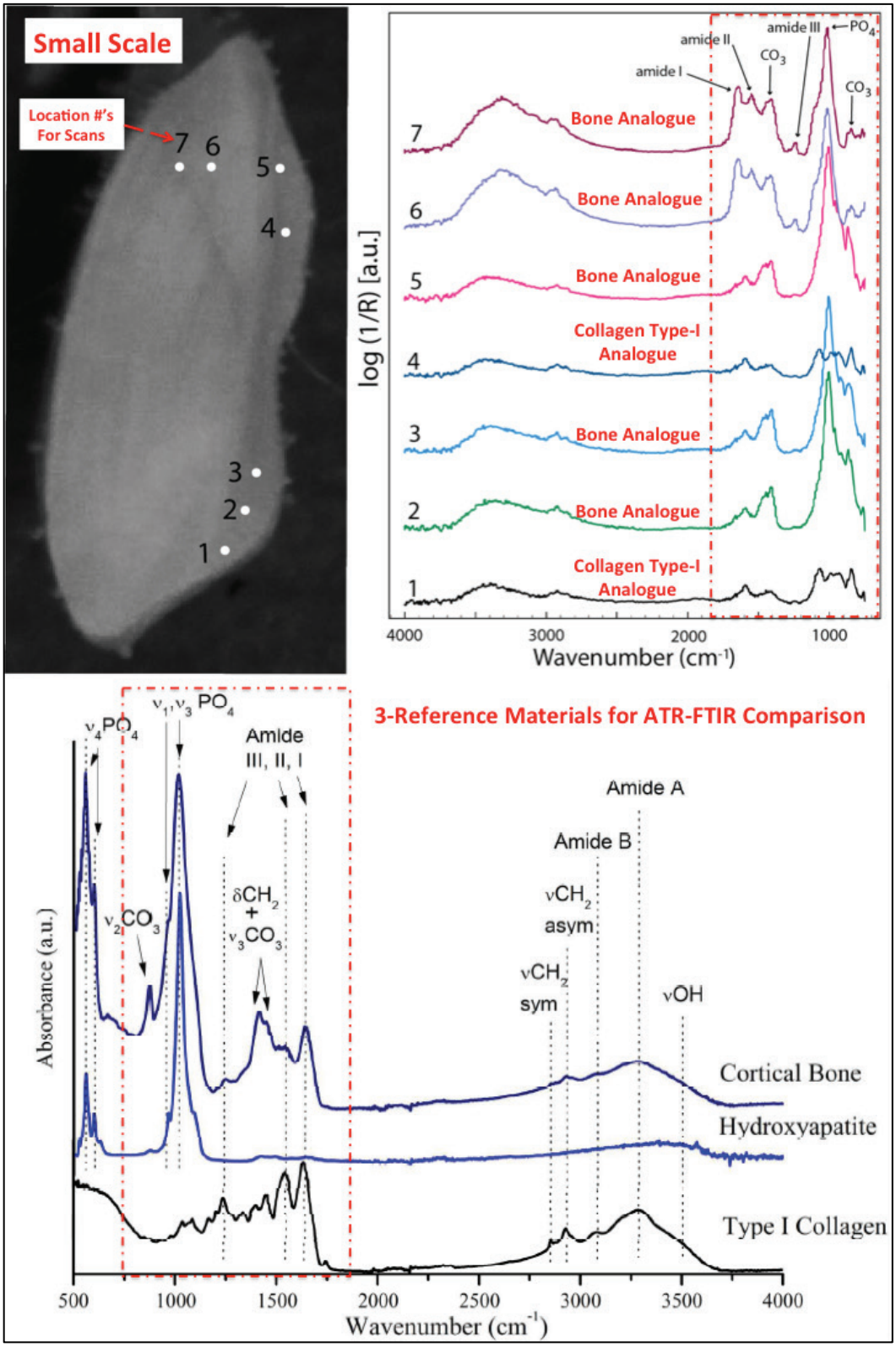

Also detected in both layers were the amide peaks, which are associated with Type-I collagen. The peaks were shown to be much less prominent in the denser outer layer than the inner layer. Yet, the spectra at locations 1 and 4 appear different than other spectra in the denser layer. The cause for the differences is uncertain but could be attributed to morphology changes in the structure. A review of locations 1 and 4, in Figure 4.37, indicated the measurements were taken at the layers' interface. Shown during the SEM investigation, separation at the interface caused by fracture or shrinkage can occur exposing fibrous collagen. Recall, the FTIR analysis was conducted on fully dehydrated specimens; the hydration-dependent Collagen-rich inner layer may have contracted, thus exposing the separated collagen fibers at the layer interface leading to the differing spectral measurements.

4.2.6 μm-XEDS and EMPA

The μm-XEDS and EMPA were used to identify the lighter periodic elements, by molar concentration (M), which could not be measured from Synchrotron X-ray, TGA, SS-NMR, and FTIR experiments. First, μm-XEDS data were collected to identify the bulk composition followed by EMPA, which was used for spatially correlating elemental distribution. The information gathered was used to assist with estimating the stoichiometric composition in the fish scale's structure. Typically, the electron signal for the micro-probe is calibrated to mineral standards.

The mineral standards were selected based on the likely compositional elements for carbonated bioapatites (Fleet 2015, Iyengar and Tandon 1999). The premise for using known mineral standards with EMPA is two-fold (Russ 1984; Marinenko 1991; Reed 1996; Sanchez-Quevedo et al. 1998; Goldstein et al. 2007). Firstly, the mineral standards are used to identify unknown elements for a substance. Secondly, the standards are used to determine if there are impurities present in embedded inorganic-organic bound phases, based on electron signal loss that may not be straightforwardly measured directly (e.g., carbonates and phosphates). The minerals standards used were Albite, Zaby Enstatite, and Chlorapatite. Collectively the mineral standards represent known molar concentrations for periodic elements of aluminum (Al), calcium (Ca), chlorine (Cl), chromium (Cr), fluorine (F), iron (Fe), potassium (K), magnesium (Mg), manganese (Mn), sodium (Na), oxygen (O), phosphorous (P), silicon (Si), and titanium (Ti). Notice elements of carbon (C), hydrogen (H), and nitrogen (N) are not represented. The C, H, and N elements are essential for

maintaining life in organic matter, but because of oxidation or storage states accurate measurements tend to be difficult to achieve and were not taken.

The mineral standards discussed above were used to calibrate a JOEL 8600™ microprobe, interfaced with Philips EM 420™ TEM, and equipped with an Oxford™ EDS detector. To detect the elements in the biomineralized fish scale structure, 15-keV at 40x magnification was used. Both the small and medium fish scales were investigated using EMPA. Three line scans per polished fish scale cross section were collected to spatially resolve elemental composition. Each location in the line scan had a 20-μm diameter spot size.

Prior to conducting line scans the entire fish scale's cross section was mapped to identify any periodic elements that are common for most biomineralized structures. The elemental compositional μm-XEDS maps for the gray-scale backscattered small fish scale image are shown in Figure 4.38. The individual elemental maps for Al, Ca, C, Cl, Mg, N, O, P, Si, Na, Sr, S, and Zn are interpreted as the lighter colors and the highest concentration areas with the darker-shaded colors being the least concentrated areas for the same color bands. The maps show periodic elements of C, N, Si, Sr, S, and Zn were not detectable. However, the trace elements that could be detected were Al, Cl, and P. The element of aluminum may be an artifact caused by the alumina suspension remnants used during polishing. Higher Cl concentrations are in the less dense layer whereas the concentrations for P elements are observed in the densest upper layer. The major electron signals of Ca, Mg, Na, and O elements were detected. The highest concentrations of Ca and Na were identified in the densest upper layer compared to the highest concentrations of Mg and O in the less dense lower layer.

In addition to mapping the individual elements, EMPA was used to measure the atomic percent of molar concentrations. The atomic unit for each element was based on electron energies that could be sufficiently measured in the medium fish scale's cross section by line scans and are shown in Figure 4.39. The combined results from Synchrotron X-ray, TGA, SS-NMR, FTIR, μm-XEDS and EMPA indicate the fish scale structure is a carbonated bioapatite that contain periodic elements of Al, C, Ca, Cl, Fe, H, Mg, Mn, N, Na, O, P, and Zn. The experiments delineated the elements contributing to the fish scales' structural formation, now the overall chemical compound can be estimated. The measured units can be

used to determine the first approximated stoichiometric relationship for the assumed molecular formulation of $Ca_{(10-x)}\bullet[]_x[(PO_4)_{(6-x)}(CO_3)_x]\bullet(OH)_{(2-x)}\bullet[]_x$ (Tonsuaadu et al. 2012; Wopenka and Pasteris 2005). To allow for equation balancing the carbon oxidation state is fixed with a 2^+ charge. The shortcoming for the assumption is directly determining what atomic units are bound to both inorganic and organic phases is not trivial.

Figure 4.38. µm-XEDS elemental distribution maps for small fish scale's cross section.

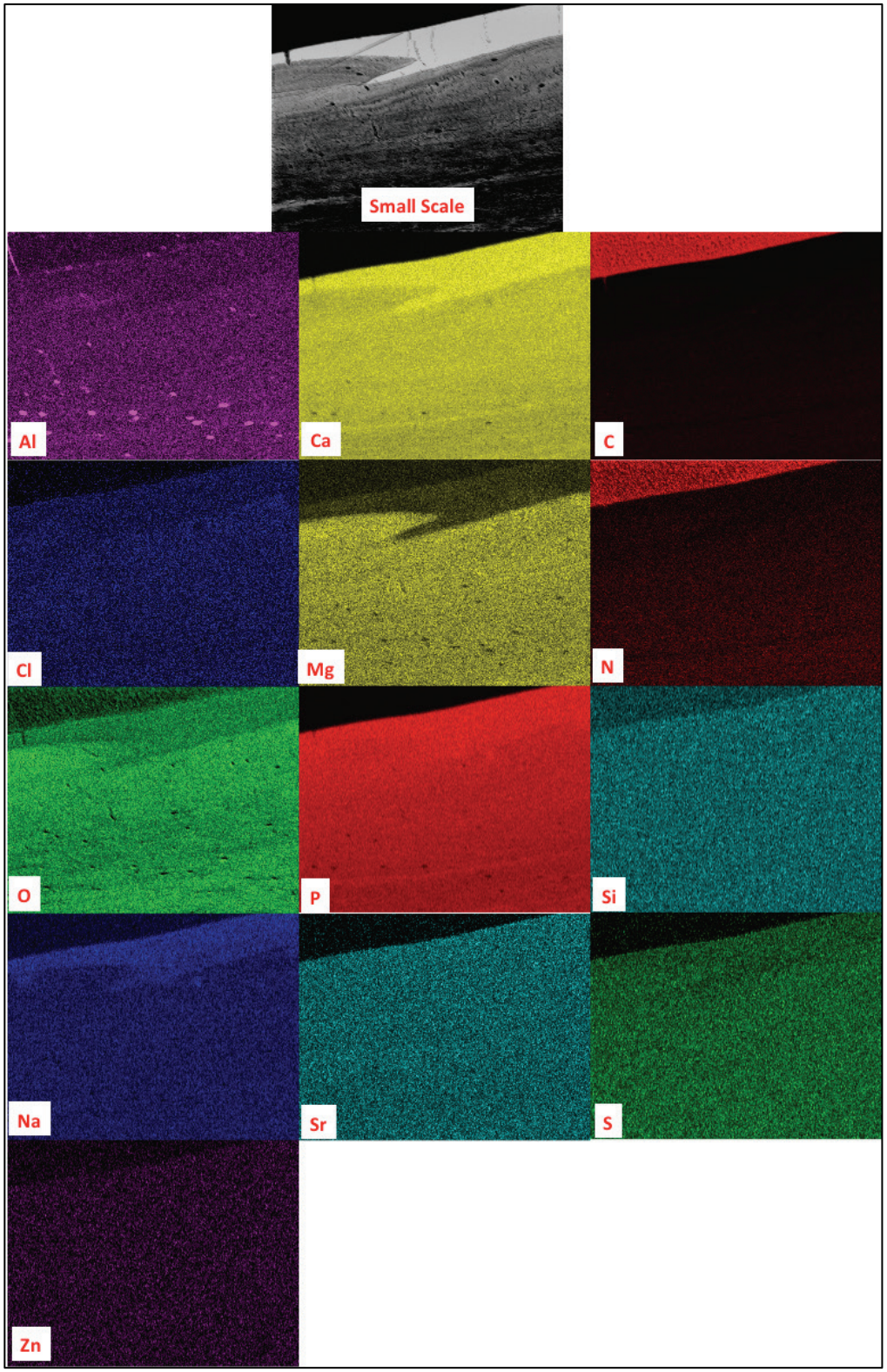

Figure 4.39. EMPA line scan elemental maps for medium fish scale's cross section.

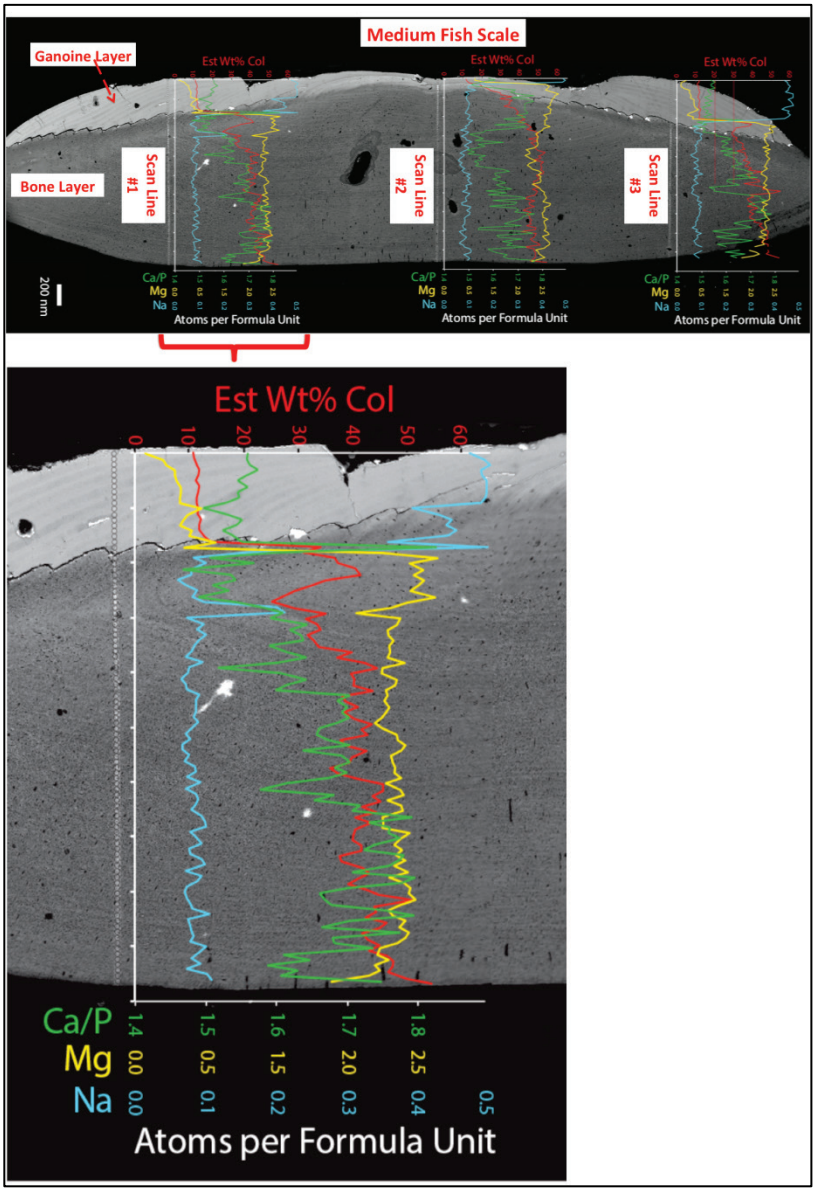

Plotted from the line scans, in Figure 4.39, are calculated mineral formulae for the inorganic hydroxyapatite (HAp) reported as atoms per formula unit at the bottom. On the top, in red, is plotted a first approximation of the collagen content, which is estimated by subtracting the sum of the inorganic oxides from one hundred percent. Because line scans were able to confirm the layer elemental concentrations, the structural layers can be identified by layer names as defined by previous researchers (Yang et al. 2012; Yang et al. 2013a; Yang et al. 2013b). The denser outer layer is known as ganoine, while the inner less dense layer is bone. The three traverse scans across the scale are each somewhat

different. The commonalities are: the ganoine is higher in Na, lower in Mg and collagen, and has a lower Ca/P ratio than the bone regions. The Ca/P ratio in the ganoine layer range was 1.55 to 1.66 while in the bone layer 1.55 to 1.90.

Of the three calculated mineral formulae Ca/P ratio is the most informative. The ratio is used to determine the degree of mineralization. In the extracellular matrix the mineralized tissues contain phosphorus, which is highly anionic and, hence, has the ability to bind to calcium. As a result, the strength and density for the biomineralized structure depends on the degree of binding for calcium in the presence of the phosphorus (Boskey 1991; Shapiro et al. 2014; Fleet 2015; Chang and Tanaka 2002; Grunenwald et al. 2014). The ideal calcium-to-phosphorus ratio for the standard geological apatite is 1.67. When Ca/P ratios are less than 1.67, usually the mineralization is decreasing whereas for higher ratios mineralization is increasing (Fleet 2015). In bio-applications the Ca/P ratio is typically used as a diagnostic parameter to evaluate health of vertebrate or determination for biosynthesis stability/compatibility (Boskey 1991; Shapiro et al. 2014; Mucalo 2015; Fleet 2015). For the fish scale investigation the Ca/P ratio was used to interpret the biomineralization process and identify the difficult-to-measure supplementary carbonate phase. Carbonate ions are found to substitute anions in biological apatites. The carbonates can substitute ions for OH^- (type A carbonate) and PO_4^{3-} (type B carbonate), which can possibly be quantified by the Ca/P ratio.

Focusing on the ITZ that corresponds to just under the ganoine where the structure is densest, as shown earlier in Figure 4.21, the HAp and collagen there are highly oriented and densely packed. Further away from the ganoine, beyond the transition zone, the estimated collagen (Est. Col.) content increases and the overall Ca/P ratio increases. However, as the microprobe samples bands of bright intensity, in general, the collagen and Mg content drop while the Ca/P and Na increase.

Remember, until now all experimental evidence has shown the densest layer is in the ganoine regions, so why does Bone HAp + Collagen have a higher Ca/P? The following reasons are provided: (a) CO_3^{-2} substitutes for PO_4^{-3} in HAp. CO_3^{-2} could be increasing away from the Ganoine interface, lowering P, raising Ca/P. The substitution is consistent with other reported findings that young HAp has more CO_3^{-2} than mature HAp (Fleet

et al. 2004; Tonsuaadu et al. 2012; Fleet 2015; Figueiredo 2015). (b) The level of carbonation is also known to increase with the maturity of the HAp, see TGA result in Figure 4.35, so more vacancies in P are expected to occur further away from the (higher mineralized) ganoine, while aging vacancies decrease.

Apatite compounds are often nonstoichiometric due to the presence of vacancies in calcium and hydroxide sites. Still unknown are the effects of CO_3^{-2} and vacancy content on the physical/mechanical properties of HAp versus collagen. The presence of carbonation ions can clearly influence crystallization processes. The ions may also provide stabilization for the collagen embedded inside the apatite crystalline structure. Furthermore, the phosphates are related to mineral crystallinity as well. An increase in the mineral crystallinity is indicative of an increase in mineral size and/or decrease in the non-stoichiometric substitutions (Boskey 1991; Fleet et al. 2004; Bigi et al. 1997; Bahrololoom et al. 2009; Grunenwald et al. 2014; Figueriredo 2015). To better understand the effects that chemistry has on the fish scale's crystalline structure and mechanical properties, further analysis was conducted at the nanometer-length scale using TEM, STEM-HAADF, STEM-EELS, and nanoindentation.

4.3 Investigation of length scale [1-1,000] nm

4.3.1 TEM observations

To this point the discussion of results, for the current research effort, have illuminated pertinent information with respect to the fish scale's chemical content and structure at both the millimeter- and micron-length scale. However, information is lacking for the description of the biomineralized structure at the nanometer-length scale. Therefore, TEM will be used to better clarify the structural details for the individual biomineralized collagen-HAp units for the composite system.

The fish scales have been shown to be an extremely complex biological system in itself with anticipated complexity increasing when exploring the lower nanometer-length scale. As a result only the medium fish scale's cross section was investigated. The thought process for selecting only the medium fish scale for exploration was based on the required detailed investigative efforts to probe the nanometer scale that are very extensive along with specimen preparation being quite rigorous. So the main objective set forth was to use TEM efficiently to examine the fish scale,

specifically at the nanometer range, to define geometries for subunits of collagen and HAp. Contingent to TEM and as continuation of the main objective, STEM based experiments are better suited to identify the assemblages and chemistry for the combined subunits of the layered system if there is greater disparity. Ultimately, the medium fish scale is thought to offer the greatest disparity because of its size and age, which were used to interpret formation processes for the layers when both STEM and TEM experimental results are combined.

Shown in Figure 4.40 is an electron image produced using the Philips EM 420™ TEM instrument. The specimen was prepared using the FIB sectioning technique from an osmium tetroxide (OsO_4) stained fish scales' cross-section. Staining was used to irradiate the collagen (soft tissue) fibers within the biomineralized scale. The image indicates there are three distinctly different layers. From top to bottom is the highly mineralized-densely packed ganoine, densely woven ganoine-bone interface, and loosely woven bone layers.

Figure 4.40. TEM image prepared using FIB sectioning technique from an osmium tetroxide stained medium fish scale's cross section.

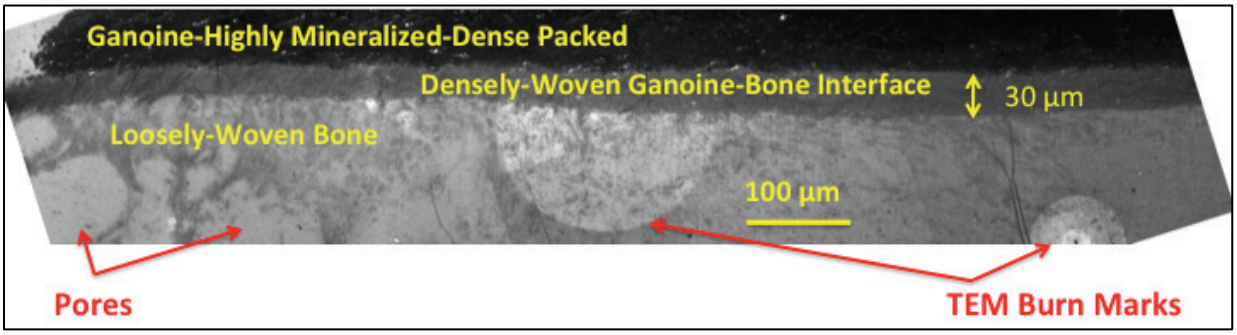

At the finer 5-µm magnification, in Figure 4.41, is a TEM montage image showing the ITZ for the ganoine and bone layers. To highlight the stained collagen fibers, the contrast for each layer was set independently. The contrasting identifies the packing arrangement for the collagen fibers. The darker region, from staining, indicates the highest packing density occurs in the ganoine for the collagen. Also from contrasting at 1-µm magnification, in Figure 4.42, there seems to be a packing density gradient; it shows collagen packing decreasing when progressing from the highly mineralized ganoine, through the densely woven ITZ, into the loosely woven bone layers. Collagen fibers have 67-nm periodicity subunits within the chain and are approximately 70-nm in diameter with an unidentifiable total length. Additionally, in Figure 4.41, the dark ITZ region inside the yellow-dashed

box was investigated at a much finer magnification. When viewing the ITZ at the 200-nm magnification, Figure 4.43, the collagen appears to bridge the interface and penetrate both layers.

Figure 4.41. TEM montage image showing the ITZ for the ganoine and bone layers from a stained medium fish scale's cross section at the finer 5-µm magnification.

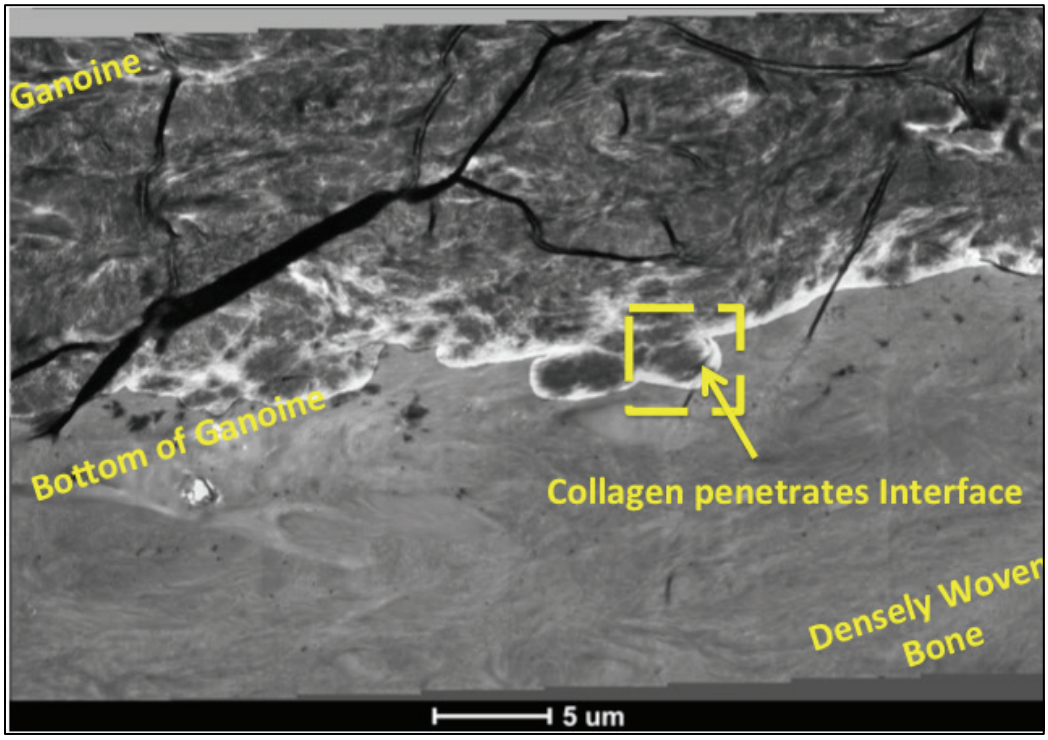

Figure 4.42. TEM montage image showing the collagen packing density gradient for a medium fish scale layers from the stained cross section at 1-µm magnification.

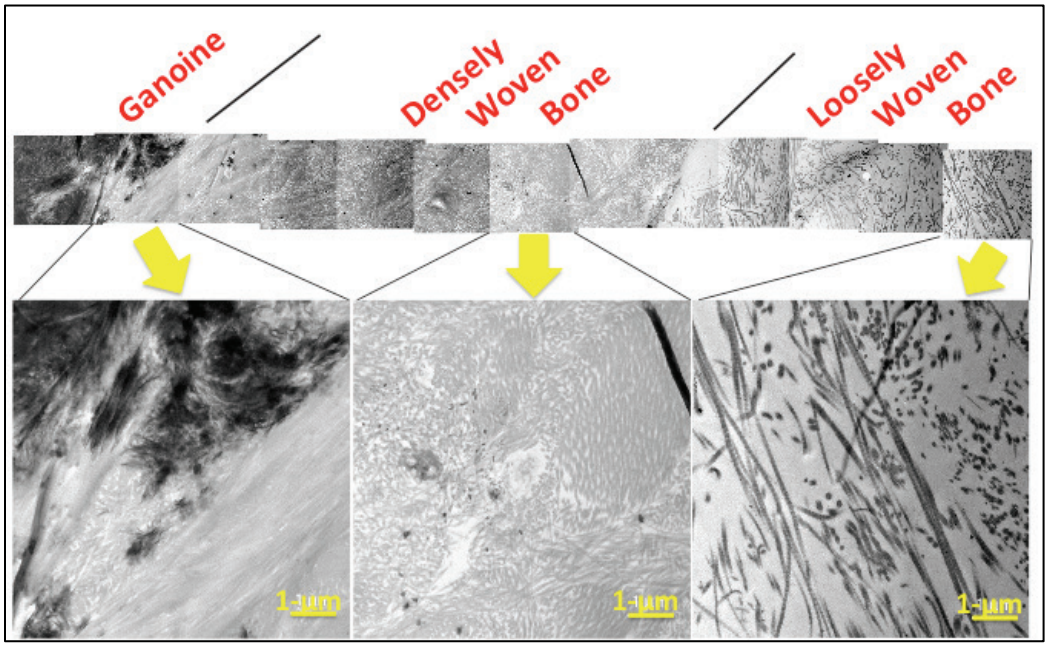

Figure 4.43. TEM image showing the highly ordered collagen arrangement in the ITZ at the finer 200-mm magnification.

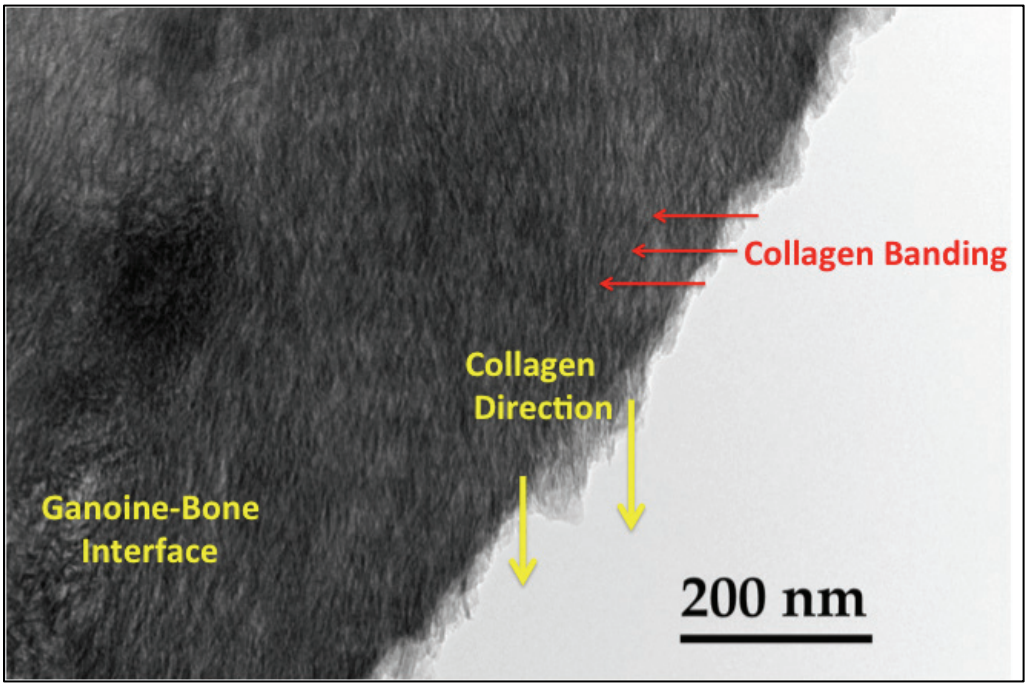

The collagen arrangement is highly ordered at the ganoine-bone interface. Yet, illustrated by Figure 4.44, the collagen arrangement much further into the bone layer seems to be more chaotically ordered. Further away from the ganoine, the bone become less dense, more open and having collagen-HAp composite fibrils that are more twisted. After zooming into the rectangular-dashed sections there are randomly woven patterns visible. Inside the woven patterns there are tubules (cavities) that are lined with amorphous materials. The tubules may be related to cavities and canals discussed earlier in Figures 4.14 and 4.17.

Figure 4.44. EM image showing the chaotic ordered collagen arrangement in the bone layer at the finer 200-mm magnification.

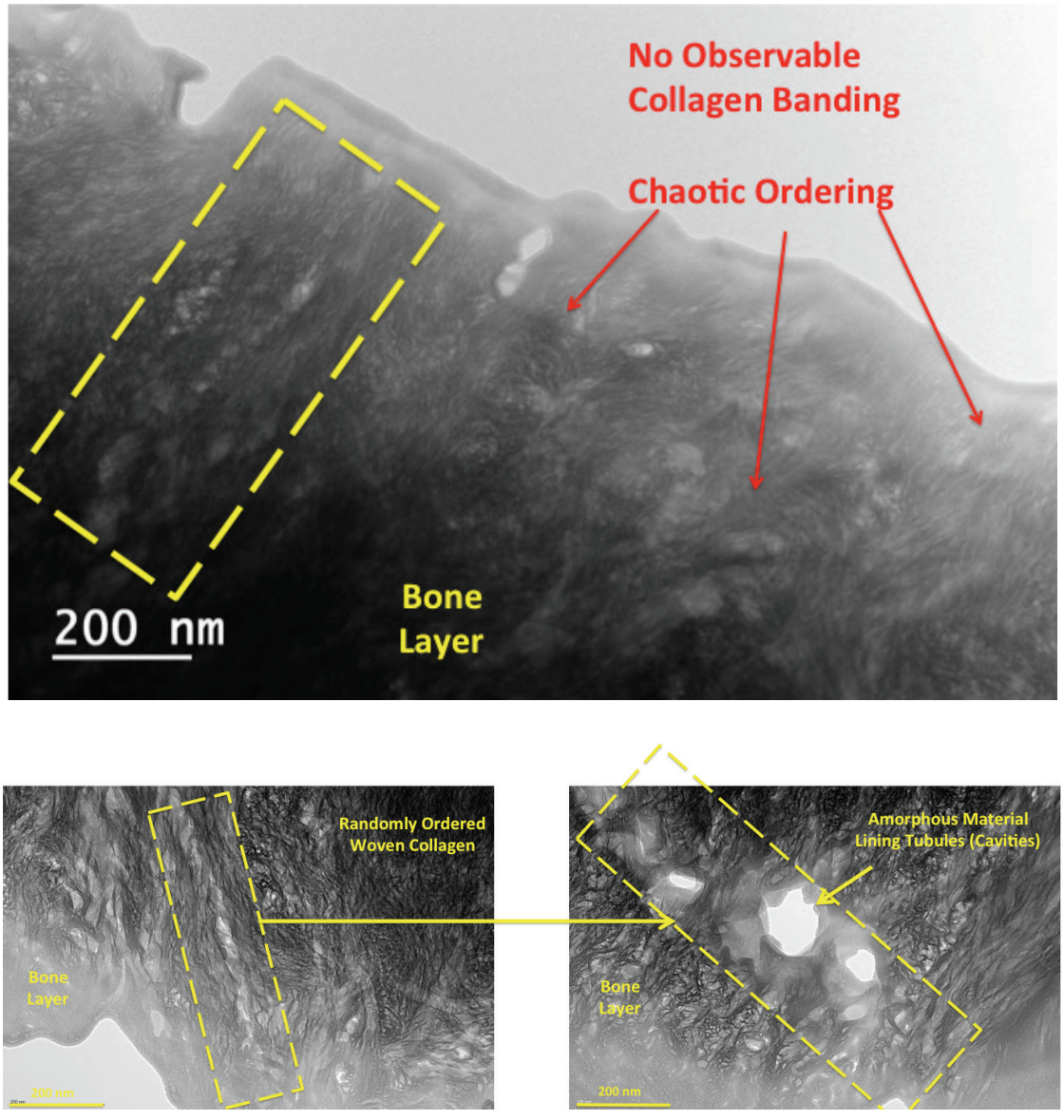

To better identify the HAp crystals, unstained specimen were cryo-milled from fish scales' cross sections. The scales were cold-treated with a hydrazine inorganic compound. The hydrazine treatment was used to chemically remove the collagenous (proteins) bound materials (Bigi et al. 1997).

Before further TEM analysis was performed, FTIR experiments were conducted to verify the HAp crystalline atomic structure was not altered.

Shown in Figure 4.45 are FTIR spectra measured in both the ganoine and bone layers for untreated and hydrazine-treated fish scales. When comparing untreated to hydrazine-treated ganoine and bone layers for fish scaleshow, there are no appreciable differences in FTIR spectra. Therefore, the hydrazine inorganic compound did not affect the HAp crystalline atomic structure.

The de-collagenized HAp structure has differing crystal sizes. The HAp platelets in Figure 4.46 appear to show larger non-uniform sizes are present in the ganoine layer, and they tend to be ovals with smooth outlines. In the bone layer the platelets have irregular outlines and are linked together to form a porous film structure. The primary bone HAp particles have a narrower size distribution. The average HAp oval sheets have dimensions that are approximately [20-?] × [60 – 200] × 5 nm. The sheets have irregular rolling "cornflake-like" topologies. As previously stated, researchers believe the crystalline size/maturity is a function of the degree on mineralization, which is controlled by the distribution of carbonate concentration (Fleet et al. 2004; Fleet 2015; Mathew and Takagi 2001; Grunenwald et al. 2014; Figueriredo 2015). Now that TEM has successfully identified the individual subunits for collagen and HAp crystals the combined parts will be investigated using STEM techniques.

Figure 4.45. FTIR spectra comparing untreated/hydrazine-treated ganoine and bone layers for gar fish scale.

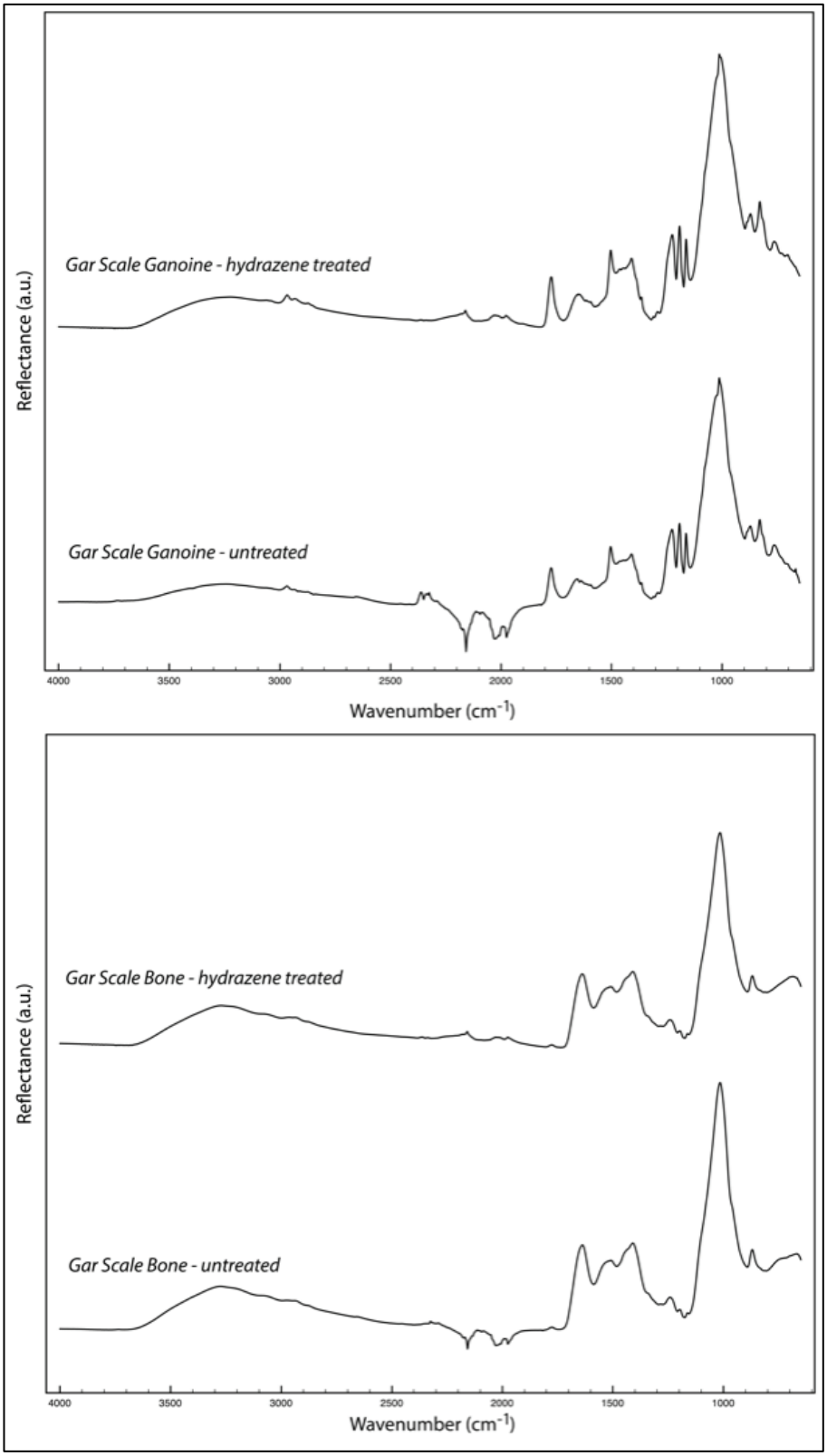

Figure 4.46. TEM image comparing de-collagenized hydrazine-treated HAp crystals in ganoine and bone layers for gar fish scale.

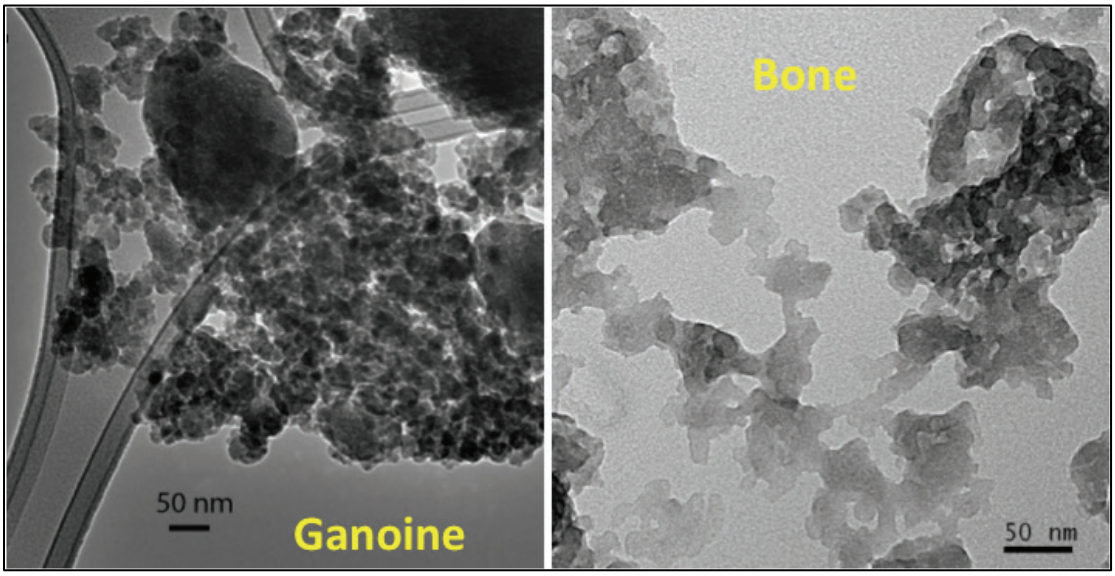

4.3.2 STEM-HAADF-EELS

One of the challenges of probing the biomineralized fish scale structure is the ability to identify the embedded mineral and fiber compositions at the nanometer scale. Moreover, when using TEM the HAp crystals do not readily diffract when combined with the collagen because the crystal thickness (5-nm) for the individual crystals are 14 orders of magnitude smaller than collagen. Because the subunits for collagen and HAp interfaces are difficult to delineate, the combined STEM-HAADF-EELS experimental techniques are helpful at lower nanometer range for probing biomineralized chemical composition and structural arrangement for the fish scale.

Scanning transmission electron microscopy (STEM), when combined with high-angle annular dark-field can produce images from contrasting intensities that correlate with the mean atomic number (Z) for known periodic elements. Typically electron energy-loss spectroscopy (EELS) data is simultaneously collected with STEM-HAADF. The addition of EELS allows the investigation of the chemical state and electron density at the nanoscale. The combined experiments use the secondary electron signatures to identify the periodic elements, based on their mean atomic number, which provide contrast for structures that have opaque interfaces when imaged.

The current STEM investigation used a FEI CM 300™ FEG equipped with Gatan 200 EELS™, Oxford™ EDS, and HAADF detectors. The CM 300™ instrument has a 300 keV atomic magnification with a field emission gun capable of point-to-point characterization of material at the nanoscale (<0.2 nm). The instrument is also equipped with a high-current probe capable of extremely high-magnification (~1 nm) chemical analyses.

The STEM-HAADF-EELS study was conducted at the highest magnification. Shown in Figure 4.47 is the correlated STEM-HAADF-EELS image of the medium fish scale's bone layer. The bright contrasting intensity means there is high occurrence for mean atomic number. In this case the mean atomic number is used to identify HAp are inside collagen and also align along the collagen long axis. The gap and overlap banding have very sharp boundaries. HAp crystals run vertically, but not exactly parallel with the collagen fibers, and cut through both the GAP and OVERLAP bands. On the right are STEM (K and $L_{3,2}$) Electron Energy-Loss Spectroscopy Maps of C, O, P, and Ca. Here, the light bands correspond to Ca-rich, C-poor GAP bands, while the dark band is C-rich OVERLAP band. The STEM imaging contrast is the opposite of conventional TEM images of bone layers. Even though Ca is greater in the GAP band, there are immense amounts of Ca in the OVERLAP bands and also lots of C in the GAP band. So Ca is not simply limited to the GAP-band of collagen. In fact, the majority of Ca may be in HAp platelets that are larger than the GAP or OVERLAP bands. Additionally, the ordering for GAP and OVERLAP banding for collagen is unique to Type-I Collagen (Nudelman et al. 2010; Jantou-Morris et al. 2010; McNally et al. 2012; McNally et al. 2013). Inferred from the STEM-HAADF-EELS analysis, the calcium concentrations are embedded in collagen. The concentration of calcium is not all part of the HAp mineral phase; some are contributing to the collagen phase, but even more contribute to the carbonate phase.

Figure 4.47. STEM-HAADF-EELS image of the medium fish scale's bone layer.

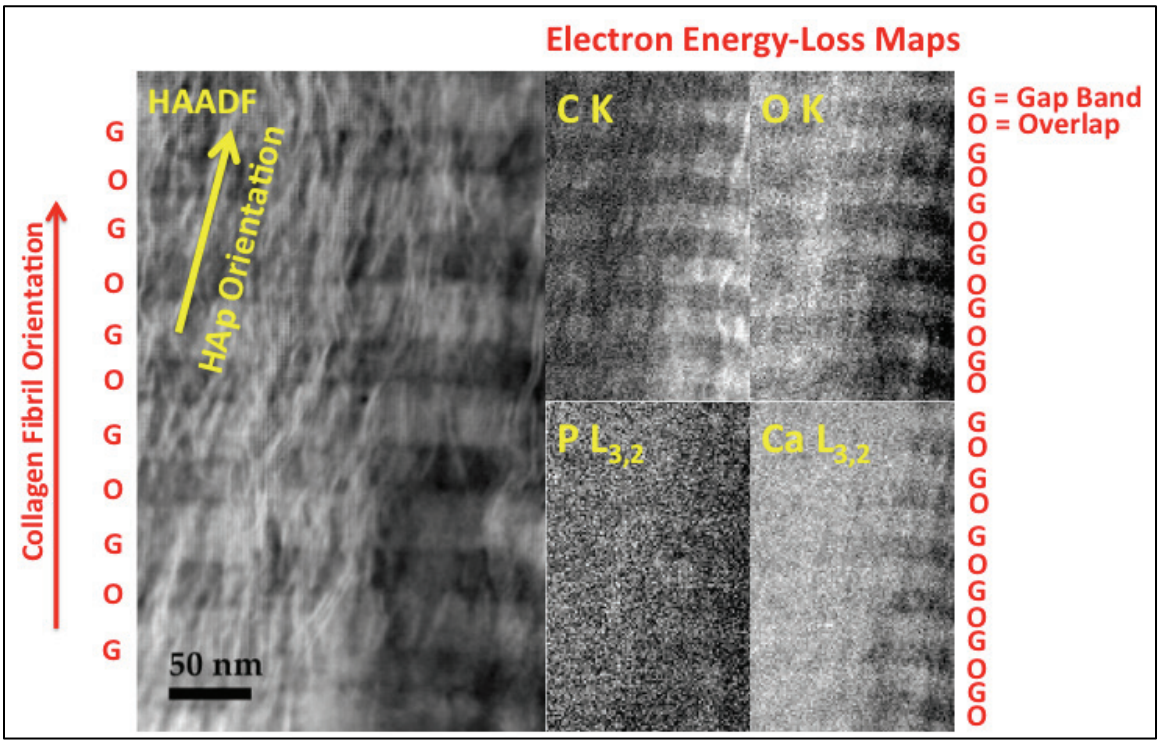

4.3.3 Nanoindentation mechanical analysis

Thus far Chapter 4 has been dedicated to discussing the hierarchical description of the chemical composition and structural assemblage.

Nanoindentation experiments were used to provide further details of how the biomineralized ganoine and bone layers respond to external loading. Additionally, the experimental measurement was used to interpret how collagen fiber and HAp mineral structural phases contribute to the fish scales' mechanical strengthening.

Analysis of nano-indentation experiments assumes the measured response is that of a linear homogenous or near homogenous material system (Constantinides et al. 2006). The assumption permits interpretation of physical measurement using *classical continuum mechanics* based on elasticity, plasticity, and/or viscoelasticity, all three of which assume material parameters do not depend on specimen size (Ostojic and McPherson 1987). For heterogeneous materials this assumption breaks down, especially when the material is composed of discrete components that are large compared to the size of the probe. For example, most materials exhibit size-dependent phenomena in the length scale range of

1–10 nm due to surface energy effects that become increasingly appreciable due to the large surface-to-volume ratios available at the nanoscale (Maranganti and Sharma 2007). The practical application of *classical continuum mechanics* assumes the length scale over which deformation varies is much larger than the discrete size of the particles. Further, the assumption of size-invariant properties for discrete and heterogeneous systems breaks down when the experiments are analyzed *using the equations for homogeneous material* in conjunction with averaged material parameters (Brandstatter 1963; Pethica and Oliver 1989). Properties so determined depend on specimen size unless there is a large separation between specimen size and the size of material components. Moreover, such materials display scale-dependent features such as wave dispersion, force chains, and finite sizes of shear bands and fractures whereas continuum mechanics tells us wave velocities should be independent of wave length and force chains, shear bands, and fractures should have zero size. Accordingly, the governing equations for homogenized discrete and heterogeneous systems must be based on non-local stress-strain relationships, which impart a characteristic scale not available using the locality assumption of classical continuum mechanics. Such relationships are essential for proper modeling of material damage and softening. However, the relationships have yet to be sufficiently developed by the community of practice.

Biological materials cannot be considered homogenous due to their hierarchical structure. The key issue is the difference (or scale separation) between the discrete components and domain size. Here the discrete components are minerals and fibers with separation of length scale for the domain being attributed to the much larger radius of curvature for the indenter probe used to conduct the indentation experiment (Rettler et al. 2013). Since the minerals and fibers are much smaller than the probe size, further considerations are needed when interpreting the mechanical response from nanoindentation measurements. Specifically, for biomineralized composite materials that have bound compliant soft (fibers) fixed inside rigid (mineral) nano phases, capturing the energy dissipative response is difficult. Therefore, it is important to understand the suitability of experimental techniques used to capture the discrete elastic and viscous properties for highly heterogeneous material systems. For the fish scale, the instrumented nanoindentation (INI) techniques were selected as the most appropriate technique that could best capture the effects of the hierarchical structure.

The primary advantages of the INI technique are the ability to characterize small volumes of material and measure properties with high spatial resolution. However, characterizing small volumes of materials creates a conflict when attempting to capture the heterogeneity attributes for the fish scale. That is, to get meaningful properties, we need to average over some representative volume, but doing so masks the mechanical property attributes gained from the local material variation. The viscoelastic properties are of critical importance in the fish scales' structure because they can describe how the bone layer stores energy (storage modulus), like a spring, and how the internal network of collagen fibers uses friction to convert mechanical energy into heat (loss modulus) – the energy that is lost/dissipated through heat generation.

The (INI) experiments were carried out using strain-rate-displacement controlled, dynamic indention measurements. Strain-rate controlled, dynamic indention measurements are sensitive to small deformations (less than one micron). To correctly capture the small deformations, a two-step process was carried out during the experiment for the small and medium dehydrated fish scales. During polishing, the specimen's surface is typically and unavoidably work-hardened. The work-hardened layer is roughly one-third to one-half the size of the particle size used for polishing. As a result, the measured elastic modulus could reflect the value of the work-hardened layer, or the underlying substrate or some combination thereof, thus giving a false reading. Moreover, the false reading can give a false sense of layering. So the first step for conducting INI experiments is to determine what is the minimum displacement needed to penetrate the work-hardened polished surface.

The experiments were conducted using a Nanomechanics iNano™ nanoindenter with the setup parameters listed in Table 4.1. A Berkovich grid indented array was used to map the fish scales' cross section, Figure 4.48. The converged penetration depth determined in Step 1 was extracted from the elastic modulus-penetration depth and hardness-penetration depth plots for the small and medium scales, in Figures 4.49 and 4.50, respectively. The mechanical properties show excellent convergence in the ganoine and bone regions by 300 nm of surface penetration.

Table 4.1. Nanoindentation setup parameters for determining minimum penetration depth, modulus, and hardness.

Input Parameter	Value
Tip Geometry (Angle/Curvature)	Berkovich (142.3°/~150 nm)
Tip Material Type	Diamond
Indentation Strain Rate	0.2 s^{-1}
Maximum Indention Depth, (D_{Max})	1-µm
Spacing Between Indents, 10x(D_{Max})	10-µm
Poisson's Ratio, (v)	0.35
Penetration Range for Averaging Results	[500-800]-µm

Figure 4.48. Berkovich indented array for mapping the fish scales' cross section.

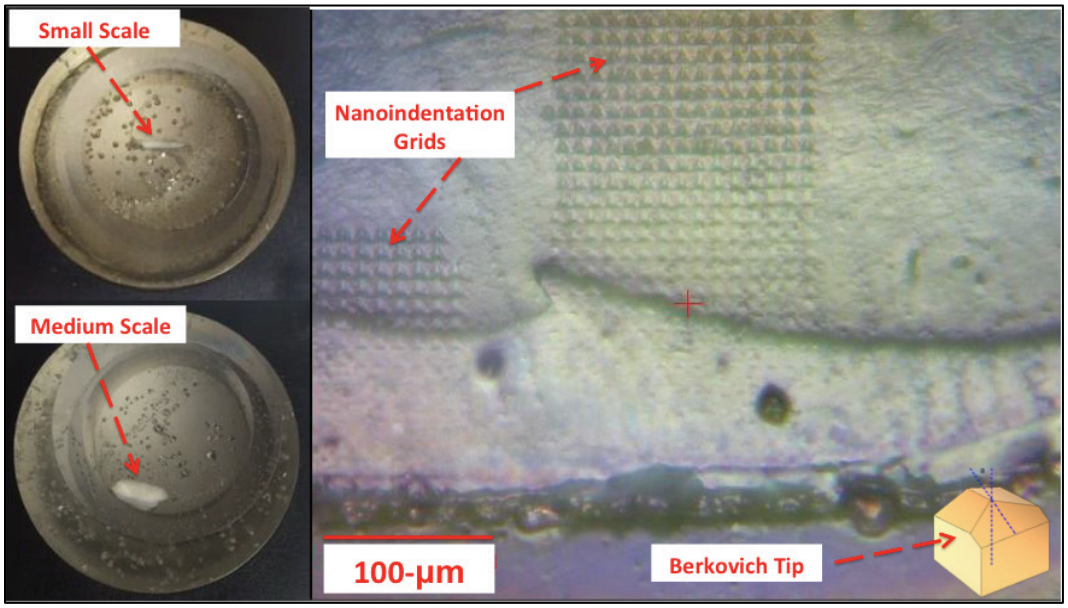

Next, for Step 2 the data for mechanical properties in each experiment were analyzed over the penetration range from 500 to 800 nm and used spatially resolved line plots and surface maps to report the measured mechanical properties. Using the dynamic indentation technique allowed for the continuous acquisition of hardness and elastic modulus as the tip penetrated through the surface of the sample. An array totaling 1,680 and 3,600 indents with a 10-µm spacing between indents were used to map the small and medium fish scales' cross sections, respectively. Shown in Figures 4.51 and 4.52 are the measured elastic moduli and hardness for both the small and medium scales. Also, illustrated in Figures 4.51 and 4.52 are snapshots showing how the mechanical properties transitions across the ganoine-bone interface.

Figure 4.49. Nanoindentation elastic modulus-penetration depth and hardness-penetration depth plots for the small dehydrated fish scale.

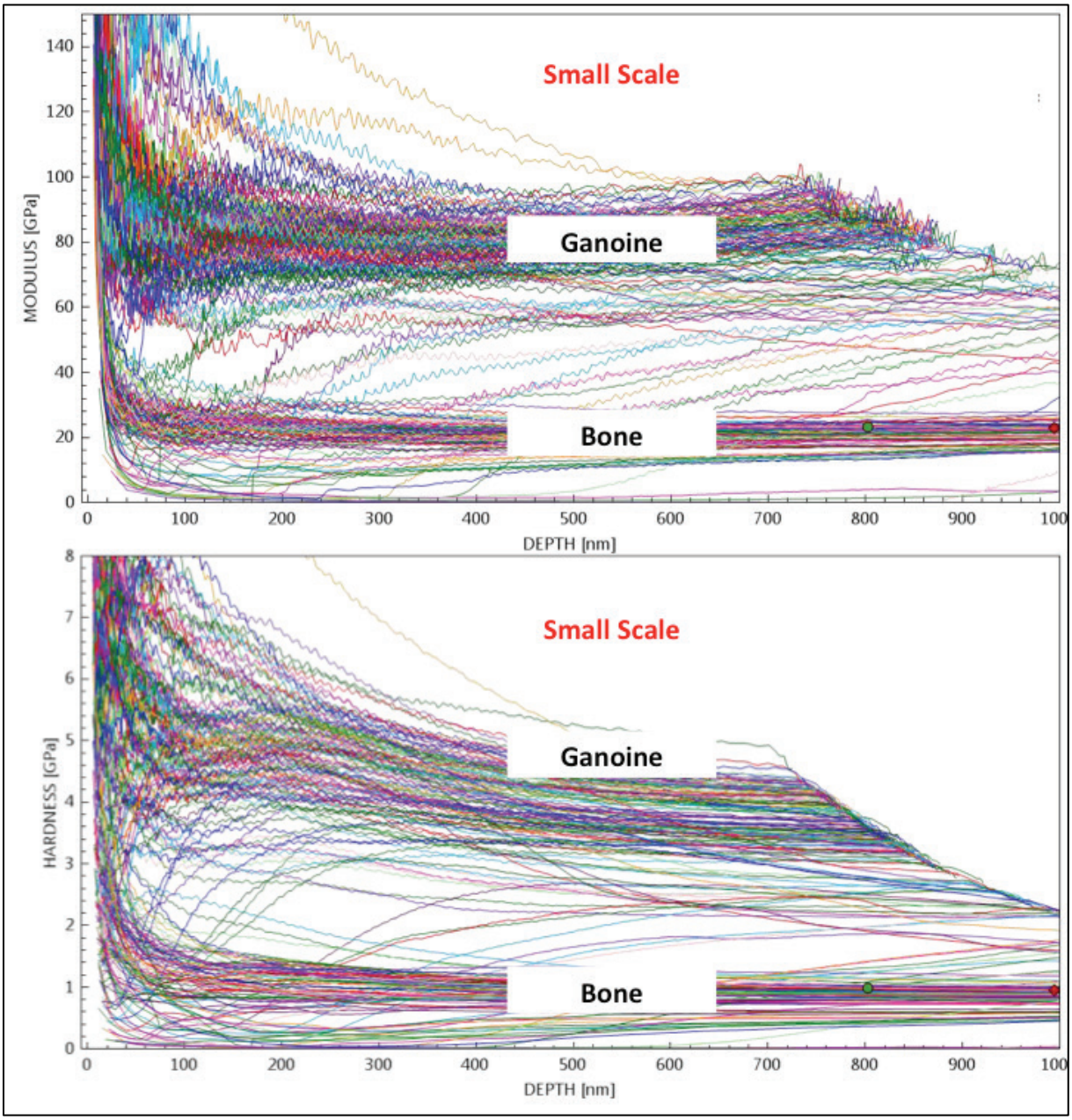

Figure 4.50. Nanoindentation elastic modulus-penetration depth and hardness-penetration depth plots for the medium dehydrated fish scale.

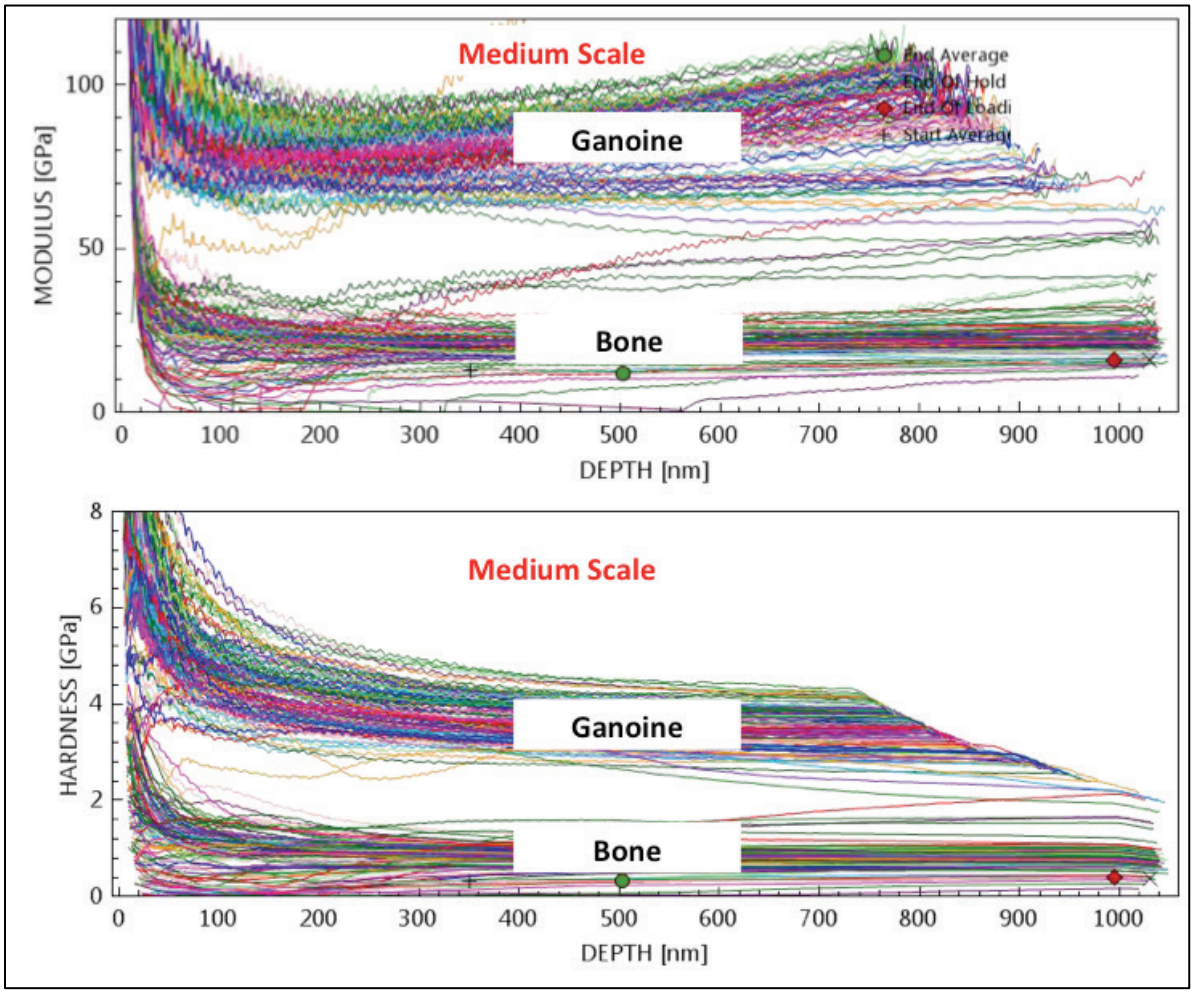

Both elastic moduli and hardness have property gradients occurring through the ITZ from 0.11-0.25 and 0.02-0.23 normalized distances, with respect to layer thickness, for the small and medium fish scales, separately. In the outset of each line plot, the median properties for small and medium scales are shown using blue diamonds and red circles, respectively. Each data point represents the average measured mechanical property positioned equidistant from the interface. The corresponding colored dashed line represented by two standard deviations (2σ) show the upper and lower bound for the orthogonal property grading. Meaning the upper and lower lines are respectively twice the standard deviations from the mean making the zone between four standard deviations. The surface plots better show three-dimensional variation for the local maxima and minima results.

Figure 4.51. Nanoindentation elastic modulus for dehydrated small and medium fish scale.

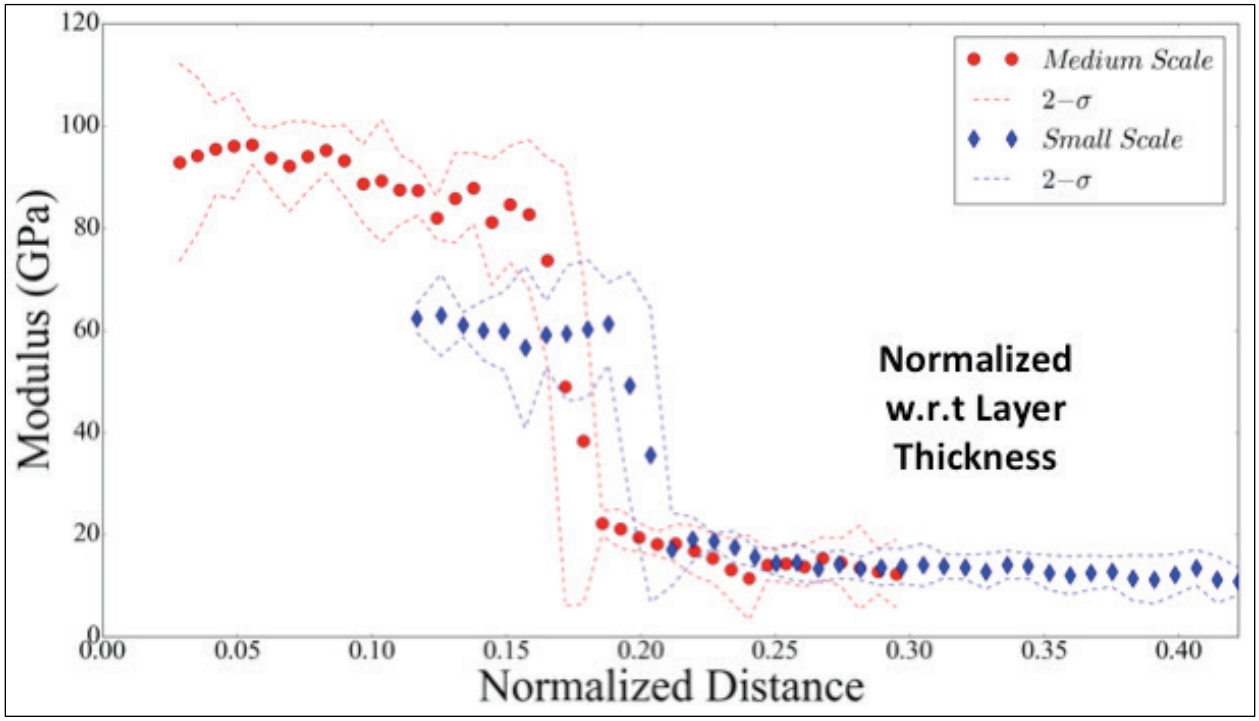

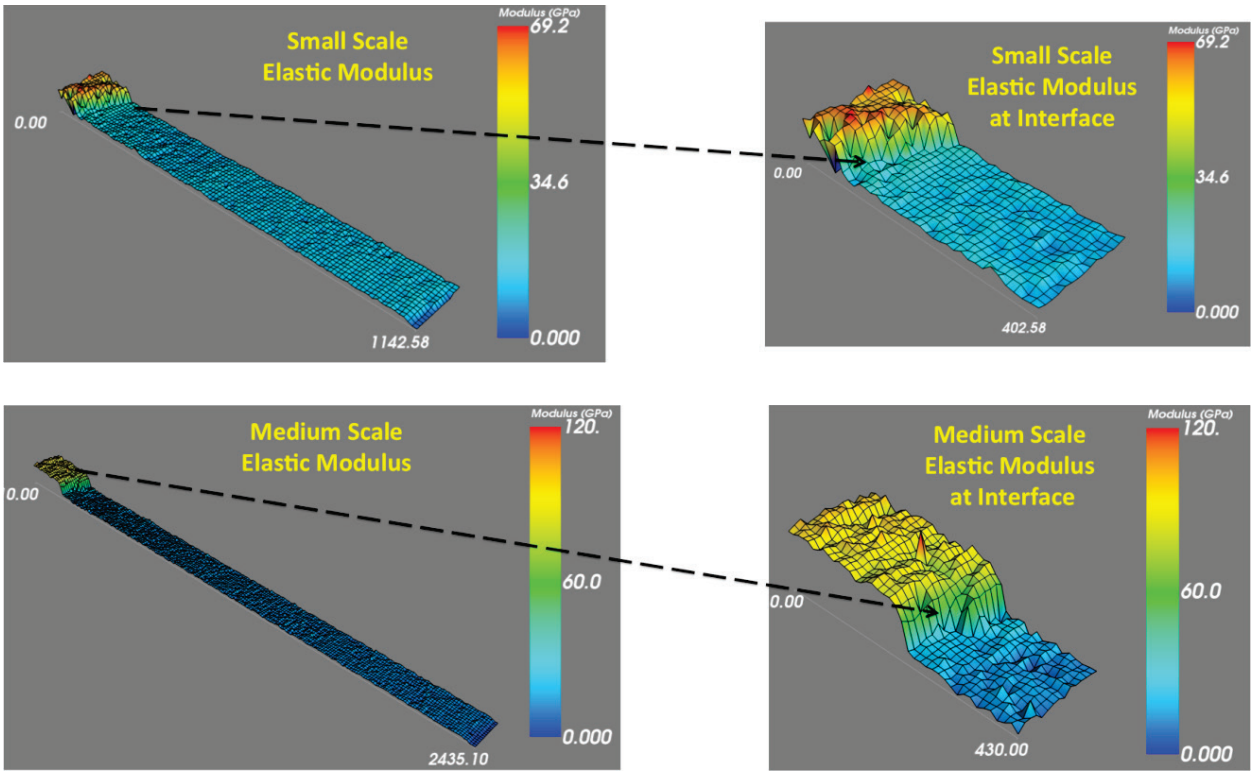

Figure 4.52. Nanoindentation hardness for dehydrated small and medium fish scale.

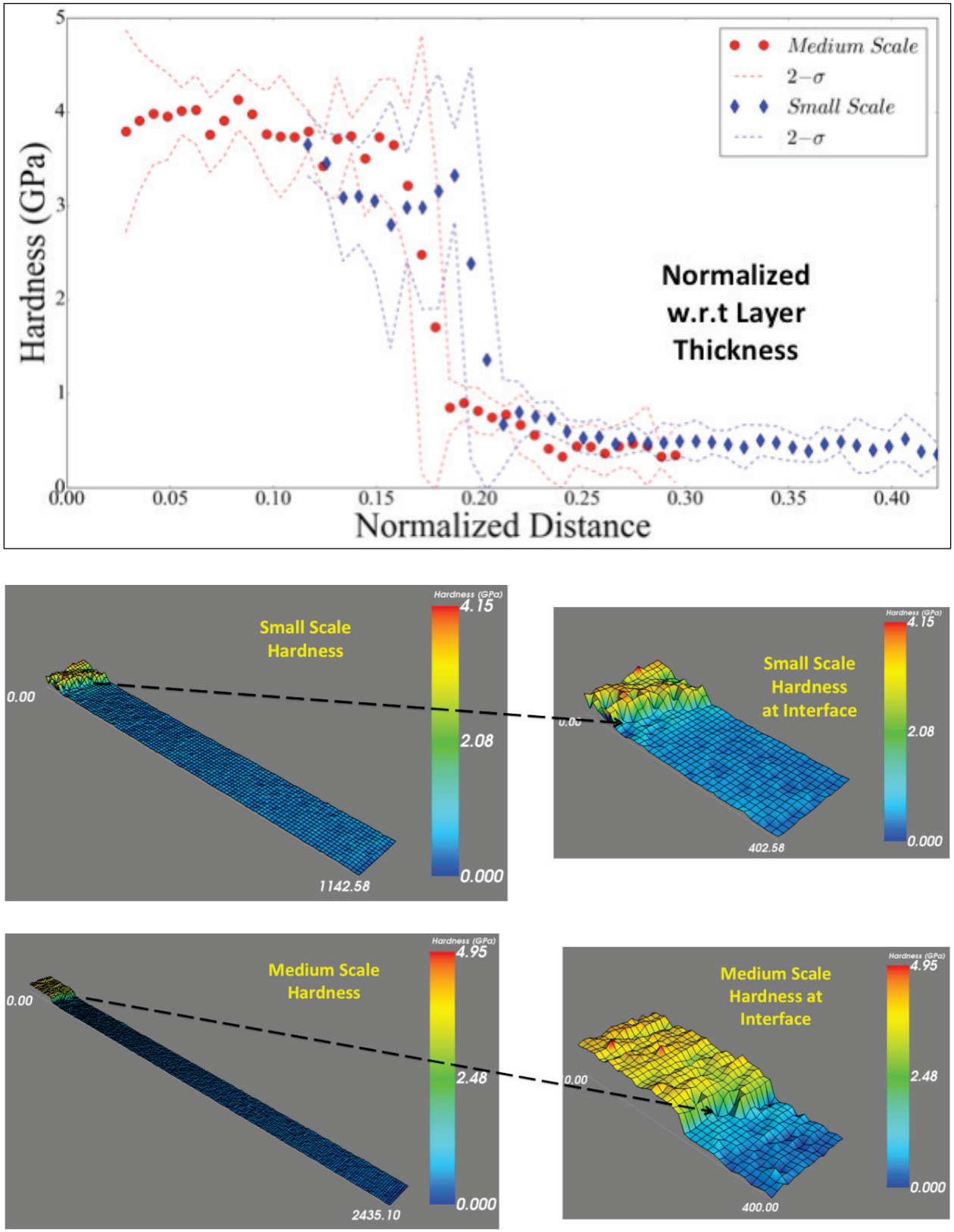

In the line plots, elastic modulus in the ganoine layer for the medium scale shows a continuous decrease as the interface is approached with the maximum measured elastic modulus occurring at the outer edge of the ganoine layer, whereas the small scale shows an increase in elastic modulus as the interface is approached, with the maximum elastic modulus in the bone layer occurring at the interface. The hardness shows the same trend as compared to the elastic modulus for both fish scale sizes.

Noticeably the ganoine layer has elastic moduli ranging from 60 to 66 GPa in the small scale compared to 98 to 80 GPa in the medium scale, while both scales' bone layers have an average elastic modulus of 18 GPa. Similarly, the ganoine layers have hardness values ranging from 3.0 to 3.4 GPa in the small scale compared to 3.6 to 4.0 GPa in the medium scale; while both scales' bone layers have an average elastic modulus of 0.5 GPa. For comparison purposes, shown in Chapter 1 by Figure 1.3, the elastic modulus for the fish scale's ganoine layer closely resemble human tooth enamel while the bone layer has comparable modulus as human bone. As a reminder, the tooth has a fixed 2-layer structure with harder outer protective enamel layer covering a less dense softer dentin layer while the bone has a more woven medium compact structure containing osteon gap zones that are used for constant bone remolding throughout life.

Continuing with the indentation analysis, both fish scale sizes have comparable slopes occurring in the ITZ with average elastic modulus changing from 60 to 18 GPa in the small scale compared to 80 to 16 GPa. However, the average hardness shows much less change ranging from 3.4 to 0.5 GPa in the small scale compared to 3.6 to 0.5 GPa. Even more interesting, both the medium and small scales show similar mechanical properties in the bone layer over the same distance from the interface, suggesting that size and age of the scale does not influence the size of the transition zone in the bone layer. Yet in the ganoine layer an increase in the elastic modulus is observed for the medium scale with an additional steady increase in elastic modulus as the outer edge of the scale is approached. The overall findings, from modulus and hardness, indicate the fish scale grows from the bone-ganoine interface as the fish grows and the scale becomes more mineralized and denser/stronger in the ganoine layer while the bone layer maintains a consistent lower modulus and hardness.

Recall, from the analytical chemical speciation and structural characterization the bone layer is much less compact than at the interface

and ganoine layers, leading to the much lower elastic modulus and hardness. In addition, the bone layer has a collagen-rich, chaotic, randomly ordered structure. To better capture the heterogeneity effects collagen has on viscoelastic response in the ganoine and bone layer, dynamic mechanical measures were also taken during the INI experiments for elastic modulus and hardness. The current study used the phase lag (tan ϕ), determined using dynamic mechanical analysis (DMA), to map the viscoelastic response for the corresponding indenter locations for both the small and medium fish scales in Figures 4.51 and 4.52.

Note the calculated values of *E'* and *E"* can be affected by the uncertainties in accuracy for the measured the contact area, especially at lower indentation depth where full contact may not have been established. However, the Berkovich indenter tips usually maintain full contact for at least the "***unhydrated case,"*** allowing for an accurately determined contact area (Sneddon 1965; Rho et al. 2002; Swadener et al. 2002; Bei et al. 2005; Fischer-Cripps 2006; Pharr et al. 2009; Pharr et al. 2010; Randall et al. 2011). Thus, the dynamic INI experimental technique is ideally suited for measuring the viscoelastic effect of the indented materials at shallow depths (Oliver and Pharr 1992; Hay and Pharr 2000; VanLandingham 2003; Oliver and Pharr 2004; Golovin 2008; Pharr et al. 2009; Hay 2009; Ryou et al. 2012; Sun et al. 2014).

Viscoelastic materials are commonly characterized by their *E'* and *E"* moduli where the former represents the stored energy or the elastic response, and the latter corresponds to the amount of energy dissipated or the viscous response, as well as their ratio – the loss tangent is calculated as the ratio of loss to storage. During the dynamic INI experiment as the indenter tip penetrates the specimen, illustrated in Figure 4.53, a harmonic force oscillation is applied to the tip, which generates an oscillatory harmonic displacement response at the same frequency of force application. A phase-locked harmonic oscillating force is applied to measure the frequency specific harmonic displacement response and determine the phase angle (ϕ) — also termed the phase lag — between the two harmonic signals (Figure 4.54.) The phase-locked harmonic oscillation allows the harmonic displacement to be in phase with the applied harmonic force, causing an instantaneous displacement response due to the external force

Figure 4.53. Illustration of indenter tip penetrating a specimen (Pharr et al. 2009).

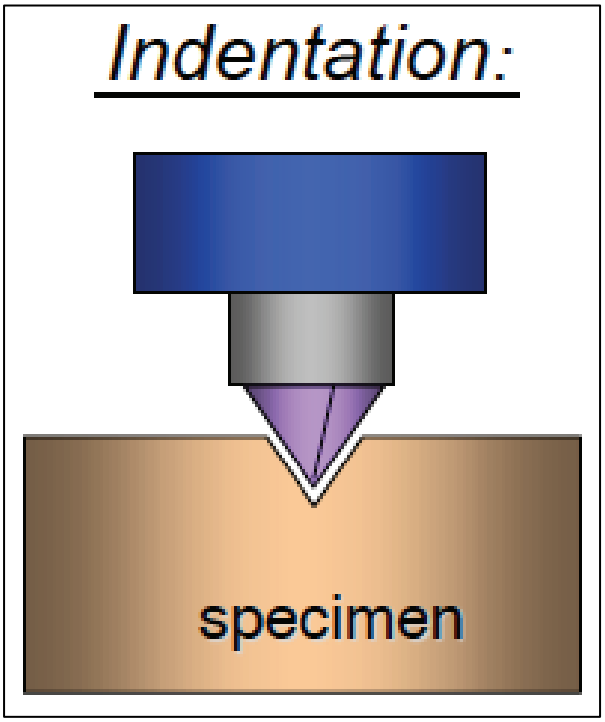

application. As damping is introduced into the sample, through the viscoelastic collagen fibers, the displacement response starts to lag behind the force application. The lag is measured through the phase angle separation between the harmonic force application and the frequency specific displacement response. To isolate the response of the sample, the instrument is modeled as a force, damped oscillator with a modified *Voigt* model to capture the viscoelastic behavior (Wright et al. 2007; Herbert et al. 2008; Jager and Lackner 2008; Hay and Crawford 2011).

The schematic viscoelastic model used when conducting the INI experiment is a modified Voigt solid model, having a spring in series with a spring and dashpot that are in parallel and connected in parallel with a simple spring with an adjacent parallel dashpot, illustrated by Figure 4.55 (Golovin 2008), whereas the Voigt model denotes the mass (m), contact stiffness (S), contact damping, (D_S), machine damping (D_m), finite stiffness (k_f), and spring stiffness (k_s), as shown in Wright et al. (2007). The models' configuration allows for determination of the energy dissipative behavior for differing storage and loss modulus relaxation times as a function of tan(ϕ).

Figure 4.54. Phase lag (tan Φ) determined from storage and loss modulus for viscoelastic behaving materials (Hay and Crawford 2011).

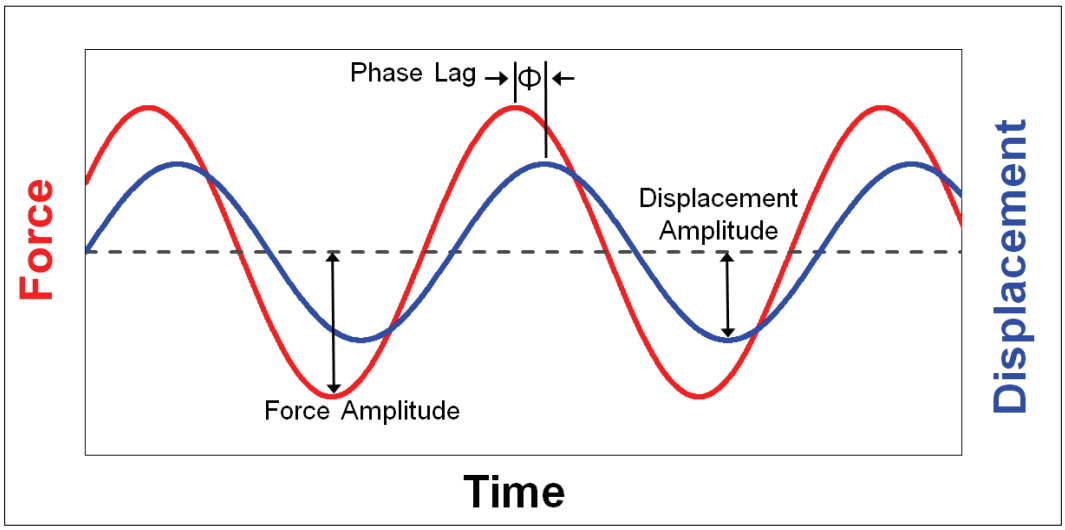

Assuming (1) the instrument can be modeled as a forced, damped oscillator that is limited to one degree of freedom, (2) the contact measurements must be made in the linear viscoelastic regime of the sample, and (3) measurements are only performed under conditions of steady-state harmonic motion linear viscoelastic behavior, then the phase lag (tan ϕ) for the sinusoidal phases, show in Figure 4.54, can be computed from the data using the following the calculations (Herbert et al. 2008):

$$S = \frac{F_0}{h_0} \cos \varphi \tag{1}$$

$$C\omega = \frac{F_0}{h_0} \sin \varphi \tag{2}$$

and

$$\frac{C_\omega}{S} = \tan \varphi \tag{3}$$

where:

F_o = harmonic force amplitude
h_o = harmonic displacement amplitude
ϕ = phase angle between the two harmonic signals

Figure 4.55. Illustration of modified Voigt model used for dynamic instrumented indentation analysis (Wright et al. 2007).

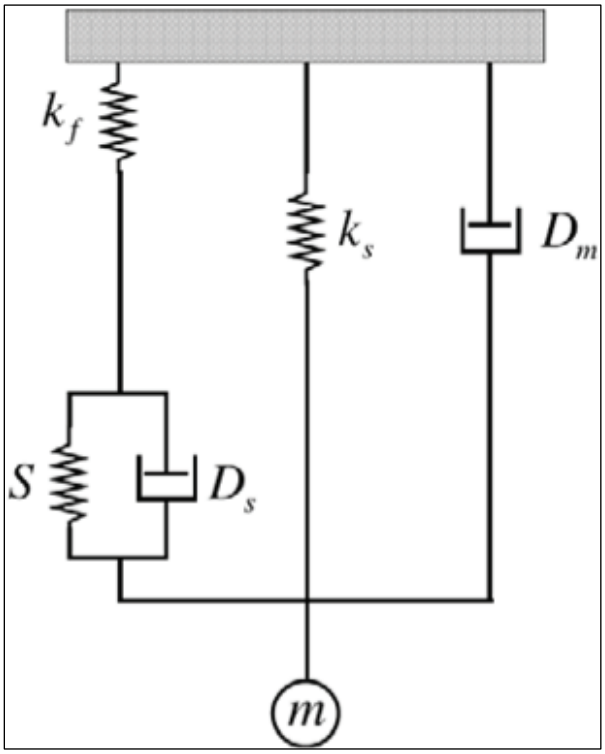

To isolate the response of the sample, the instrument is modeled as a force, damped oscillator.

To better elucidate the instantaneous dampening response in the dynamic INI experiment, a single frequency in the lower quasi-static frequency range of 5-Hz was used as opposed to traditionally conducting a full frequency sweep for DMA, although the biomineralized fish scale has complex highly heterogeneous structure conducting the INI-DMA experiment at a single frequency is sufficient and a novel approach to use the measured tan ϕ parameter to show energy dissipative response. Shown in Figure 4.56 is the calculated phase angle of both the small and medium scales.

Figure 4.56. Nanoindentation phase angle, tan (ϕ), for storage and loss modulus for small and medium dehydrated fish scale.

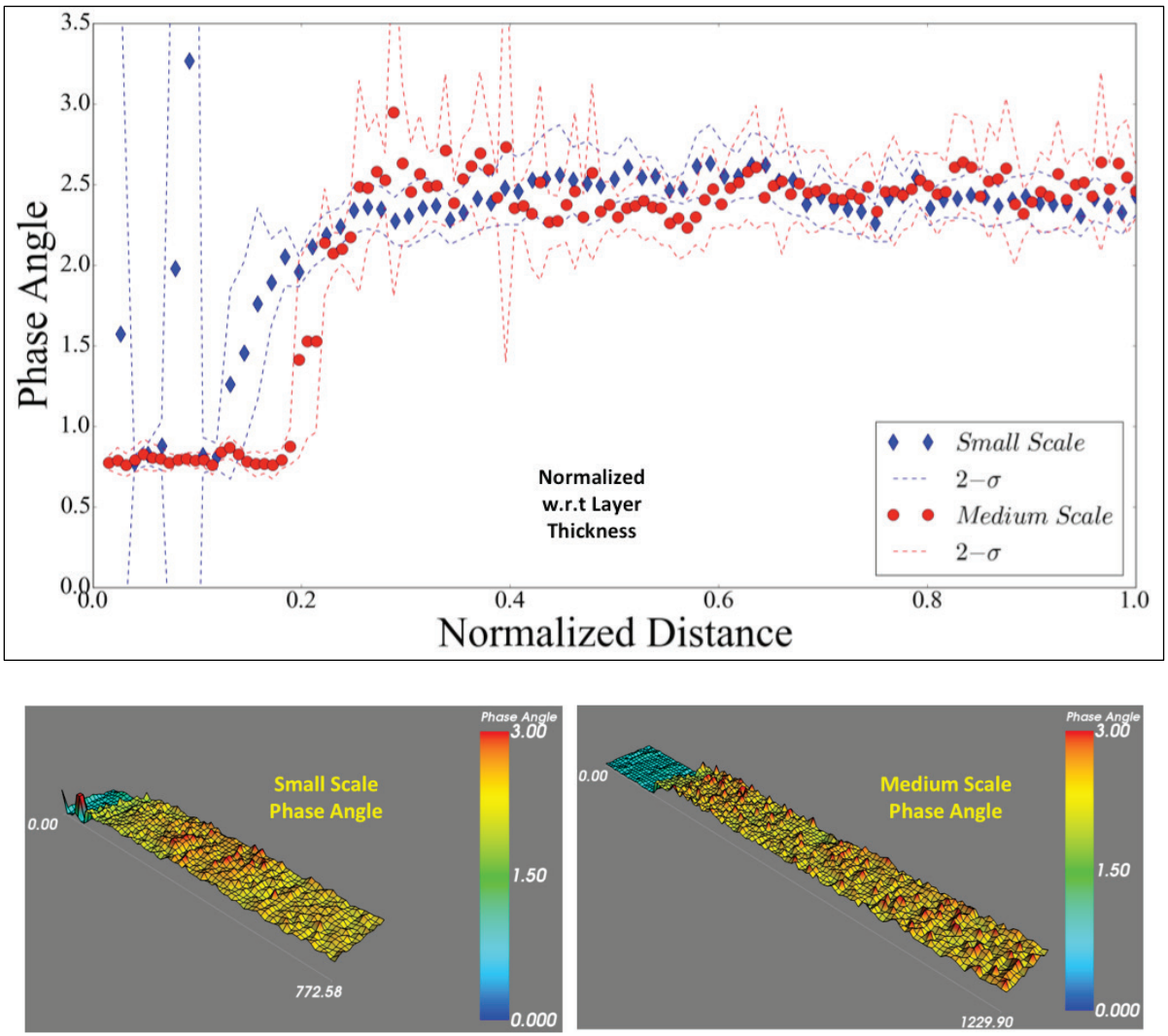

Like the previously measured mechanical properties, the phase angle gradients are occurring through the ITZ from 0.20 to 0.40 and 0.10 to 0.40 normalized distances, with respect to layer thickness, for the small and medium fish scales, separately. In the outset of each line plot, the median properties for small and medium scales are shown using blue diamonds and red circles, comparatively. Each data point represents the average calculated. The corresponding colored dashed lines represented by two standard deviations (2σ) show the upper and lower bound for the orthogonal phase angle parameter grading,.meaning the upper and lower lines are respectively twice the standard deviations from the mean making the zone between four standard deviations. The (tanϕ) value is interpreted as the higher the value, the more energy dissipative at the local indention

site and vice versa. The surface plots better show three-dimensional variation for the local maxima and minima results.

The line plots in the ganoine layer for the medium scale shows a near-constant but much lower (tan ϕ) away from the interface; whereas, the small-scale plots show lower (tan ϕ) that have large variations in the ganoine layer when crossing the interface. Shown in the surface plots, for the bone layer the average phase angle is comparable for both scale sizes with the difference being the medium scale has a wider variation nearer to the interface. Distinctively the ganoine layer has a phase angle ranging from [0.75-3.5^{+}]° in the small scale compared to [0.75-0.80]° in the medium scale. But in the bone layer the small and medium scales consistently have much higher phase angles with ranges of [2.30-2.40]° and [2.25-2.50]°, comparably.

The medium fish scale has a sharp slope occurring in the ITZ with average phase angle changing from [0.75-2.00]° unlike the small fish scale, which has more of a gradual slope with the same phase angle values. The phase angles for the medium and small scales show an interesting trend in the bone layer over the same distance from the interface. The trend tends to show as the fish scale grows; the bone layer for the medium scale becomes more energy dissipative with a higher variation than the small scale in the bone layer. Unlike in the ganoine layer for the medium scale there is much lower energy dissipative behavior observed with the minimal variation. For the small scale in the ganoine layer the dampening behavior is fairly inconsistent and changing. The trends also suggest the ITZ is the key and heavily influences the maturation of the layers. With aging the ganoine layer becomes more mineralized, shown by the sharper phase angle gradient, thus being denser/stiffer whereas the bone layer becomes more porous/compliant. There is much greater variation in the energy dissipative behavior than suggested by the measured elastic and hardness properties, suggesting the material in the ITZ is not as discrete as the measured mechanical properties might indicate. This difference is marked by an increased energy response occurring on the bone side immediately adjacent to the interface. Evidently the difference grows with age. Thus, the geometrically connected sawtooth structured interface, combined with the additional energy dissipative/damping effect, might minimize stress localization and delamination in the ITZ. When the layers are combined, the outer ganoine layer achieves high strength and is possibly used as a protective layer whereas the interior layer achieves high toughness, a

combination that produces an advanced high-performance composite material provided delamination is resisted. Understanding delamination resistance allows the development of better composites.

While there remains a level of uncertainty for identifying all contributors to the energy dissipative/damping behavior in the fish scale, the phase angle results indicate the loosest compact biomineralized region in the fish scale exhibits much higher energy dissipative potential. The higher dampening behavior is unique to the bone layer and is more than likely attributed to the loosely packed, chaotically ordered collagen fibers. The loosely packed bone layer identified throughout the hierarchal chemical/ structural analysis appears to mostly use collagen fiber bundles to introduce anisotropic reinforcement at the nanoscale. The nanoscale collagen fiber reinforcement seems to dampen/dissipate energy at the largest length scale for the composite when loaded externally.

4.4 Summary of findings

A systematic detailed approach was used to identify controlling mechanisms by discovering the scale-dependent fish scale structure that governs its mechanical response as a function of chemical composition and hierarchal structural arrangement. The fish scale was found to be a robust advanced composite, having a simple elemental composition. Subtle differences in chemical processes appear to form the fish scale's layered structure while using elements that remain relatively uniform throughout the scale. Within the fish scales the structural hierarchy takes on several morphological arrangements that are not obvious from individual microscopy techniques (Optical, HR-SEM, or TEM) when used alone. Innovative experimental and data analysis techniques were employed for interpreting the relationship between these chemically based differences with differences in mechanical response. A novel application of nanoscale engineering measurements was used to isolate and better understand the extremely complex contributions for the assembled structural components and their subunits. For better clarity the scientific and engineering results presented in Chapter 4 will be discussed in greater detail in Chapter 5. Also addressed in Chapter 5 are the specific questions raised by the hypothesis, insight provided for the biological design principles, and suggested methodologies for developing bioinspired engineered composite designs that exhibit advanced high -performance.

5 Discussion

The results discussed in Chapter 4 provided sufficient evidence to test the hypothesis *(H)*. The hypothesis *(H)* stated was the fish scales are effective in resisting cracks, dissipating energy, and transferring loads across interfaces because of the grading of the composite layer properties. The hypothesis is found to be consistent with the data and from the comprehensive experimental investigation the results verified the following: (a) interfaces exist and (b) the layers are graded. In the test of *H*, there is a significant difference in the material above, below, or between layers and the difference in material arrangement is the reason for the fish scale's attributes. To further expand on how the results were used to test and prove the hypothesis to be true, a discussion addressing the overall research objective is provided for the remainder of Chapter 5.

The overall objective was to use experimentation to provide insight on what are the inherent chemical, structural, and mechanical attributes of bio-engineered fish scale composites found in the alligator gar's exoskeleton. Experiments were used to determine (a) how is the natural composite system assembled, (b) how do the layer thickness and the functionalized gradient properties interact to achieve high toughness, (c) what are the design principles of natural armor systems, and (d) how can these design principles be applied to the design of manmade engineered composite systems. The pertinent information gathered helped provide the necessary details to allow an adequate assessment of the biomineralized fish scale attributes that led to the development of the superior performing advanced composite.

5.1 Discussion

5.1.1 Natural composite system assembly

The fish scale's composite system is assembled using periodic elements most often found in nature. The fish scale uses eight elements to develop, maintain, and evolve its structure. The elements of carbon, phosphorus, oxygen, nitrogen, and hydrogen are used to form the amide, phosphate, and carbonate chemical groups. The carbonate compound controls the degree of mineralization by substituting with magnesium and sodium. Finally, calcium is the primary element used to mineralize the bio-structure.

The fish scale was observed to use at least 3 levels of length scale hierarchy to form its structure. The biomineralized composite uses the chemical groups to form the two structural sub-units of bioapatite (B-Ap crystals) and Type I-Collagen (fibrils) phases at the nanoscale. Although the geometric dimensions of the collagen are 14 orders of magnitudes larger than the bioapatite crystals, by volume the crystals occupy at least 90 percent of the fish scale's space. Furthermore, at the nanoscale, the collagen and B-Ap crystals are not attached by their surfaces; rather the crystal subunits are embedded, at sharp angles, along the collagen fiber strand's length.

At the micron level the collagen bundles + B-Ap crystals (C/B-Ap) form a distinctive two-layered system that is connected by what is described as saw-tooth geometrically structured interface. The outermost layer for the fish scale is called ganoine while the inner layer called bone. The ganoine layer does not provide full coverage over the bone layer. Additionally, as the layers grow, the ratio of their thicknesses remain relatively constant. As an aside, the current research effort has provided never before shown proof that collagen does not tend to appear as ridged/stiff rods at any length scale as reported by many previous researchers (Bruet et al. 2008; Bruet 2008; Chen et al. 2011; Allison et al. 2013; Yang et al. 2013b; Han et al. 2011). In fact collagen fibers were shown to possess degrees of freedom that allow for bending, stretching, and twisting and therefore cannot be appropriately described as having a rigid needle structure. What had been interpreted as the needle-like collagen strands were actually the hidden fine nanometer cornflake-structured B-Ap crystals passing through the banded collagen bundles. As a result, when conducting morphological studies using HR-SEM at the micron scale, the magnification is too coarse and the results are easily misinterpreted. However, at the nanometer-length scale, with the use of TEM and STEM-HAADF-EELS, the true morphology was uncovered.

Finally, at the millimeter-length scale the fish scales have long and short axis. The scale's shape appears to have subtle curvature around its perimeter that converges at the vertices to form sharp points similar to arrowheads. The layer thickness seems to lead to its overall shape. Also, the curved perimeter of the scales is thinner on the edge and overlap when connected to other scales.

5.1.2 Functionalized gradient properties

Overall the fish scale structure uses the same limited mineralogical constituents throughout the structure. The mineralogical constituents are used to form the two structural sub-units of bioapatite (B-Ap crystals) and Type I-Collagen (fibrils) in the two-layered structure. Independently the collagen fibers and hydroxyapatite minerals phases are weak. However, the ganoine and bone layers uniquely use the subunits, along with the controlling the collagen fibers and hydroxyapatite volume fractions, combined with optimizing morphological arrangements materials within in its structural hierarchy to functionally grade the properties. Additionally, the geometrically connected sawtooth structured interface, combined with the additional viscous damping effect, might minimize stress localization and delamination in the ITZ. When the layers are combined, the outer, much thinner ganoine layer achieves high strength and is possibly used as a protective layer whereas the interior's much thicker layer achieves high toughness, a combination that produces an advanced high-performance composite material provided delamination is resisted and the system is fully hydrated. The fish scale structure has the likeness of a steel plate attached to a bed of springs with varying spring stiffnesses.

5.1.3 Design principles of natural armor systems

This investigation has made new discoveries of mechanisms that can inherently describe the attributes that govern the fish scale hierarchy mechanical response as a function of chemical composition and structural arrangement. The design principles of natural armor system are as follows:

1. The structure of the biomineralized fish scale composite has both short and long range order. The ganoine layer is highly ordered. Densely compact the layer contains an abundance of B-Ap minerals and very little collagen fibrous material leading to the layer's high strength. This ordered structure is in contrast with the bone layer, which is chaotically ordered, loosely compact, and containing an abundance of collagen with similar volumes of B-Ap minerals, leading to the layers with high toughness.
2. The structure grows from the ganoine-bone curved saw-tooth geometrically structured interface outwards. The ganoine-bone interface is the oldest of the layers and has therefore shown to be the densest region in the fish scale structure. Because of geometrically

mechanical interlocking and similar material densities, a less discrete (graded) interface exists that might provide durability and delamination resistance.

3. The fish scale structure uses the same limited mineralogical constituents throughout the structure. Since the fish scale uses limited constituents, the selected materials tend to be indigenous and are routinely abundant in nature. Consequently, the same limited mineralogical constituents allow for chemical, structural compatibility and may evolve when queued by external stressors.
4. The fish scale creatively uses the minimal components of collagen fibers and bioapatite minerals materials to efficiently optimize the structural composite. Remember the fish scale's structure is efficiently produced at ambient conditions using minimal material types. Nature focuses mainly on making use of the structural hierarchy to optimize the geometric arrangement, the volume fractions, and grading of properties for the components during the growth processes. The resulting structure ultimately dictates the mechanical response at the system level.

As a result of the aforementioned design principles for the natural armor fish scale system, a high-performance advanced composite structure is formed. The simple two phases are used to form a very robust complex hierarchal functionally property-graded composite structure. The exoskeleton fish scale is very attractive to the design community because layered composite possesses the attributes of being lightweight, high-strength, high-stiffness, and energy absorbent/dissipative. In addition, the fish scale appears to be delamination resistant when fully hydrated.

5.1.4 Application of bio-inspired design for designing manmade engineered composite systems

Shown in Figure 5.1 is the illustration I developed for an effective application of the biological design principles to design manmade engineered composites made possible by the evolving additive manufacturing technology, in concert with a computational test bed for optimizing material properties for the structural design.

Figure 5.1. Illustration of how research findings can make use of modeling and rapid prototyping methods to better understand mechanisms that transfers stress across interfaces.

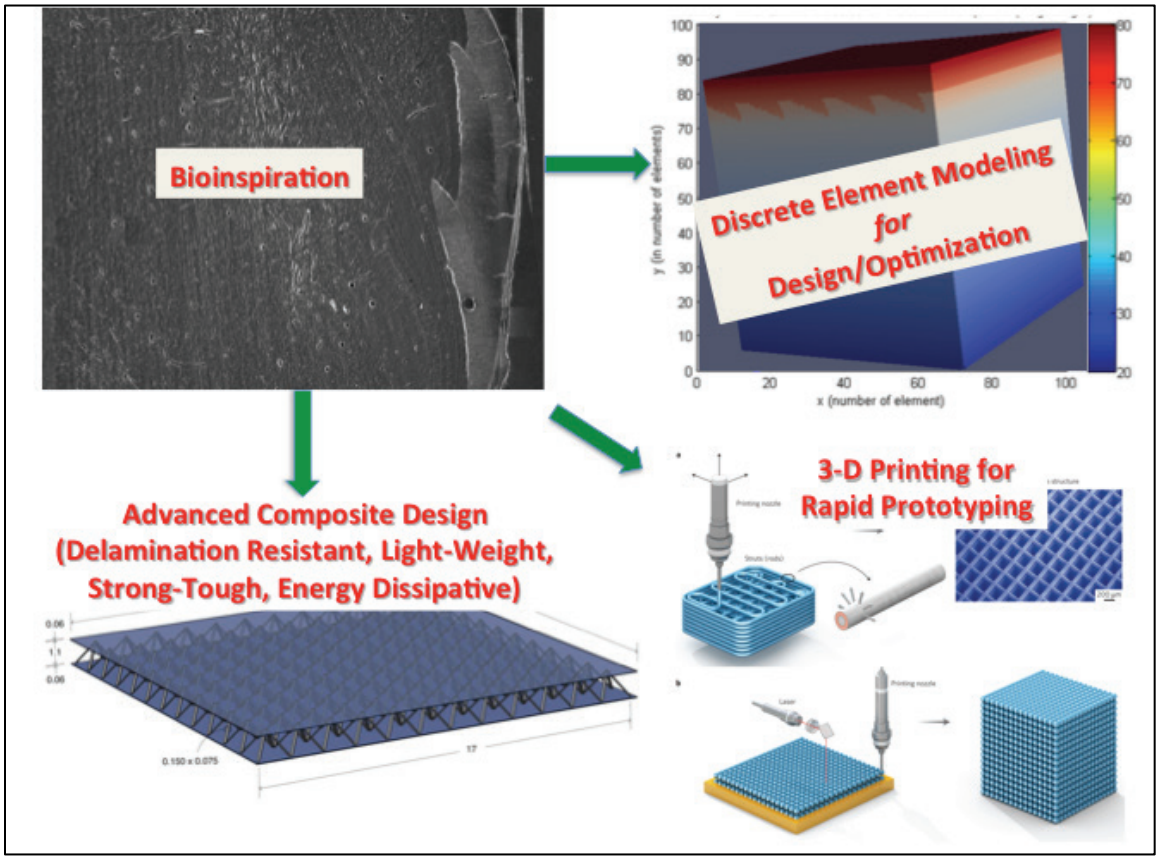

The results in Chapter 4 showed the fish scale is highly detailed due to the complex biological formation processes at the lower nanometer range. Because the formation processes are not well-understood, attempting to incorporate the intricate details from the nano- to millimeter-length scale in manufacturing is not feasible at present. However, building the layered system, observed at the micron scale with the structured interface, which included property grading, is an ideal controllable approach when employing additive manufacturing technologies.

Additive manufacturing technologies such as three-dimensional (3-D) printing allows the flexibility to ***"control the manufacturing process"*** down to tens of microns. Another advantage of 3-D printer bench scale designs is that they can be rapidly prototyped in less than one day unlike subtractive (traditional) manufacturing processes that require retooling and resetting dyes each time designs are changed. Also worth mentioning is laminated composites, the current industry standard, are designed/ manufactured to at best include orthotropic reinforcement. The

current 3-D printing technologies also accommodate the use of a variety of multiple materials (e.g., polymers and plastics) that have variance in mechanical properties, allowing for the design/manufacturing of anisotropic-strengthened composites beyond simple composite designs.

Specifically, 3-D printing could be used as a means to manufacture a scaled-up geometric model for the fish scale, using the principles of similitude and dimensional analysis, to isolate and study the roles the layer thickness and structured interface play in transferring load across the layers for a single material type. Also, by using a computational test bed, the structural design can first be optimized for the irregular geometry.

As a first approximation of the averaged mechanical properties using finite element modeling may be sufficient when optimizing single material type in a one-controllable structural parameter design. However, finite element modeling (FEM) is not adequate to discern the four attributes of functionally graded properties found in the fish scale: varied multilayered thickness, anisotropic reinforcement structures, heterogeneous material system, and a structured saw-tooth interface. Each attribute is a discrete feature having its own length scale and, to some extent, interacts in an imbricated structure that is difficult to capture in an averaged representative volume as required by a continuum approach such as FEM. A more appropriate modeling technique for optimizing the multi-structural parameters, using the computational test bed, is the discrete element method (DEM) to ascertain the relevance of each structural parameter describing fish scale.

As discussed in Chapter 4 in the nanoindentation results Section 4.3.3, the local variation of properties is often masked with averaging techniques derived from continuum mechanics, which are primarily used to determine constitutive relationships for the global stress and strains in FEM. Although DEM uses similar phenomenological relationships to define interactions, the method is based on discrete systems rather than discrete approximations to continuous partial differential equations. In DEM, as in the actual material, incompatible degrees of freedom acting at multiple scales can interact, whereby it is possible to analyze particle-scale deformation, stress, rotations, and couples that develop within locally grouped particles. Additionally, DEM can be used to identify the internal connectivity of the systems using coordination number to determine where force chains are likely to occur before shear banding percolates to the surface as

an observable defect. Therefore, the discreteness of DEM allows for a thorough sensitivity analysis to determine which discrete combinations of structural design parameters have the most effect over the mechanical response.

The optimization process using DEM and 3-D printing as complimentary tools can be further used to reduce the composite's weight while maintaining the same strength-to-weight ratio. The materials can be varied in 3-D printing to match the microstructures designed using DEM. The caveat is the materials used should be chemically compatible to minimize the debonding.

Additionally, civil engineers are interested in incorporating multifunctional materials. During the manufacturing process electronic materials could be used in 3-D printing of the structure. For instance biopolymers, carbon nanotubes, or graphene sheets could be used in the design as a self-sensing material and used as a means to self-report undesired detrimental deterioration cause by the environment or external loading conditions.

5.2 Summary of discussion

The research findings support the hypothesis that the favorable mechanical properties of fish scale is enabled by graded layer structures existing over a range of length scales. The biomineralized fish scale composite is complex and hierarchically structured. Nature does not design structures; rather it designs for functionality using whatever materials are indigenous to the geographical location. In the fish scale, nature appears to have focused on optimizing the geometry of the structure to serve some unknown function. From a design perspective, nature created a composite structure that seems to be resilient and can evolve on an as-needed basis to tailor its structure to obtain the most favorable mechanical attributes. There are only two individual structural components that are used in the biological composite.

The lessons learned from the current investigation are thought to be transferable to other biomineralized composites and also valid for the bioinspired design of manmade engineered composites. Furthermore, the bioinspired design space can make use of the emerging 3-D printing additive manufacturing technologies along with using computational test bed with DEM modeling as a proving ground to optimize both the structure and materials. The future is also promising for adding

multifunctionality by adding electronic materials to the design space for self-monitoring and self-reporting on structural health. In the next chapter, Chapter 6, the major conclusions discovered and innovation that has been produced from this comprehensive research effort will be explained.

6 Summary/Conclusions/Future Work

6.1 Summary

The focus of this study was to learn how nature integrates hard and soft materials at each length scale to form a layered composite that is light weight, has high strength with good fracture toughness but does not delaminate. Previous research by others had suggested that from the nano- to millimeter-length scale the individual components of the fish scale are glued rather than integrated to form layers in the composite. My research provided a detailed description, using novel experiments, to explain how hard and soft materials are mixed and integrated at each length to form a layered structure. In addition, my research provided details on how the hard and soft materials have been optimized by volume fractions, spatial proximity, and directional placement within the layers. Furthermore, the material variations were compared to mechanical properties of modulus, hardness, and, for the first time, energy dissipation was used to explain why fish scale has high strength, good toughness, and may not delaminate.

6.2 Contributions/conclusions

The research contributions from my work for the first time provided from experimental measurements the following conclusions of how the fish scale has high strength, good toughness, and may be delamination resistant when individual hard (inorganic minerals) and soft (polymer-like organic collagen fibers) materials are used:

1. The combination of hard (inorganic minerals) and soft (polymer-like organic collagen fibers) materials are integrated instead of being glued at the nano-length scale. At the micron scale for the two-layered composite materials, the outer dental enamel (hard) layered interface uses a sawtooth geometrical-shaped joint to connect to the inner bone (hard open-like foam) layer. At the millimeter scale the material and mechanical properties are gradually graded through the thickness, away from the enamel-bone sawtooth connected interface, for approximately 150 microns into each individual layer.
2. Within each layer, at the micron scale, there are subtle variations in the spatial proximity, and directional placement of the hard and soft materials. However, the outer enamel (hard) layer has 90 percent hard

(inorganic minerals), 10 percent soft (polymer-like organic collagen fibers) by volume, and the materials in the layer are densely packed; whereas the inner bone (hard open-like foam) layer contains 60 percent hard (inorganic minerals) and 40 percent soft (polymer-like organic collagen fibers) by volume, and materials in the layer are loosely packed.

3. My research developed a new experimental technique that was used to map the local viscoelastic (energy dissipative) response, attributed to the mixing/integrating of hard (inorganic minerals) and soft (polymer-like organic collagen fibers) volume fractions, within the layers at the nano-length scale. The instrumented nanoindentation-dynamic mechanical analysis experimental method was modified and was used to show variation due to change in material volume fractions and local placement of materials within the layers. For the outer enamel (hard) layer there was minimal variation of the local viscoelastic property and there was minimal viscoelastic contribution provided by the soft (polymer-like organic collagen fibers) within the layer. For the inner bone (hard open-like foam) layer there was major variation of the local viscoelastic property and there was major viscoelastic contribution provided by the soft (polymer-like organic collagen fibers) within layer.
4. If fully hydrated, the fish scales may resist cracks and delamination because of how the hard and soft materials are mixed/integrated within the layers from the nano-to-micro length scales, along with the way the two layers grade the properties away from the interface at the millimeter scale. Evidently, the fish scale has optimized the hard (inorganic minerals) and soft (polymer like organic collagen fibers) material volume fractions, variations within the layers, and uses gradual layer property transitions to reduce the local stresses that lead to delamination and crack formation caused by impact/penetration.

6.3 Future work

The current research identified the main materials in the two-layered composite as hard (inorganic minerals) and soft (polymer-like organic fibers). The materials are integrated at the nano scale and are likely to contribute to the superior delamination resistance. The two integrated materials and the layers should be modeled using the discrete element method to rank which aspects are most important:

1. How do gradual transitions between layers that contain the same components, but with different concentrations and textures of these components, distribute load and increase desired physical properties?
2. Is the geometric sawtooth joint at the micron scale the best design to connect the two layers?
3. How can the variations in material volume fraction, layer thickness, or layer density be optimized and possibly lead to the creation of stronger, lighter, tougher, more delamination resistant composite systems?

References

Aizenberg, J., J. C. Weaver, M. S. Thanawala, V. C. Sundar, D. E. Morse, and P. Fratzl. 2005. Skeleton of Euplectella sp.: Structural hierarchy from the nanoscale to the macroscale. *Science* 309:275-278.

Albarede, F. 2003. Geochemistry: An introduction. Cambridge, UK: Cambridge University Press.

Alfaro, R. M., C. A. Gonzales, and A. M. Ferrara. 2008. Gar biology and culture: Status and prospects. *Aquaculture Research* 39:748-763.

Allison, P. G., M. Q. Chandler, R. I. Rodriguez, B. A. Williams, R. D. Moser, C. A. Weiss, Jr., A. R. Poda, B. J. Lafferty, A. J. Kennedy, J. M. Seiter, W. D. Hodo, and R. F. Cook. 2013. Mechanical properties and structure of the biological multilayered material system, *Atractosteus spatula* scales. *Acta Biomaterialia* 9(2):5289-5296.

Allison, P. G., R. I. Rodriguez, R. D. Moser, B. A. Williams, A. R. Poda, J. M. Seiter, B. J. Lafferty, A. J. Kennedy, and M. Q. Chandler. 2014. Characterization of multi-layered fish scales (*Atractosteus spatula*) using nanoindentation, X-ray CT, FTIR, and SEM. *Journal of Visualized Experiments* 89. doi: 10.3791/51535.

American Association of State Highway and Transportation Officials (AASHTO). 1993. *AASHTO guide for design of pavement structures*. Washington, DC: AASHTO.

Ashby, M. F., H. Shercliff, and D. Cebon. 2007. Materials engineering, science, processing and design. 1st ed. Massachusetts: Elsevier Ltd.

Ashish, W., Y. Mehta, D. Cleary, E. Guo, L. Musumeci, A. Zapata, and W. Kettleson. 2011. Load-transfer efficiencies of rigid airfield pavement joints based on stresses and deflections. *Journal of Materials in Civil Engineering* 23(8):1171-1180.

Bahrololoom, M. E., M. Javidi, S. Javadpour, and J. Ma. 2009. Characterization of natural hydroxyapatite extracted from bovine cortical bone ash. *Journal of Ceramic Processing Research* 10(2):129-138.

Balooch, G., G. W. Marshall, S. J. Marshall, O. L. Warren, S. A. Asif, and M. Balooch. 2004. Evaluation of a new modulus mapping technique to investigate microstructural features of human teeth. *Journal of Biomechanics* 37:1223-1232.

Baohua, J., and G. Huajian. 2010. Mechanical principles of biological nanocomposites. *Annual Reviews of Materials Research* 40:77-100.

Barthelat, F. 2007. Biomimetics for next generation materials. *Philosophical Transactions of The Royal Society: A* 365:2907-2919.

Barthelat, F., and H. Espinosa. 2007. An experimental investigation of deformation and fracture of nacre–mother of pearl. *Experimental Mechanics* 47:311-324.

Bartol, I. K., M. Gharib, D. Weihs, P. W. Webb, J. R. Hove, and M. S. Gordon. 2003. Hydrodynamic stability of swimming in ostraciid fishes: Role of the carapace in the smooth trunkfish lactophrys triqueter (teleostei: ostraciidae). *Journal Experimental Biology* 206:725-44.

Bauerlein, E., P. Behrens, M. Epple, and J. Pickett-Heaps. 2007. Handbook of biomineralization: Biological aspects and structure formation. Weinheim, Germany: Wiley-VCH.

Bei, H. B., E. P. George, J. L. Hay, and G. M. Pharr. 2005. Influence of indenter tip geometry on elastic deformation during nanoindentation. *Physical Review Letters* 95:4-pp.

Beniash, E. 2011. Biominerals-hierarchical nanocomposites: The example of bone. *Wiley Interdisciplinary Reviews: Nanomedicine and nanobiotechnology* 3(1):47-69.

Bertassoni, L. E., and M. V. Swain. 2012. Influence of hydration on nanoindentation induced energy expenditure of dentin. *Journal of Biomechanics* 45:1679-1683.

Bhushan, B. 2009. Biomimetics: lessons from nature – An overview. *Philosophical Transactions of The Royal Society: A* 367:1445-1486.

Bigi, A., G. Cojazzi, S. Panzavolta, A. Ripamonti, N. Roveri, M. Romanello, K. Noris Suarez, and L. Moro. 1997. Chemical and structural characterization of the mineral phase from cortical and trabecular bone. *Journal of Inorganic Biochemistry* 68:45-51.

Boskey, A. L. 1991. The role of extracellur matrix components in dentin mineralization. *Critical Reviews in Oral Biology and Medicine* 2(2):369-387.

Boskey, A. L. 2007. Mineralization of bones and teeth. *Elements* 3(6):385-391.

Bozec, L., J. de Groot, M. Odlyha, B. Nicholls, S. Nesbitt, A. Flanagan, and M. Horton. 2005. Atomic force microscopy of collagen structure in bone and dentine revealed by osteoclastic resorption. *Ultramicroscopy* 105:79-89.

Brandstatter, J. J. 1963. Theory of elasticity of an anisotropic elastic body. San Francisco, CA: Holden Day.

Brill, D. R. 1998. *Development of advanced computational models for airport pavement design*. FAA Technical Report DOT/FAA/AR-97/47. Washington, DC: Department of Transportation.

Bruet, B., J. Song, M. Boyce, and C. Ortiz. 2008. Materials design principals of ancient fish armour. *Nature Materials* 7:748-756.1

Bruet, B. J. F. 2008. Multiscale structural and mechanical design of mineralized biocomposites. PhD diss., Massachusetts Institute of Technology.

Buehler, J. 2007. Nano- and micromechanical properties of hierarchical biological materials and tissues. *Journal of Materials Science* 42:8765-8770.

Bull, J. W., and A. Singh. 1990. A comparison between the stresses computed for finite sized precast concrete pavement units using Westergaard's equations and a numerical design method. *Computers and Geotechnics* 9(4):325-340.

Callister, Jr., W. D., and D. G. Rethwisch. 2008. *Fundamentals of materials science and engineering: An integrated approach*. 3d edition. Hoboken, NJ: John Wiley & Sons Ltd.

Canton, J., and A. Tucker. 2009. Current knowledge of tooth development: Patterning and mineralization of the murine dentition. *Journal of Anatomy* 214:502-515.

Carlino, E., and V. Grillo. 2006. Atomic resolution STEM-HAADF imaging in the study of interfaces. *Archives of Metallurgy and Materials* 51(1):23-32.

Chandler, M. Q., P. G. Allison, R. I. Rodriguez, R. D. Moser, and A. J. Kennedy. 2014. Finite element modeling of multilayered structures of fish scales. *Journal of the Mechanical Behavior of Biomedical Materials* 4:375-389.

Chang, M. C., and J. Tanaka. 2002. FT-IR study for hydroxyapatite/collagen nanocomposite cross-linked by glutaraldehyde. *Biomaterials* 23:4811-4818.

Chang-Yu, S., and P-Y. Chen. 2013. Structural design and mechanical behavior of alligator (alligator Mississippiensis) osteoderms. *Acta Biomaterialia* 9(11):9049-9064.

Chen, P.-Y., Y.-S. Lin, W. Yang, M. I. Lopez, J. Li, E. A. Olevsky, and M. A. Meyers. 2011. Predation versus protection: Fish teeth and scales evaluated by nanoindentation. *Journal of Materials Research* 27(1):100-112.

Chen, P., J. McKittrick, and M. Meyers. 2012. Biological materials: Functional adaptations and bioinspired designs. *Progress in Materials Science* 57:1492-1704.

Chou, Y. T. 1997. *Analysis of permanent deformations of flexible airport pavements*. WES TR S-77-8. Vicksburg, MS: U.S. Army Engineer Waterways Experiment Station.

Chung, W., J. Oh, K. Kwak, B. Lee, J. Meyer, E. Wang, A. Hexemer, and S-W. Lee. 2011. Biomimetic self-templating supramolecular structures. *Nature Materials* 478:364-368.

Coates, J. 2000. Interpretation of infrared spectra, a practical approach. In *R. A. Meyers Encyclopedia of Analytical Chemistry*, 10815-10837. Hoboken, NJ: John Wiley & Sons Ltd.

Columbia Accident Investigation Board. 2003. *Vol. 1*. Washington, DC: National Aeronautics and Space Administration and the Government Printing Office.

Constantinides, G., K. S. Ravi Chandran, F.-J. Ulm, and K. J. Van Vliet. 2006. Grid indentation analysis of composite microstructure and mechanics: Principles and validation. *Materials Science and Engineering A* 430:189-202.

Currey, J. 1999. The design of mineralized hard tissues for their mechanical functions. *The Journal of Experimental Biology* 202:3285-3294.

Cuy, J. L., A. B. Mann, K. J. Livi, M. F. Teaford, and T. P. Weihs. 2002. Nanoindentation mapping of the mechanical properties of human molar tooth enamel. *Archives of Oral Biology* 47:281-291.

Daget, J., M. Gayet, F. J. Meunier, and J-Y. Sire. 2001. Major discoveries on the dermal skeleton of fossil and recent polypteriforms: A review. *Fish and Fisheries* 2:113-124.

Das, B. M. 1990. *Principles of foundation engineering*. 2nd edition. Boston, MA: PWS Publishing Company.

Das, B. M. 1994. *Principles of geotechnical engineering*. 3rd edition. Boston, MA: PWS Publishing Company.

Domingo, L., S. T. Grimes, R. Soler-Gijón, and N. López-Martínez. 2009. Analysis of the geochemical variability in lepisosteid scales from the Fontllonga-3 site (Early Danian, Tremp Formation, South Central Pyrenees, Spain): Implications for Palaeoenvironmental studies. *Palaeogeography, Palaeoclimatology, Palaeoecology* 274:204-214.

Dubey, D., and V. Tomar. 2010. Role of molecular level interfacial forces in hard biomaterial mechanics: A review. *Annals of Biomedical Engineering* 38(6):2040-2055.

Dunlop, J. W. C., and P. Fratzl. 2010. Biological composites. *Annual Review of Materials Research*. 20:1-24.

Ehrilich, H. 2010. *Biological materials of marine origin invertebrates*. New York: Springer.

Faust, C. B., J. Johnston, and N. Reed. 1998. *Modern chemical techniques*. London, UK: Royal Society of Chemistry.

Figueiredo, M. M. 2015. Infrared spectroscopy - Life and biomedical sciences, Chapter 18-Characterization of bone and bone-based graft materials using FTIR spectroscopy. http://www.intechopen.com/books/infrared-spectroscopy-life-and-biomedical-sciences.

Fischer-Cripps, A. C. 2006. Critical review of analysis and interpretation of nanoindentation test data. *Surface and Coatings Technology* 200:4153-4165.

Fleet, M. E., X. Liu, and P. L. King. 2004. Accommodation of the carbonate ion in apatite: An FTIR and X-ray structure study of crystals synthesized at 2-4 GPa. *American Mineralogist* (89):1422-1432.

Fleet, M. 2015. *Carbonated hydroxyapatite: Materials, synthesis, and application*. Boca Raton, FL: Taylor and Francis.

Fratzl, P., N. Fratzl-Zelman, K. Klaushofer, G. Vogl, and K. Koller. 1991. Nucleation and growth of mineral crystals in bone studied by small-angle X-ray scattering. *Calcium Tissue International* 48:407-413.

Fratzl, P. 2007. Biomimetic materials research: What can we really learn from nature's structural materials? *Journal of The Royal Society Interface*, 4:637-642.

Gao, H., B. Ji, M. Buehler, and H. Yao. 2004. Flaw tolerant bulk and surface nanostructures of biological systems. *Mechanics and Chemistry of Biosystems* 1(1):37-52.

Garrano, A. M. C., G. La Rosa, D. Zhang, L.-N. Niu, F. R. Tay, H. Majd, and D. Arola. 2012. On the mechanical behavior of scales from cyprinus carpio. *Journal of the Mechanical Behavior of Biomedical Materials* 7:17-29.

Gayet, M., and F. J. Meunier. 1991. First discovery of polypteridae (pisces, cladistia, polypteriformes) outside of Africa. *Geobios* 24:463-466.

Gayet, M., F. J. Meunier, and C. Werner. 2002. Diversification in Polypteriformes and special comparisons with the lepisosteiformes. *Palaeontology* 45:361-376.

Géraudie, J. 1988. Fine structural peculiarities of the pectoral fin dermoskeleton of two brachiopterygii, polypterus senegalus, and calamoichthys calabaricus (pisces, o*steichthyes*). *The Anatomical Record* 221(1):455-68.

Geubelle, P. H., and J. S. Baylor. 2008. Impact-induced delamination of composites: A 2D simulation. *Elsevier Composites Part B: Engineering* 29(5):589-602.

Gibson, R. F. 1994. *Principles of composite materials mechanics*. New York: McGraw-Hill.

Goldstein, J., D. Newbury, D. Joy, C. Lyman, P. Etchling, E. Lifshin, L. Sawyer, and J. Michael. 2007. *Scanning electron microscopy and X-ray microanalysis*. 3d edition. New York, NY: Springer.

Golovin, Y. 2008. Nanoindentation and mechanical properties of solids in submicrovolumes. Thin near-surface layers, and films: A review. *Physics of the Solid State* 50(2):2205-2236.

Goodrich, E. 1907. On the scales of fish, living and extinct, and their importance in classification. *Proceedings of The Zoological Society of London* 77(4):751-773.

Goodsell, D. 2004. *Bionanotechnology – Lessons from nature*. La Jolla, California: Wiley.

Gottfried, M. D., and D. W. Krause. 1998. First record of gars *lepissteidae actionoterygii* on Madagascar late Cretaceous remains from the Mahajanga Basin. *Journal of Vertebrate Paleontology* 18[2]:275-279.

Grandfield, K., E. A. McNally, A. Palmquist, G. A. Botton, P. Thomsen, and H. Engqvist. 2010. Visualizing biointerfaces in three dimensions: Electron tomography of the bone-hydroxyapatite interface. *Journal of Royal Society-Interface* 7(51):1497-1501.

Grandfield, K., and H. Engqvist. 2012. Focused ion beam in the study of biomaterials and biological matter. *Advances in Materials Science and Engineering* 2012:6-pp.

Grunenwald, A., C. Keyser, A. M. Sautereau, E. Crubezy, B. Ludes, and C. Drouet. 2014. Revisiting carbonate quantification in apatite (bio) minerals: A validated FTIR methodology. *Journal of Archaeological Science* 49:134-141.

Gunther, H. 2013. *NMR spectroscopy: Basic principles, concepts and applications in chemistry*. 3d ed. Hoboken, NJ: Wiley.

Gururaja, M. N. 2012. A review on recent applications and future prospectus of hybrid composites. *International Journal of Soft Computing & Engineering* 1(6):352-355.

Haines, P. J. 1995. Thermal methods of analysis. *Principles, Applications and Problems*. 1st ed. London, UK: Chapman & Hall.

Hammons, M. I., and A. M. Ioannides. 1997. *Advanced pavement design: Finite element modeling for rigid pavement joints. Report 1: Background investigation*. FAA Technical Report DOT/FAA/AR-95/85. Washington, DC: U.S. Department of Transportation.

Hammons, M. I. 1998. *Advanced pavement design: Finite element modeling for rigid pavement joints, Report II: Model development*. FAA Technical Report DOT/FAA/AR-97/7. Washington, DC: Department of Transportation.

Han, L., L. Wang, J. Song, M. C. Boyce, and C. Ortiz. 2011. Direct quantification of the mechanical anisotropy and fracture of an individual exoskeleton layer via uniaxial compression of micropillars. *Nano Letters* 11(9):3868-3874.

Hanus, M. J., and A. Harris. 2013. Nanotechnology innovations for the construction industry. *Progress in Materials Science* 58(7):1056-1102.

Hay, J. L., and G. M. Pharr. 2000. Instrumented indentation testing. In *ASM Handbook Volume 8: Mechanical Testing and Evaluation*, ed. H. Kuhn and D. Medlin, 10th ed., 232-243. Materials Park, OH: ASM International.

Hay, J. L. 2009. Introduction to instrumented indentation testing. *Experimental Techniques* 33(6):66-72.

Hay, J., and B. Crawford. 2011. Measuring substrate-independent modulus of thin films. *Journal of Materials Research* 26(6):727-738.

Henderson, G. S., D. R. Neuville, and R. T. Downs. 2014. Spectroscopic methods in mineralogy and materials sciences. *Reviews in Mineralogy and Geochemistry* 78.

Herbert, E. G., W. C. Oliver, and G. M. Pharr. 2008. Nanoindentation and the dynamic characterization of viscoelastic solids. *Journal of Physics D: Applied Physics*. 41(7):074021, 9-pp.

Hoa, S. V. 2009. *Principles of the manufacturing of composite materials*. Pennsylvania: DEStech Publications.

Hodo, W. D. 2015. Investigation of the inherent chemical, structural, and mechanical attributes of bio-engineered composites found in nature: Alligator gar's exoskeleton fish scales. PhD diss., University of Arkansas.

How to Make a NMR Sample. 2015. http://chem.ch.huji.ac.il/nmr/preparation.html.

Huang, Y. H. 1993. *Pavement analysis and design*. Englewood Cliffs, NJ: Prentice Hall.

Hughes, J. M., M. Cameron, and K. D. Crowley. 1989. Structural variations in natural F, OH, and Cl apatites. *American Mineralogist* 74:870-876.

Hughes, J. M., M. Cameron, and K. D. Crowley. 1991. Ordering of divalent cations in the apatite structure: Crystal structure refinements of natural Mn- and Sr-bearing apatite. *American Mineralogist* 76:1857-1862.

Ikoma, T., H. Kobayashi, J. Tanaka, D. Walsh, and S. Mann. 2003. Microstructure, mechanical, and biomimetic properties of fish scales from pagrus major. *Journal of Structural Biology* 142:327-333.

Ioannides, A. M., and G. T. Korovesis. 1990. Aggregate interlock: A pure shear load transfer mechanism. *Transportation Research Record* 1286:14-24. Washington, DC: Transportation Research Board of the National Academies.

Iyengar, G. V., and L. Tandon. 1999. Minor and trace elements in human bones and teeth. Vienna, Italy: International Atomic Energy Agency (IAEA) -- Nutritional and Health-Related Environmental Studies (NAHRES).

Jager, A., and R. Lackner. 2008. Identification of viscoelastic model parameters by means of cyclic nanoindentation testing. *International Journal of Materials Research*. 99(8):829-835.

Jantou, V., M. Turmaine, G. D. West, M. A. Horton, and D. W. McComb. 2009. Focused ion beam milling and ultramicrotomy of mineralized ivory dentine for analytical transmission electron microscopy. *Micron* 40:495-501.

Jantou-Morris, V., M. A. Horton, and D. W. McComb. 2010. The nano-morphological relationships between apatite crystals and collagen fibrils in ivory dentine. *Biomaterials* 31:5275-5286.

Joint Light Tactical Vehicle. 2015. https://en.wikipedia.org/wiki/Joint_Light_Tactical_Vehicle.

Jones, R. M. 1999. *Mechanics of composite materials second edition*. Philadelphia, PA: Taylor and Francis.

Kennedy, A. J., D. R. Johnson, J. M. Seiter, J. H. Lindsay, R. E. Boyd, A. J. Bednar, and P. G. Allison. 2012. Tungsten toxicity, bioaccumulation, and compartmentalization into organisms representing two trophic levels. *Environmental Science and Technology* 46:9646-9652.

Kim, S-K. 2013. *Marine biomaterials: Characterization, isolation, and applications*. Philadelphia, PA: CRC Press, Taylor and Francis.

Kizilyaprak, C., J. Daraspe, and B. M. Humbel. 2014. Focused ion beam scanning electron in biology. *Journal of Microscopy* 254(3):109-114.

Klosowski, M. M., R. J. Friederichs, R. Nichol, N. Anolin, R. Carzaniga, W. Windl, S. M. Best, S. J. Shefelbine, D. W. McComb, and A. E. Porter. 2015. Probing carbonate in bone forming minerals on the nanometer scale. *Acta Biomaterrialia* 20:129-139.

Kumar, K., R. S. Rana, and B. S. Paliwal. 2005. Osteoglossid and lepisosteid fish remains from the Paleocene palana formation, Rajasthan, India. *Palaeontology* 48(6):1187-1209.

Lambe, T. W., and R. V. Whitman. 1969. *Soil mechanics*. London: John Wiley and Sons.

Landis, W. J. 1995. The strength of a calcified tissue depends in part on the molecular structure and organization of its constituent mineral crystals in their organic matrix. *Bone* 16(5):533-544.

Lee, S., E. Novitskaya, B. Reynante, J. Vasquez, R. Urbaniak, T. Takahashi, E. Woolley, L. Tombolato, P. Chen, and J. McKittrick. 2011. Impact testing of structural biological materials. *Materials Science and Engineering: C* 31(4):730-739.

Leng, Y. 2008. *Materials characterization: Introduction to microscopic and spectroscopic methods*. Chichester, UK: John Wiley & Sons Ltd.

Levinson, R., M. Berry, J. Johnston, C. Osborne, and M. Pack. 2001. *More modern chemical techniques*. London, UK: Royal Society of Chemistry.

Liao, C-J., F-H. Lin, K-S. Chen, and J-S. Sun. 1999. Thermal decomposition and reconstruction of hydroxyapatite in air atmosphere. *Biomaterials* 20(19):1807-1813.

Lin, Y. S., C. T. Wei, E. A. Olevsky, and M. A. Meyers. 2011. Mechanical properties and the laminate structure of Arapaima Gigas scales. *Journal of the Mechanical Behavior of Biomedical Materials* 4:1145-1156.

Liou, S-C., S-Y. Chen, H-Y. Lee, and J-S. Bow. 2004. Structural characterization of nano-sized calcium deficient apatite powders. *Biomaterials* 25:189-196.

Liu, W. T., Y. Zhang, G. Y. Li, Y. Q. Miao, and X. H. Wu. 2008. Structure and composition of teleost scales from snakehead channa argus (cantor) (perciformes: channidae). *Journal of Fish Biology* 72:1055-1067.

Luz, G., and J. Mano. 2009. Biomimetic design material biomaterial inspired by the structure of nacre. *Philosophical Transactions of The Royal Society: A* 367:1587-1605.

Makhecha, D. P. 2005. Dynamic fracture of adhesively bonded composite structures using cohesive zone models. PhD diss., Virginia Polytechnic Institute and State University.

Mallick, R. B., and T. El-Korchi. 2009. *Pavement engineering principles and practice*. Boca Raton, FL: CRC Press Taylor and Francis Group.

Mann, S. 2001. *Biomineralization principles and concepts in bioinorganic materials chemistry*. New York: Oxford University Press.

Maranganti, R., and P. Sharma. 2007. Length scales at which classical elasticity breaks down for various materials. *Physical Review Letters* 98(19):195504.

Marinenko, R. B. 1991. Standards for electron probe microanalysis, in electron probe quantitation. In *Plenum*, ed. K. F. J. Heinrich and D. E. Newbury, pp.251-260.

Markovic, M., B. O. Fowler, and M. S. Tung. 2004. Preparation and comprehensive characterization of a calcium hydroxyapatite reference material. *Journal of Research of the National Institute of Standards and Technology* 109(6):553-568.

Mathew, M., and S. Takagi. 2001. Structures of biological minerals in dental research. *Journal of Dental Research* 106(6):1035-1044.

McNally, E. A., H. P. Schwarcz, G. A. Botton, and A. L. Aresnault. 2012. A model for the ultrastructure of bone based on electron microscopy of ion-milled sections. *PLoS ONE* 7(1): e29258. doi:10.1371/journal.pone.0029258.

McNally, E. A., F. Nan, G. A. Botton, and H. P. Schwarcz. 2013. Scanning transmission electron microscopic tomography of cortical bone using Z-contrast imaging. *Micron* 49:46-53.

Meyers, M., P. Chen, A. Lin, and Y. Seki. 2008. Biological materials: Structure and mechanical properties. *Progress in Materials Science* 53:1-206.

Meyers, M., P. Chen, M. Lopez, Y. Seki, and A. Lin. 2011. Biological materials: A materials science approach. *Journal of the Mechanical Behavior of Biomedical Materials* 4(5):626-657.

Mine-Resistant Ambush Protected. 2015. https://en.wikipedia.org/wiki/MRAP.

Mucalo, M. 2015. *Hydroxyapatite (HAp) for biomedical applications. 1st ed.* Cambridge, UK: Woodhead Publishing Series in Biomaterials-Elsevier.

Nalla, R. K., A. E. Porter, C. Daraio, A. M. Minor, V. Radmilovic, E. A. Stach, A. P. Tomsia, and R. O. Ritchie. 2005. Ultrastructural examination of dentin using focused ion-beam cross-sectioning and transmission electron microscopy. *Micron* 36:672-680.

Needleman, A. 1989. An analysis of decohesion along an imperfect interface. *International Journal of Fracture* 42(1):21-40.

Nieto, F., and K. J. T. Livi. 2013. Minerals at the nanoscale. *European Mineralogical Union: Notes In Mineralogy* 14.

Nudelman, F., K. Pieterse, A. George, P. H. Bomans, H. Friedrich, L. J. Brylka, P. A. Hilbers, G. de With, and N. A. Sommerdijk. 2010. The role of collagen in bone apatite formation in the presence of hydroxyapatite nucleation inhibitors. *Nature Materials* 9:1004-1009.

Ochsner, A., and W. Ahmed. 2011. *Biomechanics of hard tissues modeling, testing, and materials. 4th ed.* Hoboken, NJ: Wiley-VCH.

Oliver, W. C., and G. M. Pharr. 1992. An improved technique for determining hardness and elastic modulus using load and displacement sensing indentation experiments. *Journal of Materials Research* 7(6):1564-1583.

Oliver, W. C., and G. M. Pharr. 2004. Measurement of hardness and elastic modulus by instrumented indentation: Advances in understanding and refinements to methodology. *Journal of Materials Research* 19(1):3-20.

Olszta, M., X. Cheng, S. Jee, R. Kumar, Y-Y. Kim, M. Kaufman, E. Douglas, and L. Gower. 2007. Bone structure and formation: A new perspective. *Materials Science and Engineering: R: Reports* 58(3-5):77-116.

Ostojic, P., and R. McPherson. 1987. A review of indentation fracture theory: Its development, principles and limitations. *International Journal of Fracture* 33:297-312.

Oyen, M. L. 2011. *Handbook of nanoindentation with biological applications*. Singapore: Stanford Publishing.

Pethica, J. B., and W. C. Oliver. 1989. Mechanical properties of nanometer volumes of material: Use of the elastic response of small area indentations. *Materials Research Society Symposium Proceedings* 130:13-23.

Pharr, G. M., J. H. Strader, and W. C. Oliver. 2009. Critical issues in making small-depth mechanical property measurements by nanoindentation with continuous stiffness measurement. *Journal of Materials Research* 24(3):653-666.

Pharr, G. M., E. G. Herbert, and Y. Gao. 2010. The indentation size effect: A critical examination of experimental observations and mechanistic interpretations. *Annual Review of Materials Research* 40:271-292.

Qiao, P., M. Yang, and F. Bobaru. 2008. Impact mechanics and high-energy absorbing materials: Review. *Journal of Aerospace Engineering* 21(4):235-248.

Rakovan, J., Y. Luo, and O. Borkiewicz. 2008. Synchrotron microanalytical methods in the study of trace and minor elements in apatite. *Mineralogia* 39(1-2):31-40.

Randall, N. X., M. Vandamme, and F-J. Ulm. 2011. Nanoindentation analysis as a two-dimensional tool for mapping the mechanical properties of complex surfaces. *Journal of Materials Research* (24):v679-690.

Raschi, W., and C. Tabit. 1992. Functional aspects of placoid scales: A review and update. *Australian Journal of Marine and Freshwater Research* 43(1):123-147.

Ratner, B. D., A. S. Hoffman, F. J. Schoen, and J. E. Lemons. 2013. *Biomaterials science: An introduction to materials in medicine. 3d ed.* London: Elsevier.

Reed, S. J. B. 1996. *Electron microprobe analysis and scanning electron microscopy in geology*. Cambridge, UK: Cambridge University Press.

Reinhardt, C. 2001. *Chemical sciences in the 20th century: Bridging boundaries*. Weinheim, Germany: Wiley-VCH.

Resnikov, N., R. Shahar, and S. Weiner. 2014. Three-dimensional structure of human lamellar bone: The presence of two different materials and new insights into the hierarchical organization. *Bone* 59:93-104.

Rettler, E., S. Hoeppener, B. W. Sigusch, and U. S. Schubert. 2013. Mapping the mechanical properties of biomaterials on different length scales: Depth-sensing indentation and AFM based nanoindentation. *Journal of Materials Chemistry B* 1:2789-2806.

Rho, J-Y., and G. M. Pharr. 1999. Effects of drying on the mechanical properties of bovine femur measured by nanoindentation. *Journal of Materials Science: Materials in Medicine* 10:485-488.

Rho, J. Y., P. Zioupos, J. D. Currey, and G. M. Pharr. 2002. Microstructural elasticity and regional heterogeneity in human femoral bone of various ages examined by nano-indentation. *Journal of Biomechanics* 35:189-198.

Richter, M., and M. Smith. 1995. A microstructural study of the ganoine tissue of selected lower vertebrates. *Zoological Journal of the Linnean Society* 114(2):173-212.

Ritchie, R. 2011. The conflicts between strength and toughness. *Nature Materials* 10(11): 817-822.

Rodriguez-Florez, N., M. L. Oyen, and S. J. Shefelbine. 2013. Insight into differences in nanoindentation properties of bone. *Journal of the Mechanical Behavior of Biomedical Materials* 18:90-99.

Russ, J. C. 1984. *Fundamentals of energy dispersive X-ray analysis*. London, UK: Butterworths.

Ryou, H., E. Romberg, D. H. Pashley, F. R. Tay, and D. Arola. 2012. Nanoscopic dynamic mechanical properties of intertubular and peritubular dentin. *Journal of the Mechanical Behavior of Biomedical Materials* 7:3-16.

Sahi, N., and M. A. A. Schoonen. 2006. Medical mineralogy and geochemistry. *Reviews in Mineralogy and Geochemistry* 64.

Salonitis, K., J. Pandremenos, J. Paralikas, and G. Chryssolouris. 2010. Multifunctional materials: Engineering applications and processing challenges. *International Journal of Advanced Manufacturing Technology* 49:803-826.

Sanchez-Quevedo, M. C., O. H. Nieto-Albano, J. M. Garacia, M. E. Gomez de Ferraris, and A. Campos. 1998. Electron probe microanalysis of permanent human enamel and dentine. A methodological and quantitative study. *Histology and Histopathology* 13:109-113.

Sarikaya, M., H. Fong, D. Frech, and R. Humbert. 1999. Biomimetic assembly of nano-structured materials. *Material Science Forum* 293:83-98.

Schonborner, A. A., F. J. Meunier, and J. Castanet. 1981. The fine structure of calcified Mandl's corpuscles in teleost fish scales. *Tissue and Cell* 13(3):589-597.

Shapiro, J. R., P. H. Byers, F. H. Glorieux, and P. D. Sponseller. 2014. *Osteogenesis imperfecta: A translational approach to brittle bone disease*. London: Elsevier.

Shark. 2015. http://www.britannica.com/EBchecked/topic/53bb51/shark.

Sire, J-Y. 1989a. Scales in young polypterus senegalus are elasmoid new phylogenetic implications. *American Journal of Anatomy* 186(3):315-323.

Sire, J-Y. 1989b. From ganold to elasmoid scales in the actinopterygian fishes. *Netherlands Journal of Zoology* 40(1-2):75-92.

Sire, J-Y. 1995. Ganoine formation in the scales of primitive actinopterygian fishes, lepisosteids and polypterids. *Connective Tissue Research* 33(1-3):213-222.

Smith, J. B., B. S. Grandstaff, and M. S. Abdel-Ghani. 2006. Microstructure of polypterid scales (*Osteichthyes: Actinopterygii: Polypteridae*) from the upper Cretaceous Bahariya formation, Bahariya Oasis, Egypt. *Journal of Paleontology* 80(6):1179-1185.

Sneddon, I. N. 1965. The relation between load and penetration in the axi-symmetric Boussinesq problem for a punch of arbitrary profile. *International Journal of Engineering Science* 3(1):47-57.

Song, J., S. Reichert, I. Kallai, D. Gazit, M. Wund, M. Boyce, and C. Ortiz. 2010. Quantitative microstructural studies of the armor of the marine threespine stickleback (*Gasterosteus aculeatus*). *Journal of Structural Biology* 171:318-331.

Song, J., C. Oriz, and M. C. Boyce. 2011. Threat-protection mechanics of an armored fish. *Journal of the Mechanical Behavior of Biomedical Materials* 4(5):699-712.

Srinivasan, A. V., G. K. Haritos, and F. L. Hedberg. 1991. Biomimetics: Advancing man-made materials through guidance from nature. *Applied Mechanical Reviews* 44(11):463-481.

Strong, A. B. 2008. *Fundamentals of composites manufacturing - Materials, methods, and applications, second edition*. Dearborn, MI: Society of Manufacturing Engineers.

Structural composites and sandwich panels. 2015. http://www.engineeredmaterialsinc.com/products/structural-composites-and-sandwich-panels/.

Sudo, S., K. Tsuyuki, Y. Ito, and T. Ikohagi. 2002. A study on the surface shape of fish scales. *JSME International Journal. Mechanical Systems, Machine Elements and Manufacturing* 45(4):100-1105.

Sun, J., M. Ling, Y. Wang, D. Chen, S. Zhang, J. Tong, and S. Wang. 2014. Quasi-static and dynamic nanoindentation of some selected biomaterials. *Journal of Bionic Engineering* 11:144-150.

Swadener, J. G., E. P. George, and G. M. Pharr. 2002. The correlation of the indentation size effect measured with indenters of various shapes. *Journal of the Mechanics and Physics of Solids* 50:681-694.

Tai, K., H. J. Qi, and C. Ortiz. 2005. Effect of mineral content on the nanoindentation properties and nanoscale deformation mechanisms of bovine tibial cortical bone. *Journal of Materials Science: Materials In Medicine* 16:947-959.

Terzaghi, K. 1943. *Theoretical soil mechanics*. London: John Wiley and Sons.

The Electromagnetic Spectrum. 2015. http://herschel.cf.ac.uk/science/infrared.

Timoshenko, S., and J. M. Lessels. 1925. *Applied elasticity*. Pittsburgh, PA: Westinghouse Technical Night School Press.

Tippetts, T. 2005. Non-linear models of composite laminate. *Proceedings of the 23rd International Modal Analysis Conference*. Orlando, FL.

Tonsuaadu, K., K. A. Gross, L. Pluduma, and M. Veiderma. 2012. A review on the thermal stability of calcium apatites. *Journal of Thermal Analysis and Calorimetry* 110: 647-659.

Torres, F. G., O. P. Troncoso, J. Nakamatsu, C. J. Grande, and C. M. Gomez. 2008. Characterization of the nanocomposite laminate structure occurring in fish scales from arapaima gigas. *Materials Science and Engineering C* 28:1276-1283.

Unified Facilities Criteria (UFC), Pavement Design for Airfields. 2001. *UFC 03-260-02. Construction Criteria Base*. Washington, DC: National Institute of Building Sciences.

VanLandingham, M. R. 2003. Review of instrumented indentation. *Journal of Research of the National Institute of Standards and Technology* 108(4):249-265.

Waite, J. H., and C. C. Broomell. 2012. Review: Changing environments and structure–Property relationships in marine biomaterials. *The Journal of Experimental Biology* 215:873-883.

Wegst, U. G. K., and M. F. Ashby. 2004. The mechanical efficiency of natural materials. *Philosophical Magazine* 84(21):2167-2181.

Wegst, U., H. Bai, E. Saiz, A. Tomsia, and R. Ritchie. 2015. Bioinspired structural materials. *Nature Materials* 14(1):23-36.

Wegst, U., M. Schecter, A. Donius, and P. Hunger. 2010. Biomaterials by freeze casting. *Philosophical Transactions of The Royal Society: A* 368:2099-2121.

Weiner, S., A. Veis, E. Beniash, T. Arad, J. W. Dillion, B. Sabsay, and F. Siddiqui. 1999. Peritubular dentin formation: Crystal organization and the macromolecular constituents in human teeth. *Journal of Structural Biology* 126:27-41.

Weiner, S., L. Addadi, and H. D. Wagner. 2000. Materials design in biology. *Materials Science and Engineering C* 11:1-8.

Westergaard, H. M. 1925. Computation of stresses in concrete roads. In *Proceedings Highway Research Board. National Research Council* 5(1):90-112.

Wheeler, A. J., and A. R. Ganji. 2001. *Introduction to engineering experimentation. 2nd ed.* Upper Saddle River, NJ: Pearson-Prentice Hall.

Wiley, E. O. 1976. The phylogeny and bio geography of fossil and recent gars (*Actinopterygii: Lepisosteidae). University of Kansas Museum of Natural History Miscellaneous Publication* 64:1-111.

Williams, D. B., and C. B. Carter. 2009. *Transmission electron microscopy: A textbook for materials science, 2nd ed.* New York, NY: Springer.

Williamson, W. C. 1849. On the microscopic structure of the scales and dermal teeth of some ganoid and placoid fish. *Philosophical Transactions-Royal Society of London. Physical Sciences and Engineering* 139:435-475.

Willmott, P. 2011. *An introduction to synchrotron radiation: Techniques and applications*. Chichester, UK: John Wiley & Sons Ltd.

Wilson, R. M., J. C. Elliot, and S. E. P. Dowker. 1999. Rietveld refinement of the crystallographic structure of human dental enamel apatites. *American Mineralogist* 84: 1406-1414.

Wopenka, B., and J. D. Pasteris. 2005. A mineralogical perspective on the apatite in bone. *Materials Science and Engineering C* 25:131-143.

Wright, W. J., A. R. Maloney, and W. D. Nix. 2007. An improved analysis for viscoelastic damping in dynamic nanoindentation. *International Journal of Surface Science and Engineering* 1(2-3):274-292.

X-Ray DATA BOOKLET. 2015. http://xdbl.llbl.gov.

Yang, W., I. H. Chen, J. McKittrick, and M. A. Meyers. 2012. Flexible dermal armor in nature. *Journal of the Minerals, Metals & Materials Society* 64(4):475-485.

Yang, W., I. H. Chen, B. Gludovatz, E. A. Zimmermann, R. O. Ritchie, and M. A. Meyers. 2013a. Natural flexible dermal armor. *Advanced Materials* 25(1):31-48.

Yang, W., B. Gludovatz, E. A. Zimmermann, H. A. Bale, R. O. Ritchie, and M. A. Meyers. 2013b. Structure and fracture resistance of alligator gar (*Atractosteus Spatula*) armored fish scales. *Acta Biomaterialia* 9(4):5876-5889.

Yoder, E. J., and M. W. Witczak. 1975. *Principles of pavement design, 2nd ed.* London: John Wiley and Sons.

Young, R. A. 1974. Implications of atomic substitutions and other structural details in apatites. *Journal of Dental Research* 53(2):193-203.

Zhang, J., G. L. Niebur, and T. C. Ovaret. 2008. Mechanical property determination of bone through nano- and micro-indentation testing and finite element simulation. *Journal of Biomechanics* 41:267-275.

REPORT DOCUMENTATION PAGE

Form Approved
OMB No. 0704-0188

1. REPORT DATE *(DD-MM-YYYY)*	2. REPORT TYPE	3. DATES COVERED *(From - To)*
April 2019	Final	

4. TITLE AND SUBTITLE

Investigation of the Mechanisms for the Delamination Resistance Found In Bio-Engineered Composites Found in Nature: Bi-Layered Exoskeleton Fish Scales

5a. CONTRACT NUMBER

5b. GRANT NUMBER

5c. PROGRAM ELEMENT NUMBER
61101

6. AUTHOR(S)

W. D. Hodo

5d. PROJECT NUMBER
MR018

5e. TASK NUMBER
02

5f. WORK UNIT NUMBER

7. PERFORMING ORGANIZATION NAME(S) AND ADDRESS(ES)

Geotechnical and Structures Laboratory
U.S. Army Engineer Research and Development Center
3909 Halls Ferry Road
Vicksburg, MS 39180-6199

8. PERFORMING ORGANIZATION REPORT NUMBER

ERDC/GSL TR-19-20

9. SPONSORING / MONITORING AGENCY NAME(S) AND ADDRESS(ES)

U.S. Army Corps of Engineers
Washington, DC 20314-1000

10. SPONSOR/MONITOR'S ACRONYM(S)

USACE

11. SPONSOR/MONITOR'S REPORT NUMBER(S)

12. DISTRIBUTION / AVAILABILITY STATEMENT

Approved for public release; distribution is unlimited.

13. SUPPLEMENTARY NOTES

14. ABSTRACT

The focus of this study was to learn how nature integrates hard and soft materials at each length scale to form a layered composite that better resists delamination. This research provided a detailed description, using novel experiments, to explain how hard and soft materials have been mixed/integrated at each length scale, optimized by volume fractions, which affect the fish scales' mechanical response due to external loading. The results from the study showed the following:

1. The combination of the hard (inorganic minerals) and soft (organic collagen fibers) are integrated instead of being glued at the nano scale. At the micron scale for the two-layered composite, the outer dental enamel (hard) layered interface uses a sawtooth-shaped joint to connect to the inner bone (hard open-like foam) layer. At the millimeter scale, the material and mechanical properties are gradually graded through the thickness away from the interface.
2. The outer hard layer has 90 percent hard (inorganic minerals) and 10 percent (collagen fibers) by volume. Whereas, the inner bone layer has 60 percent hard (inorganic minerals) and 40 percent (organic collagen fibers) by volume. The property variation seems to delocalize stresses, which increase delamination resistance at the interface.

15. SUBJECT TERMS

Biomineralized
Exoskeleton Fish Scale
Biocomposite
Delamination Resistant
Alligator Gar
Composite materials – evaluation
Atractosteus spatula
Composite materials – delamination

16. SECURITY CLASSIFICATION OF:			17. LIMITATION OF ABSTRACT	18. NUMBER OF PAGES	19a. NAME OF RESPONSIBLE PERSON
a. REPORT	b. ABSTRACT	c. THIS PAGE			19b. TELEPHONE NUMBER *(include area code)*
Unclassified	Unclassified	Unclassified		168	